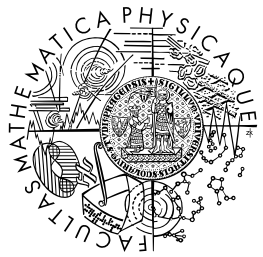

FACULTY
OF MATHEMATICS
AND PHYSICS
Charles University

MASTER THESIS

Bc. Matúš Rojik

Ab-initio description of nuclear reactions

Institute of Particle and Nuclear Physics

Supervisor of the master thesis: Ing. Martin Schäfer, PhD.

Study programme: Particle and Nuclear Physics (N0533A110014)

Study branch: FCJFP (0533TA110014)

Prague 2025

I declare that I carried out this master thesis independently, and only with the cited sources, literature and other professional sources. It has not been used to obtain another or the same degree.

I understand that my work relates to the rights and obligations under the Act No. 121/2000 Sb., the Copyright Act, as amended, in particular the fact that the Charles University has the right to conclude a license agreement on the use of this work as a school work pursuant to Section 60 subsection 1 of the Copyright Act.

In ..... date ....

Author's signature

First and foremost, I would like to thank my supervisor, Dr. Martin Schäfer, for his guidance, patience and for introducing me to the wonderful world of nuclear effective field theories.

Chcel by som sa poďakovať mojim rodičom za ich lásku a podporu, bez ktorej by som túto prácu nemohol dokončiť.

Title: Ab-initio description of nuclear reactions

Author: Bc. Matúš Rojik

Institute: Institute of Particle and Nuclear Physics

Supervisor: Ing. Martin Schäfer, PhD., Nuclear Physics Institue of the Czech Academy of Sciences, Řež

Abstract: Study of few-nucleon reactions is a highly contemporary topic in nuclear physics. Nowadays, the few-body Schrödinger equation can be solved with very high accuracy which allows us to compare different models of the nucleon-nucleon potential. In this work, we derive the interaction from the so-called pionless effective field theory ($\not\pi$EFT), the simplest possible nuclear EFT consisting only of contact interactions. The breakdown scale of the theory is set by the pion mass, making it ideal for the study of very low energy nuclear processes. Our interaction is renormalizable and the Coulomb potential is accounted for non-perturbatively in the used power counting scheme. We apply this interaction in a systematic study of up to four-nucleon scattering, making our work the first ever test of $\not\pi$EFT in four-body charged particle-target nuclear reactions. The scattering phase shifts are calculated using a harmonic oscillator trap corrected for the long-range Coulomb interaction - the first time this method has been used in few-body calculations. The bound-state energies needed as input are calculated using the Stochastic Variational Method in a correlated Gaussian basis.

Keywords: pionless effective field theory, few-nucleon scattering, harmonic oscillator trap, Stochastic Variational Method, correlated Gaussian basis

Contents

Introduction **3**

1 Scattering Theory **6**
1.1 Scattering of Two Charged Particles 6
1.1.1 Solutions of the Radial Equation 8
1.1.2 The Regular Solution and Jost Function 12
1.1.3 Effective Range Expansion 13
1.2 Scattering of Two Nuclei in a Harmonic Oscillator Trap 16
1.2.1 Neutral Case - The BERW Formula 16
1.2.2 Coulomb Corrections to the BERW Formula 20
1.2.2.1 Derivation 20
1.2.2.2 Numerical Solution 24

2 Correlated Gaussians Approach to Few-Body Systems **33**
2.1 The Few-Body Problem 33
2.1.1 Jacobi Coordinates 34
2.1.2 Antisymmetrization 35
2.2 Correlated Gaussian Basis 36
2.3 Stochastic Variational Method 37

3 Pionless Effective Field Theory **41**
3.1 Effective Field Theories 42
3.2 Pionless Theory 44
3.2.1 The Return of the Effective Range Expansion 47
3.2.2 Coulomb Effects 51
3.3 Pionless EFT Interaction 54
3.3.1 Two-Body, Three-Body and Four-Body Potential . . . 54
3.3.2 Regularization, Renormalization and Power Counting . 57
3.3.2.1 Three- and Four-Body Forces 60
3.3.3 Fitting the Low Energy Constants 62
3.3.3.1 Leading Order 63

3.3.3.2 Next-to-leading Order 64

4 Few-Nucleon Scattering Results **70**
4.1 Three Nucleons 71
4.1.1 Binding Energy of ^{3}He 71
4.1.2 Proton Scattering off the Deuteron 72
4.2 Four Nucleons 77
4.2.1 Binding Energy of ^{4}He 77
4.2.2 Scattering of Two Deuterons 78
4.2.3 Proton Scattering off ^{3}He 79

Conclusion **85**

Bibliography **87**

List of Figures **97**

A Numerical Methods For Two-Body Scattering **101**
A.1 Numerov 101
A.2 R-Matrix 102

B Calculation of Matrix Elements in the Correlated Gaussian Basis **104**

C Low-Energy Constants **108**

Introduction

Over the last few decades, nuclear structure calculations have made considerable progress and a large range of so-called '*ab initio*' methods has been developed [1]. The attribute '*ab initio*,' meaning from first principles, reflects the fact that these methods are microscopic and they make no assumptions about the nuclear dynamics. Their success can be by part attributed to the increase in available computational power over the years, which has made it possible to reach even medium-mass nuclei. However, perhaps the key ingredient has been the development of realistic nuclear interactions derived from effective field theories [2]. Using these potentials, the properties of light nuclei can be predicted highly accurately [3].

Since these potentials are usually fitted to reproduce two-body scattering data and binding energies of light nuclei, further insight into the inter-nucleon force can be gained by studying nuclear reactions. Unlike structure calculations, reactions probe the behaviour of the interaction not only in bound systems but also in free space. However, the exact *ab initio* treatment of continuum is a much more challenging problem compared to bound states. Rigorous calculations that take into account the degrees of freedom of each nucleon and include many-particle breakup channels are usually limited to less than five nucleons. The usual approaches try to formulate the problem in such a way that bound-state techniques may be applied [4, 5, 6, 7].

Nevertheless, discrepancies between the predictions of state-of-the-art potentials and experimental data have been observed already in the few-body sector. For example, the tensor analyzing powers A_y in proton-deuteron [8, 9] and proton-^{3}He [10] scattering are underpredicted. Furthermore, recent electron scattering experiments on the alpha particle have revealed large deviations of the theoretical predictions in comparison with the measurement [11].

Studies of few-body nuclear reactions are also motivated by nuclear astrophysics. According to current cosmological models, the lightest elements were being synthesized only a few seconds to minutes after the Big Bang. The so-called Bing Bang Nucleosynthesis (BBN) theory predicts that about

a quarter of the mass of the universe comes from Helium [12]. The accuracy of the BBN predictions depends on the baryon-to-photon ratio, or the baryon density in early universe. In order to determine this ratio precisely, cross-sections of reactions such as

$$
\begin{aligned}
d + p &\longrightarrow {}^3\mathrm{He} + \gamma\,, \\
d + d &\longrightarrow {}^3\mathrm{He} + n\,, \\
d + d &\longrightarrow p + t
\end{aligned}
$$

have to be known with very small uncertainties [13]. Furthermore, fusion reactions of light nuclei such as ^{3}H(d,n)^{4}He and ^{3}He(d,p)^{4}He play not only an important role in BBN but also fusion power generation on earth.

Because the temperature in the early universe was no higher than 1 MeV, the cross sections need to be determined for very low scattering energies. This makes experimental measurements difficult because, in beam-target experiments at these energies, the target nuclei are screened by the electrons present in atomic shells [13, 12]. This is, however, not the case in the early-universe plasma. Furthermore, the strong low-energy Coulomb repulsion makes measuring low-energy fusion reactions very difficult due to extremely low counting rates [12]. The importance of theoretical calculations, where the bare nucleus-nucleus cross sections are accessible, is then obvious.

In this work, we study s-wave few-nucleon scattering (pd, p^3He and dd) in the framework of the so-called pionless effective field theory ($\not\pi$EFT) [2], which is the simplest possible nuclear EFT consisting only of contact interactions. The pion degrees of freedom are integrated out, and following the EFT paradigm, the lagrangian density is expanded only in nucleonic fields and their derivatives. Consequently, the breakdown scale of the theory is set by the pion mass, which makes it ideal for the study of very low-energy nuclear processes such as the astrophysical reactions mentioned above.

We derive a potential which, thanks to the adapted renormalization and power-counting schemes, offers predictions independend of any artificial momentum regulators. The regulators generally need to be introduced to supress divergences stemming from the fact that the high-momentum physics is not described by the effective theory. Furthermore, consistent with the fact that we are ultimately interested in descriptions of very low-energy nuclear reactions, we treat the Coulomb interaction non-perturbatively as a genuine low-energy scale and it is accounted for in the power-counting scheme. This makes our work unique, as there are currently no studies that solve the few-body Schrödinger equation with $\not\pi$EFT interactions at next-to-leading order [2, 14], while being fully consistent with the perturbative power-counting of the theory including isospin-symmetry breaking Coulomb terms.

To solve the few-nucleon scattering problem, we use the harmonic-oscillator trap method generalized to include the long-range Coulomb interaction. In this *ab initio* approach, the two interacting nuclei are trapped in a harmonic oscillator potential, which discretizes the continuum and creates an infinite tower of bound states. A quantization condition that relates these bound-state energies to free-space scattering phase shifts can be derived [15]. Recently, this method has been applied to two-body scattering in Ref. [16], but the authors were able to apply it in only limited energy intervals. These issues were solved in Ref. [17], which was co-authored by the author of this thesis.

To study phase shifts with the harmonic oscillator method, one only needs to calculate the bound-state energies. We handle this by using the stochastic variational method (SVM) with an explicitly correlated Gaussian (CG) basis [18]. This method was proven to be one of the most accurate and efficient approaches to few-body systems [19] and is particularly fit for applications to ≠EFT, where the interaction is represented by coordinate-space Gaussians, which allows for an analytic evaluation of matrix elements in the CG basis.

This thesis is devided into four chapters and it is structured as follows: In the first chapter, we introduce some important concepts from non-relativistic scattering theory of charged particles. Then, the quantization condition in the harmonic oscillator trap is derived for both the neutral and charged particles and the method is discussed. In the second chapter, we introduce the SVM and the CG basis. In the third chapter, we introduce the concept of effective field theories in nuclear physics. Here, we pay special attention to the ≠EFT as a low-energy effective theory made for systems with large scattering lengths. In the second part of the chapter, the ≠EFT interaction and its power-counting, together with the fitting of the low-energy constants are discussed. In the fourth chapter, our results for the pd, p^3He and dd scattering are presented. Lastly, a conclusion follows in which the presented work and its most important results are summarized.

Some technical details of calculating two-body scattering phase shifts and matrix elements in the correlated Gaussian basis can be found in Appendices A and B, respectively. The low-energy constants of the nuclear potential derived and fitted in this work are presented in Appendix C.

Chapter 1

Scattering Theory

In this chapter, we summarize some basics of scattering theory in non-relativistic quantum mechanics and thereby introduce definitions and concepts that we will refer to throughout the thesis. This chapter is by no means fully comprehensive - for that we refer the reader to the monograph by Taylor [20] or to the book by Newton [21], both of which were used as a reference. We begin by studying the case of two charged particles, the neutral case can be then obtained by sending their charge to zero. The relations and equations presented here are used in Chapter 3 to fit two-body nucleon-nucleon interactions. From this point of view, the Sections 1.1.2 and 1.1.3 are especially important.

We then describe a novel approach to calculation of elastic scattering phase-shifts - the harmonic oscillator trap. This method is technically simple but powerful and can be used to calculate collisions of nuclei microscopically (*'ab initio'*), i.e., the dynamics of each nucleon are treated explicitly. In Chapter 4, this method is applied in a study of charged few-nucleon scattering within the framework of $\not\pi$EFT.

Throughout this work, we use the natural unit system $\hbar = c = 1$. Unless explicitly stated otherwise, masses, energies and momenta are given in units of MeV.

1.1 Scattering of Two Charged Particles

Scattering of two charged particles interacting through a central interaction is described by the radial Schrödinger equation

$$-\frac{d^2}{dr^2}u_l(r) = 2\mu\left[E - \frac{1}{2\mu}\frac{l(l+1)}{r^2} - V_c(r) - V(r)\right]u_l(r), \qquad (1.1)$$

where r is the relative coordinate between the particles and $u_l(r)$ is the (partial) radial wave function with the boundary condition

$$u(r) \xrightarrow[r\to 0]{} 0 \tag{1.2}$$

at the origin. Note that this condition does not fix the normalization of the scattering wave function, this will be done later by studying its asymptotic behaviour. The radial equation is obtained from the standard time-independent Schrödinger equation

$$\left[-\frac{1}{2\mu}\boldsymbol{\Delta} + V_c(r) + V(r)\right]\psi_l(\boldsymbol{r}) = E\psi_l(\boldsymbol{r}) \tag{1.3}$$

by seperating the wave function $\psi_l(\boldsymbol{r})$ into a radial and angular part

$$\psi_l(\boldsymbol{r}) = \frac{u_l(r)}{r}Y_{lm}(\theta,\phi), \tag{1.4}$$

where Y_{lm} are the well-known spherical harmonics defined as the eigenfunctions of the orbital angular momentum operator $\boldsymbol{L}$ squared

$$\boldsymbol{L}^2 Y_{lm}(\theta,\phi) = l(l+1)Y_{lm}(\theta,\phi). \tag{1.5}$$

In Eq. (1.1), E stands for the energy related to the relative particle momentum k as

$$E = \frac{k^2}{2\mu} \tag{1.6}$$

and μ is the reduced mass of the two-particle system defined as

$$\mu = \frac{m_1 m_2}{m_1 + m_2}, \tag{1.7}$$

where m_1 and m_2 are the particle masses. The Coulomb potential $V_c(r)$ between two particles with charges Z_1 and Z_2 is defined as

$$V_c(r) = \frac{Z_1 Z_2 e^2}{r}, \tag{1.8}$$

where $e^2 = 4\pi\alpha\epsilon_0\hbar c \approx 1.44$ MeV·fm. We will refer to the potential $V(r)$ as the short-range interaction and its form will be discussed in great detail in the third chapter. For now, it is sufficient to remark that $V(r)$ is sufficiently 'well-behaved', meaning its not too singular at origin, $\lim_{r\to 0} r^2 V(r) = 0$, and it falls off faster than all powers of $1/r$ at infinity. In practice, this means that there exists such an r_0 that $V(r) \approx 0$ for $r > r_0$. As is apparent from the

notation $V(r) = V(|\boldsymbol{r}|)$, this potential is assumed to be central. In nuclear physics, the short range interaction is such that r_0 is of the order of a few femtometers. Unlike $V(r)$, the Coulomb potential $V_c(r)$ is not well-behaved from the point of view of scattering theory. The reason is that it falls off too slowly and strongly influnces the particales even as they are far apart - the asymptotic conditions usually assumed do not hold (see the first thirteen chapters of [21]). Nevertheless, the solutions of the differential equation (1.1) with Coulomb interaction only can still be given in closed form for every l and k.

1.1.1 Solutions of the Radial Equation

The general solution of the pure Coulomb problem, $V(r) = 0$ in Eq. (1.1), is given in terms of two special functions, the regular Coulomb function F_l and the irregular Coulomb function G_l [22]. Both of these solve the equation (1.1), but they differ by their behaviour at the origin and by their asymptotic behaviour at infinity. The function F_l vanishes at the origin

$$F_l(\eta, kr) \xrightarrow[kr\to 0]{} C_l(\eta)(kr)^{l+1}, \tag{1.9}$$

where the coefficient $C_l(\eta)$ is given by

$$C_l(\eta) = \frac{2^l|\Gamma(l+1+i\eta)|}{e^{\pi\eta/2}(2l+1)!} \tag{1.10}$$

and η is the dimensionless Sommerfeld parameter

$$\eta = \frac{Z_1 Z_2 e^2 \mu}{k}. \tag{1.11}$$

The asymptotic behaviour of F_l is

$$F_l(\eta, kr) \xrightarrow[kr\to\infty]{} \sin(kr - \frac{1}{2}l\pi - \eta \ln 2kr + \sigma_l). \tag{1.12}$$

The irregular function G_l diverges as the argument approaches zero

$$G_l(kr) \xrightarrow[kr\to 0]{} \frac{(kr)^{-l}}{(2l+1)C_l(\eta)} \tag{1.13}$$

and has the asymptotic behaviour

$$G_l(\eta, kr) \xrightarrow[kr\to\infty]{} \cos(kr - \frac{1}{2}l\pi - \eta \ln 2kr + \sigma_l), \tag{1.14}$$

where the σ_l is the so-called Coulomb phase shift

$$\sigma_l = \arg\Gamma(l+1+i\eta). \tag{1.15}$$

The function G_l goes to r^{-l} as $r \to 0$ and plays no role in the Coulomb-only scattering problem. Setting $\eta = 0$, we obtain the free-wave solutions of the radial Schrödinger equation with $V_c(r) = 0$ and $V(r) = 0$

$$F_l(0, kr) = r j_l(kr), \tag{1.16}$$
$$G_l(0, kr) = r n_l(kr) = -r y_l(kr), \tag{1.17}$$

where $j_l(kr)$ and $y_l(kr)$ are the spherical Bessel functions[1] of the first and second kind.

If both the short-range interaction $V(r)$ and the Coulomb potential $V_c(r)$ are non-zero, the asymptotic behaviour of the radial scattering wave function $u_l(r)$ is given by

$$u_l(r) \xrightarrow[r\to\infty]{} constant \times \left[F_l(\eta, kr) + \tan\delta_l\, G_l(\eta, kr)\right], \tag{1.18}$$

where we have introduced the important quantity δ_l, called phase shift, which measures the effect of the additional short-range interaction added to the Coulomb potential. Although we have omitted any kind of energy E or momentum k index in δ_l and $u_l(r)$, please do note that both of them are energy (momentum) dependent. Again, in the neutral case the Coulomb functions would be replaced by $r j_l(kr)$ and $r n_l(kr)$. The meaning of the additional phase shift δ_l becomes clearer when we insert Eq. (1.12) and Eq. (1.14) into Eq. (1.18), then

$$u_l(r) \xrightarrow[r\to\infty]{} constant \times \sin(kr - \frac{1}{2}l\pi - \eta \ln 2kr + \sigma_l + \delta_l), \tag{1.19}$$

where we could define the total phase shift as

$$\delta_l^c = \sigma_l + \delta_l. \tag{1.20}$$

Notice the presence of the $\ln(r)$ term - by substituing back into the radial equation we see that it cancels the Coulomb interaction. It also means that the definition of phase shift is problematic, since the asymptotic solution continues to pick up phase as r increases. This behaviour is caused by the fact that the conditions for well-bahaved potentials do not hold for $V_c(r)$, as was discussed at the end of the previous section. Indeed, if we switch off

[1]Properties of every special function can be found in the NIST Digital Library of Mathematical Functions, `https://dlmf.nist.gov/`, cited as of Sep. 30th 2024.

the electromagnetic interaction by setting $\eta = 0$ then the shift compared to the asymptotic solution of the free radial equation $rj_l(kr) \to \sin(kr - \frac{1}{2}l\pi)$ would be just δ_l. One way to deal with the issue of defining phase shift for the Coulomb potential is to consider a screened Coulomb potential, which is almost always the case in experimental setups. One can then define Coulomb amplitudes and cross-sections consistently (see Chapter 14 in [20])[2]. However, our quantity of interest is the additional phase shift δ_l and there are no such problems with its defintion, since it is defined with respect to the asymptotics F_l and G_l.

Equation (1.18) represents a convenient form for numerical calculation of the phase shift δ_l. Let us asssume that we know the values of the solution $u_l(r)$ at some two points r_1 and r_2 such that $r_1, r_2 \gg r_0$ and $r_1 \neq r_2$. Then by calculating the ratio $u_l(r_1)/u_l(r_2)$ and doing some elementary algebraic manipulations we obtain

$$\tan\delta_l = \frac{r_2 u_l(r_1) F_l(\eta, kr_2) - r_1 u_l(r_2) F_l(\eta, kr_1)}{r_1 u_l(r_2) G_l(\eta, kr_1) - r_2 u_l(r_1) G_l(\eta, kr_2)}. \tag{1.21}$$

Alternatively, the phase shift may be computed by matching the solution $u_l(r)$ to the asymptotic form (1.18) at some $r = R$, which is chosen to be large enough so that the phase shift does not depend on it. The matching follows from the continuity of the logarithmic derivative of the wave function at $r = R$, we have

$$\frac{u_l'(R)}{u_l(R)} = \frac{F_l'(\eta, kR) + G_l'(\eta, kR)\tan(\delta_l)}{F_l(\eta, kR) + G_l(\eta, kR)\tan(\delta_l)} \tag{1.22}$$

and after some manipulations we get

$$\tan\delta_l = \frac{W[u_l(r), F_l(\eta, kr)]_R}{W[G_l(\eta, kr), u_l(r)]_R}, \tag{1.23}$$

where $W[f, g]_{x_0} = f(x_0)g'(x_0) - f'(x_0)g(x_0)$ is the Wronskian determinant.

The solution $u_l(r)$ can be obtained by integrating out the Schrödinger equation (1.1) from $r = 0$ to some $r = r_{max}$ with the boundary condition (1.2) by means of, e.g., the Numerov algorithm (see Chapter 2 in [23] and Appendix A). This method is exact and easily generalized to multi-channel problems, it is, however, costly because we are dealing with a numerical integration on a dense grid.

[2]This place marks the start of a neverending struggle with the unsavoury properties of the Coulomb interaction that permeates the entire thesis.

The asymptotic form of the partial scattering solution $u_l(r)$ may be recast in another convenient form. Let us define an ingoing wave as

$$I_l(\eta, kr) = G_l(\eta, kr) - iF_l(\eta, kr) \tag{1.24}$$

and an outgoing wave as

$$O_l(\eta, kr) = G_l(\eta, kr) + iF_l(\eta, kr). \tag{1.25}$$

It is obvious that they differ only by complex conjugation. The asymptotic condition (1.18) can then be rewritten as

$$u_l(r) \xrightarrow[r\to\infty]{} constant \times \left[I_l(\eta, kr) - S_l O_l(\eta, kr)\right], \tag{1.26}$$

where the *constant* here is generally different from the one in Eq. (1.18) and Eq. (1.19) and its value is related to the normalization of the wave function. As an example, if we want the partial scattering solutions $u_l(r)$ to be normalized to $\delta(k - k')$, then

$$constant = \frac{i}{\sqrt{2\pi}} \exp(-i\delta_l). \tag{1.27}$$

The equation (1.26) defines an important quantity - the S-matrix element S_l. Since in this work we are dealing only with a single ingoing and outgoing channel defined by the same l, the S-'matrix' element is just a number

$$S_l = \exp(2i\delta_l). \tag{1.28}$$

Note that in literature the S-matrix element in Coulomb scattering is usually defined as $S_l = \exp[2i(\sigma_l + \delta_l)]$ and (1.28) is sometimes called the collision matrix element U_l [24].

Now we will construct the full stationary solution. For an outgoing wave we have

$$\psi^+(\boldsymbol{r}) = (2\pi)^{-1}(2kr)^{-1} \sum_{l=0}^{\infty} (2l+1) i^l e^{i\sigma_l + i\delta_l} P_l(\cos\theta) u_l(r), \tag{1.29}$$

where $P_l(\cos\theta)$ is the Legendre polynomial and we have chosen the *constant* according to (1.27). The factor i^l is purely conventional. The scattering solution (1.29) behaves asympotically as a sum of an outgoing Coulomb wave and a spherical wave

$$\psi^+(\boldsymbol{r}) \xrightarrow[r\to\infty]{} \psi_c^+(\boldsymbol{r}) + f_{add}(\theta, \phi)(2\pi)^{-3/2} \frac{e^{i(kr - \eta \ln 2kr)}}{r}. \tag{1.30}$$

The Coulomb wave propaging in a direction given by the dot product of $\boldsymbol{k}$ and $\boldsymbol{r}$ has the form (see Chapter 14 in [21])

$$\psi_c^+ = (2\pi)^{-3/2} e^{-\pi\eta/2} \Gamma(1+i\eta) e^{i\boldsymbol{k}\cdot\boldsymbol{r}} {}_1F_1(-i\eta, 1, i(kr - \boldsymbol{k}\cdot\boldsymbol{r})), \tag{1.31}$$

where ${}_1F_1$ is the confluent hypergeometric function of the first kind, in literature also known as the Kummer's function of the first kind and denoted by M. The quantity f_{add} is the additional scattering amplitude caused by the short-range interaction with respect to the Coulomb potential. Expressed in partial waves it reads

$$f_{add}(\theta, \phi) = \frac{1}{2ik} \sum_{l=0}^{\infty} (2l+1) e^{2i\sigma_l} (S_l - 1) P_l(\cos\theta). \tag{1.32}$$

The pure Coulomb scattering amplitude f_c is given by (see Chapter 14 in [20, 21])

$$f_c(\theta, \phi) = -\frac{\eta}{2k \sin^2\left(\frac{1}{2}\theta\right)} e^{2i(\sigma_0 - \eta \ln \sin \frac{1}{2}\theta)}. \tag{1.33}$$

Finally, the differential cross-section is then calculated as

$$\frac{d\sigma}{d(\theta, \phi)} = |f_{add}(\theta, \phi) + f_c(\theta, \phi)|^2. \tag{1.34}$$

1.1.2 The Regular Solution and Jost Function

In the previous section, we have discussed the *physical* solution $u_l(r)$ of the radial equation, which is defined by the boundary conditions at the origin (1.2) and at infinity (1.19). Let us now define the *regular* solution $\varphi_l(r)$ of Eq. (1.1), which is completely characterized by its behaviour at the origin. For $l = 0$ the boundary condition reads

$$\varphi_0(0) = 0, \tag{1.35}$$
$$\varphi_0'(0) = 1. \tag{1.36}$$

The reason for the construction of this solution is that the normalization of $\varphi_0(r)$ is fixed by these two conditions. In comparison, the normalization of the solution $u_l(r)$ depends on the exact value of the constant in Eq. (1.18), which is generally not fixed when we solve the radial equation numerically, using e.g. the Numerov method. While this is not a problem when calculating phase shifts using the ralation (1.23) or (1.22) since the normalization coefficients in the numerator and denominator cancel, we may run into problems in cases where the normalization of the wavefunction needs to be consistenst, such as

when calculating expectation values, e.g. in Eq. (3.64). For this reason, we prefer to work with the regular solution in this work.

Due to the presence of the centrifugal term $\sim 1/r^2$, the boundary condition $\varphi_0'(0) = 1$ needs to be modified for higher angular momenta. It depends on the value of l and has the form (see Chapter 12.2 in [21])

$$\lim_{r\to 0} r^{-l-1}\varphi_l(r) = 1. \tag{1.37}$$

The regular solution is related to the physical one through the Jost function $\mathfrak{F}(k)$

$$u_l(r) = \frac{e^{i\pi l/2}k}{\mathfrak{F}_l(k)}\varphi_l(r). \tag{1.38}$$

The Jost function is especially useful for evaluating the S-matrix element, which is given by the ratio of $\mathfrak{F}_l(k)$ and its complex conjugate

$$e^{2i\delta_l^c} = e^{i\pi l}\frac{\mathfrak{F}_l(-k)}{\mathfrak{F}_l(+k)}, \tag{1.39}$$

where δ_l^c is given by Eq. (1.20). Knowing the regular solution, we may then calculate the Jost function using its integral representation [21]

$$\mathfrak{F}_l(k) = \mathfrak{F}_l^{(c)}(k) + 2\mu\int_0^\infty dr F_l^{(c)}V(r)\varphi_l(r), \tag{1.40}$$

where $\mathfrak{F}_l^{(c)}(k)$ is the 'pure Coulomb Jost function' given by

$$\mathfrak{F}_{l,\pm}^{(c)}(k) = \frac{e^{\eta\pi/2\pm i\pi l/2}\Gamma(2l+2)}{(2k)^l\Gamma(l+1\pm i\eta)} \tag{1.41}$$

and the function $F_l^{(c)}$ is defined as

$$F_{l,\pm}^{(c)} = e^{\pi\eta/2}\mathcal{W}_{\mp i\eta,l+1/2}(\mp 2ikr), \tag{1.42}$$

where $\mathcal{W}$ is the irregular Whittaker function [22]. Hence, after we have found the regular solution, the S-matrix is easily evaluated using Eq. (1.40), since the integral needs to be computed only on a small interval due to the quick fall-off of the short-range interaction. For more details about Jost functions, their properpies and applications, we refer the reader to [25].

1.1.3 Effective Range Expansion

The low energy behaviour of phase shifts can be described by only two scattering parameters. This approximation is known as the effective range

expansion and it is invaluable for analysis of experimental scattering data and their comparison to theory. It was first discovered by Schwinger [26] and a simpler proof was then given later by Bethe [27]. A nice proof, which relies on the properties of Coulomb functions and which we shall replicate here, is given in Ref. [28].

To assess the low energy behaviour of phase shifts we search for the Taylor expansion of $\cot\delta_l$, see Eq. (1.23), for $k = 0$. The issue that we run into is that the function G_l diverges for zero momentum, see Eq. (1.13), and as consequence $\cot\delta_l(k)$ has a pole at the origin. We can, however, use the analytic decomposition of the irregular Coulomb function [28]

$$G_l(\eta, kr) = \frac{e^{2\eta\pi}}{\pi}\left[h_l(\eta)F_l(\eta, kr) + \frac{1}{w_l(\eta)}\tilde{I}_l(\eta, kr)\right]. \tag{1.43}$$

Here

$$w_l(\eta) = \frac{(i\eta)^{2l+1}\Gamma(-l+i\eta)}{\Gamma(l+1+i\eta)}. \tag{1.44}$$

and

$$h_l(\eta) = \frac{\psi_D(l+1+i\eta) - \ln(i\eta) + \psi_D(l+1-i\eta) - \ln(-i\eta)}{2}, \tag{1.45}$$

where $\psi_D(z)$ is the digamma function - the logarithmic derivative of the gamma function. Since G_l is a solution of the Coulomb-only Schrödinger equation (1.1), the function $\tilde{I}_l(\eta, kr)$ is also one and we may consider the equation (1.43) to be its definition. It has been constructed so that all divergences are contained in the factors $h_l(\eta)$ and $w_l(\eta)$ and in the zero-momentum limit it behaves the same as F_l, see Eq. (1.9), that is

$$\tilde{I}_l(\eta, kr) \xrightarrow[k\to 0]{} C_l(\eta)k^{l+1}. \tag{1.46}$$

The functions F_l/C_lk^{l+1} and $\tilde{I}_l/C_lk^{l+1}$ are therefore both analytic in the variable k (have a well-defined Taylor series) and behave as constants as momentum goes to zero.

Using the decomposition (1.43), the expression (1.23) can be recast as

$$\cot\delta_l = \frac{e^{2\pi\eta}-1}{\pi}\left[\frac{1}{w_l(\eta)}\frac{W[\tilde{I}_l(\eta, kr), u_l(r)]_R}{W[u_l(r), \tilde{F}_l(\eta, kr)]_R} - h_l(\eta)\right]. \tag{1.47}$$

Thanks to the analytic properties of the functions F_l, $\tilde{I}_l$ in the variable k, all poles in the ratio of the two Wronskians cancel and the expression

$$\frac{W[\tilde{I}_l(\eta, kr), u_l(r)]_R}{W[u_l(r), F_l(\eta, kr)]_R} = w_l(\eta)\left[\frac{\pi\cot\delta_l}{e^{2\eta\pi}-1} + h_l(\eta)\right] \equiv \varkappa_l(\eta) \tag{1.48}$$

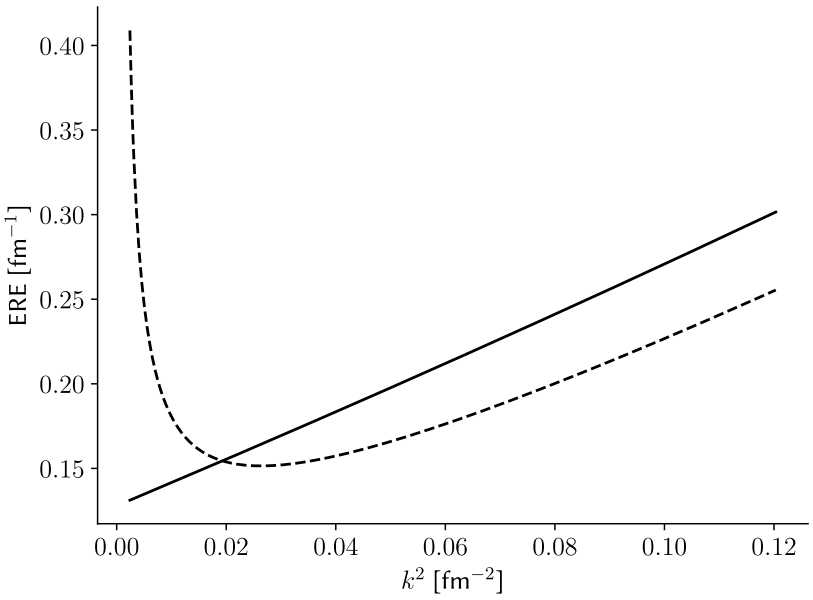

Figure 1.1 The effective range expansion (ERE) of the proton−proton spin singlet s-wave scattering for relative momenta k up to $k^2 = 0.12$ fm^{-2} (energies E_{cm} up to 5 MeV). The solid line depicts the Coulomb-corrected ERE as a function of k^2 and the dashed line is the 'bare' ERE $k \cot \delta$. We observe that the corrected ERE behaves linearly while the 'bare' ERE diverges as $k \to 0$. The phase shifts were calculated using the two-body R-matrix method with the effective Minnesota interaction [29].

is analytic in k. We can therefore expand it in powers of k and by setting $l = 0$ and multiplying $\varkappa_0(\eta)$ by $2\eta k$ we obtain the Coulomb-corrected s-wave effective range expansion (ERE) as originally given by Bethe in Ref. [27]

$$\varkappa_0(\eta) \equiv C_0^2(\eta) k \cot \delta_0 + 2k\eta h_0(\eta) = -\frac{1}{a} + \frac{1}{2} r k^2 + \mathcal{O}(k^4), \tag{1.49}$$

where $C_0^2 = \frac{2\eta\pi}{e^{2\eta\pi}-1}$. Setting $\eta = 0$ in the above equations, it is clear that for scattering of neutral particles the wave functions are analytic in k and the ERE is given by

$$\varkappa_l(0) \equiv k^{2l+1} \cot \delta_l = -\frac{1}{a} + \frac{1}{2} r k^2 + \mathcal{O}(k^4). \tag{1.50}$$

The constants a and r in (1.50) and (1.49) are known as the *scattering length* and *effective range*, respectively. These names come from their properties for $l = 0$, in which case the scattering length has dimension of length and the effective range can be related to the range of the interaction (see also the discussion in Chapter 11.2 of Ref. [21]). The expansion essentially tells us

that the function $\varkappa_l(\eta)$ behaves linearly in k^2 for small momenta and based on the knowledge of the two parameters a and r we can extrapolate the values of phase shifts for quite a large range of energies (see Figure 1.1).

From the ERE we can also asses the contribution of the different partial waves to the scattering amplitude and, by extension, the cross section. The partial-wave amplitude due to the additional short-range interaction, see Eq. (1.32), is given by

$$f_l(k) = e^{2i\sigma_l}\frac{S_l(k)-1}{2ik} = \frac{e^{2i\sigma_l}}{k\cot\delta_l - ik} \tag{1.51}$$

and so we have

$$e^{-2i\sigma_l} f_l \xrightarrow[k\to 0]{} -a_l k^{2l}. \tag{1.52}$$

It is then obvious that for small energies the s-wave dominates and higher partial waves are negligible.

1.2 Scattering of Two Nuclei in a Harmonic Oscillator Trap

This subsection presents a convenient method for calculating elastic scattering phase shifts, which is then used to obtain the main results of this work. The two interacting nuclei are trapped in an harmonic oscillator (HO) potential, which discretizes the scattering energies and leads to an infinite spectrum of bound states. A quantization condition, which relates the phase shifts to the discretized energies, can then be derived. This approach was coined by Busch, Englert, Rzażewski and Wilkens in a study of two cold atoms [30] and the quantization condition they derived is aptly known as the BERW formula. It was then later generalized for higher angular momenta in [31] and quite recently it was extended to include the long range Coulomb interaction by Guo [15]. Following these references, we will first introduce the main ideas by studying the neutral case and then generalize the method to charged particle scattering.

1.2.1 Neutral Case - The BERW Formula

We solve the Schrödinger equation (1.1) with the potential $V_c(r) = 0$ and $V(r) = V_s(r) + V_{\mathrm{HO}}(r)$, where $V_s(r)$ is an unspecified short-range interaction with range r_0 and $V_{\mathrm{HO}}(r)$ is the harmonic oscillator (HO) potential

$$V_{\mathrm{HO}}(r) = \frac{1}{2}\mu\omega^2 r^2, \tag{1.53}$$

where μ is the reduced two-particle mass, ω the oscillator frequency, or equivalently

$$b = \sqrt{\frac{1}{\mu\omega}} \tag{1.54}$$

the HO trap length. By introducing the HO potential we essentially divide the configuration space into three regions - denoted I, II and III in Figure 1.2. We assume that b is large enough so that in the first region the HO potential can be neglected and the wave function is affected only by the short-range interaction. In the second region, $r > r_0$, it is assumed that $V_s(r)$ is 0 and the HO potential is still weak so the wave function can be approximated by a scattered free wave, see Eq. (1.18),

$$u_l^{\mathrm{II}}(r) = Ckr\left[j_l(kr) - \tan\delta_l n_l(kr)\right]. \tag{1.55}$$

Since r_0 is very small, for some $r > r_0$ we can still use the limiting forms of Bessel functions [22]

$$j_l(kr) \xrightarrow[kr\to 0]{} \frac{(kr)^l}{(2l+1)!!},\ n_l(kr) \xrightarrow[kr\to 0]{} -\frac{(2l-1)!!}{(kr)^{l+1}} \tag{1.56}$$

and we obtain

$$u_l^{\mathrm{II}}(r) \xrightarrow[kr\to kr_0^+]{} \frac{C(kr)^{l+1}}{(2l+1)!!}\left[1 + (2l+1)[(2l-1)!!]^2\frac{\tan\delta_l}{(kr)^{2l+1}}\right]. \tag{1.57}$$

In the last region the HO potential becomes too strong and it cannot be neglected anymore, it starts to supress the scattering wavefunction and introduces the bound-state asymptote corresponding to the HO trap bound-state energy E. The solution is then given by [31]

$$u_l^{\mathrm{III}}(x) = e^{-x^2/2}\Big[C_1 x^{l+1}{}_1F_1\left(\tfrac{3}{4}+\tfrac{1}{2}l - \tfrac{b^2\mu}{4}E, \tfrac{3}{2}+l, x^2\right) + \\ + C_2 x^{-l}{}_1F_1\left(\tfrac{1}{4}-\tfrac{1}{2}l - \tfrac{b^2\mu}{4}E, \tfrac{1}{2}-l, x^2\right)\Big], \tag{1.58}$$

where $x = r/b$. Considering the asymptotic behaviour of the hypergeometric functions [22]

$${}_1F_1(a,b,z) \xrightarrow[z\to\infty]{} \frac{\Gamma(b)}{\Gamma(a)}e^z z^{a-b} \tag{1.59}$$

the coefficients C_1 and C_2 need to satisfy[1]

$$\frac{C_2}{C_1} = (-1)^{l+1}\left(l+\frac{1}{2}\right)\frac{[(2l-1)!!]^2}{2^{2l}}\frac{\Gamma(1/4 - l/2 - b^2\mu E/4)}{\Gamma(3/4 + l/2 - b^2\mu E/4)} \tag{1.60}$$

[1] $2^n\Gamma(n+\frac{1}{2})/\sqrt{\pi} = (2n-1)!!$

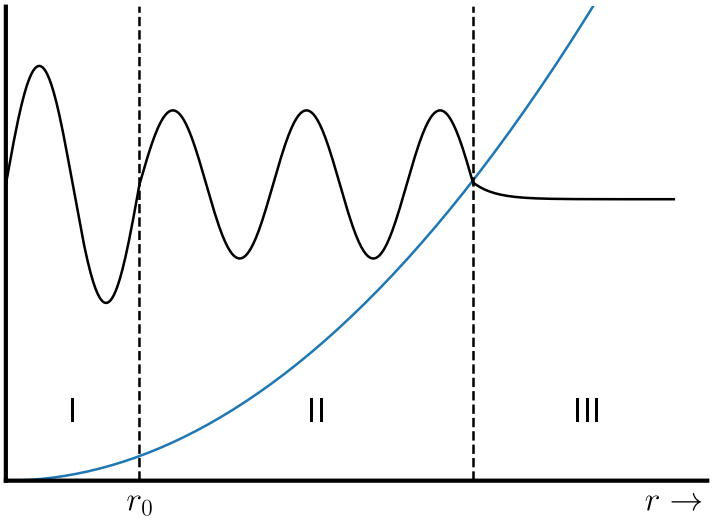

Figure 1.2 Schematic depiction of the relative radial wave function of two interacting particles trapped in a HO trap. The blue line denotes the HO potential. For regions I,II and III, see the text

so that the bound-state wave function vanishes for $x \to \infty$. Now we match the wave functions given $u_l^{\rm II}(r)$ and $u_l^{\rm III}(r)$ at the boundary of the second and third region. Since we can still assume that r is small, we use the limiting form [22]

$$ {}_1F_1(a,b,z) \underset{z\to 0}{\longrightarrow} 1 \tag{1.61}$$

and we obtain

$$ \frac{C_2}{C_1} = (2l+1)[(2l+1)!!]^2 \frac{\tan\delta_l}{(bk)^{2l+1}}. \tag{1.62}$$

From there, by doing additional elementary manipulations we get

$$ k^{2l+1}\cot\delta_l = (-1)^{l+1}\,(4\mu\omega)^{l+1/2}\,\frac{\Gamma(3/4+l/2-E/2\omega)}{\Gamma(1/4-l/2-E/2\omega)}. \tag{1.63}$$

The above formula is known as the Bush or BERW formula and it relates the scattering phase shift at momentum $k=\sqrt{2\mu E}$ to the bound-state energy E of the HO trap spectrum.

A few remarks are in order here. First of all, one might wonder if the assumptions made here are not too strong, that is, if we can ignore the HO potential in the second region. Although in theory the phase shifts are exact only in the limit $b \to \infty$, from our calculations in the subsequent chapters it will be clear that good convergence can already be achieved for trap lengths of the order ~ 10 fm. This issue was also discussed in the Appendix A of [31].

The conclusion the authors arrived to is that unless the scattering length is abnormaly large (e.g. near a resonance, or more generally in case the S-matrix has a pole near threshold) the formula (1.63) holds well. A rather complicated derivation of an improved formula which takes into account that the trap is finite was given in [32]. However, in our work we found these corrections to be negligible.

The power of the HO trap method lies in the fact that it can be very easily generalized for more than two particles. Generally, methods that treat the few- or many-body problem, such as the one introduced in Chapter 2, are based on an expansion of the total wave function into a basis. This allows for calculation of bound states, but the extension of these methods to continuum problems is rather difficult. That is where the HO trap comes in - the only needed input is the bound-state energy. We can generalize the HO potential for $A \geq 2$ particles with the same mass m as

$$V_{\mathrm{HO}}(\boldsymbol{r}) = \frac{m}{2A}\omega^2 \sum_{i<j} (\boldsymbol{r}_i - \boldsymbol{r}_j)^2, \tag{1.64}$$

where $\boldsymbol{r}_i - \boldsymbol{r}_j$ is the relative coordinate vector between the particle i and j. By adding the above term to a many-body Hamiltonian, defined later in Eq. (2.1), and using our preffered method for solving the Schrödinger equation we obtain energies that are then plugged into (1.63). The energy E in the $A = 2$ case was just the relative energy of the two particles. In many-body problems, we are interested in the scattering between two clusters of particles, let us denote them A and B. Then, the reduced mass in (1.63) is

$$\mu = \frac{m_A m_B}{m_A + m_B} \tag{1.65}$$

and the energy E is the energy with respect to the breakup threshold of the two clusters, that is

$$E = E(A+B) - E(A) - E(B), \tag{1.66}$$

where $E(A+B)$ is the bound-state energy of the trapped $A+B$ system and similarly, $E(A)$ and $E(B)$ are the trapped energies of A or B alone. If the system $A+B$ can form bound states even without the trapping potential, energy levels corresponding to these states must be disregarded.

This method can also be generalized to multi-channel problems which was done in [7]. The main drawback of the HO trap is that the energies E need to be calculated very precisely because they enter as arguments into a numerically rather sensitive ratio of two gamma functions. The precise calculation of energies becomes increasingly difficult for larger systems (see the discussion at the end of Chapter 2).

1.2.2 Coulomb Corrections to the BERW Formula

If we take into account the long-range Coulomb interaction then the Figure 1.2 no longer holds since the $\sim 1/r$ potential is felt strongly in each of the three regions. Following Ref. [15], we will now derive a generalized form of the BERW formula.

1.2.2.1 Derivation

It turns out that the quantization condition can be easily derived by considering the Lippman-Schwinger equation for the charged two-particle system in a trap. Let us, however, first consider Coulomb scattering in free space; for brewity we shall switch to bracket notation. The full scattering amplitude is given by

$$f(\boldsymbol{k}) = -(2\pi)^2\mu \langle \boldsymbol{k}_0|V|\boldsymbol{k}^+\rangle = -(2\pi)^2\mu \langle \boldsymbol{k}_0|V_c + V_s|\boldsymbol{k}^+\rangle \,, \tag{1.67}$$

where $|\boldsymbol{k}_0\rangle$ are plane waves, eigenvectors of $H_0 = H - V$, in x-representation given by

$$\langle \boldsymbol{x}|\boldsymbol{k}_0\rangle = (2\pi)^{-3/2} e^{i\boldsymbol{k_0}\cdot\boldsymbol{x}} \tag{1.68}$$

and $|\boldsymbol{k}^+\rangle$ are stationary scattering states, eigenvectors of H, in x-representaion given by Eq. (1.30). Instead of amplitudes it is simpler to work with a closely related quantity, the T-matrix defined as

$$T(\boldsymbol{k}) = -\langle \boldsymbol{k}_0|V|\boldsymbol{k}^+\rangle \,, \tag{1.69}$$

which is the same as the amplitude $f(\boldsymbol{k})$ up to the constant factor $(2\pi)^2\mu$.

The scattering states are connected to plane waves by the Lippman-Schwinger equation (see e.g. Chapter 10 in [20])

$$|\boldsymbol{k}^\pm\rangle = |\boldsymbol{k}^0\rangle + G_0(E \pm i0)(V_c + V_s)\,|\boldsymbol{k}^\pm\rangle \,, \tag{1.70}$$

where $G_0(z)$ is the resolvent or Green's operator[1] for H_0, given by

$$G_0(z) = \frac{1}{z - H_0}. \tag{1.71}$$

We may also write a similar Lippman-Schwinger equation for the pure Coulomb interaction

$$|\boldsymbol{k}_c^+\rangle = |\boldsymbol{k}^0\rangle + G_0(E + i0)V_c\,|\boldsymbol{k}_c^+\rangle \,, \tag{1.72}$$

[1]We use the same notation for operators and their representations in a basis. The nature of the symbols should be apparent from context.

where $|\boldsymbol{k}_c^{\pm}\rangle$ is the Coulomb wave. Using the conjugate of this equation

$$\langle \boldsymbol{k}_c^{-}| = \langle \boldsymbol{k}^0| + \langle \boldsymbol{k}_c^{-}|\, V_c G_0(E+i0) \tag{1.73}$$

together with (1.70), the expression for T may be recast as follows

$$\begin{aligned} T(\boldsymbol{k}) = &- \langle \boldsymbol{k}_c^{-}|V_c + V_s|\boldsymbol{k}^{+}\rangle - \langle \boldsymbol{k}_0|V_c|\boldsymbol{k}^{+} - \boldsymbol{k}_0\rangle = \\ &= - \langle \boldsymbol{k}_c^{-}|V_c|\boldsymbol{k}_0\rangle - \langle \boldsymbol{k}_c^{-}|V_s|\boldsymbol{k}^{+}\rangle = T_c(\boldsymbol{k}) + T_{sc}(\boldsymbol{k}) \end{aligned} \tag{1.74}$$

The term $T_c(k)$ on the right-hand side of the above equation is the contribution to the T-matrix due to Coulomb interaction only and the term $T_{sc}(k)$ describes the additional effect of the short-range force. Since the second term is what we are interested in, it is useful to define an operator whose matrix elements between the known Coulomb waves $|\boldsymbol{k}_c^{\pm}\rangle$ are elements of the matrix T_{sc}. To achieve this goal, we write the Lippman-Schwinger equation for V_s in the form

$$|\boldsymbol{k}^{+}\rangle = |\boldsymbol{k}_c^{+}\rangle + G_c(E+i0)V_s\,|\boldsymbol{k}^{+}\rangle\,, \tag{1.75}$$

where $G_c(z)$ can be symbolically written as

$$G_c(z) = \frac{1}{z - H_0 - V_c}. \tag{1.76}$$

Now, combining (1.75) and (1.74) we obtain

$$T_{sc}(\boldsymbol{k}) = - \langle \boldsymbol{k}_c^{-}|V_s|\boldsymbol{k}^{+}\rangle = - \langle \boldsymbol{k}_c^{-}|V_s|\boldsymbol{k}_c^{+}\rangle - \langle \boldsymbol{k}_c^{-}|\, V_s G_c(E+i0)V_s\,|\boldsymbol{k}^{+}\rangle \tag{1.77}$$

and it is obvious that the sought-after operator must satisfy the equation

$$T_{sc} = -V_s + V_s G_c(E+i0)T_{sc} \tag{1.78}$$

because then the following holds

$$T_{sc}(\boldsymbol{k}) = - \langle \boldsymbol{k}_c^{-}|V_s|\boldsymbol{k}^{+}\rangle = \langle \boldsymbol{k}_c^{-}|T_{sc}|\boldsymbol{k}_c^{+}\rangle \tag{1.79}$$

and

$$T_{sc}\,|\boldsymbol{k}_c^{+}\rangle = -V_s\,|\boldsymbol{k}^{+}\rangle\,. \tag{1.80}$$

In this way we have basically 'solved' the scattering problem; the essential knowledge is the form of the Coulomb Green's operator, which can then be iterated in the Lippman-Schwinger equation for T_{sc} (1.78) to obtain the T-matrix.

If the system is trapped, the Lippman-Schwinger equation needs to be modified to include the trapping potential, we have

$$|\boldsymbol{k}_\omega^{+}\rangle = |\boldsymbol{k}_c^{+}\rangle + G_{c\omega}(E+i0)V_s\,|\boldsymbol{k}_\omega^{+}\rangle\,, \tag{1.81}$$

where now $|\boldsymbol{k}_\omega^+\rangle$ is the stationary scattering wave distorted also by the HO potential and the operator $G_{c\omega}(z)$ is the Green's operator for $H = H_0+V_c+V_{\mathrm{HO}}$ and can be symbolically expressed as

$$G_{c\omega}(z) = \frac{1}{z - H_0 - V_c - V_{\mathrm{HO}}}. \tag{1.82}$$

For the T-operator we obtain, in the same way as for free-space scattering,

$$T_{sc\omega} = -V_s + V_s G_{c\omega}(E + i0) T_{sc\omega}. \tag{1.83}$$

Generally, the T-operator has the same analytical properties as the Green's operator - it is analytic everywhere but in the eigenenergies of the Hamiltonian, where it has poles. From Eq. (1.83) we obtain

$$T_{sc\omega} = -\left[V_s^{-1} - G_{c\omega}(E + i0)\right]^{-1}. \tag{1.84}$$

Since where T has poles T^{-1} has zeros, we may write the following condition for bound states

$$V_s^{-1} - G_{c\omega}(E + i0) = 0. \tag{1.85}$$

Going one step further, we can get rid of the V_s by substituing from Eq. (1.78). Formally, we may write

$$-V_s^{-1} = T_{sc} - G_c(E + i0) \tag{1.86}$$

and by plugging this equation into (1.85) we obtain a quantizion condition independent of the short-range interaction, given by the equation

$$\boxed{T_{sc} + G_{c\omega}(E + i0) - G_c(E + i0) = 0.} \tag{1.87}$$

This is exactly what we were looking for from the beginning - an equation that relates the bound-state energies E to the scattering phase-shifts, or here equivalently, the amplitudes T_{sc}. The Busch formula (1.63) obtained earlier is just a special case of this general condition.

Nevertheless, the alphabet soup cooked up in this section is not very useful as is; next we need to find the coordinate representation of the quantization condition and, most importantly, we need to find the form of the Green's function G_{cw} (the form of G_c is known in closed form, see e.g. [33]). Using the trivial operator identity

$$A^{-1} = B^{-1} + B^{-1}(B - A)A^{-1} \tag{1.88}$$

with $A \equiv G_{c\omega}^{-1} = z - H_0 - V_c - V_{\rm HO}$ and $B \equiv G_{\omega}^{-1} = z - H_0 - V_{\rm HO}$ we get

$$G_{c\omega} = G_\omega + G_\omega V_c G_{c\omega}. \tag{1.89}$$

The above equation relates the unknown Green's function in a trap with Coulomb interaction to the HO Green's function, whose form is known analytically [34]. In coordinate representation it is a Fredholm integral equation of the second kind.

To derive the coordinate representation of the quantization condition we may use any form of the short-range interaction, as we have argued in the previous section, the quantization condition does not depend on it. Following refs. [7, 15, 35] we choose a seperable zero-range potential

$$V_s(\boldsymbol{r}, \boldsymbol{r'}) = \frac{\delta(r)\delta(r')}{(rr')^2} \sum_{lm} \frac{V_l^s}{(rr')^l} Y_{lm}(\hat{\boldsymbol{r}}) Y_{lm}^*(\hat{\boldsymbol{r}}). \tag{1.90}$$

Using this assumption, Eq. (1.85) expressed in partial waves becomes

$$\det \left[\delta_{lm,l'm'} \frac{1}{V_l^s} - \lim_{r,r'\to 0} \frac{G^{c\omega}_{lm,l'm'}(r,r',E)}{r^l r'^{l'}} \right] = 0, \tag{1.91}$$

where in case of the HO the m and m' labels are superfluos due to the rotational symmetry. The partial wave T-matrix may be parametrized in terms of the phase shifts just like the amplitude in Eq. (1.51). Up to some constant factors which are a matter of convention we may write

$$T_l^{sc}(k) \propto \frac{e^{2i\sigma_l}}{k \cot \delta_l - ik}. \tag{1.92}$$

Now, using the fact that the partial waves of the wave function $\langle \boldsymbol{r} | \boldsymbol{k}_c^+ \rangle$ are [21, 35]

$$\psi_l^c(r) = 4\pi C_l(\eta)(ikr)^l e^{ikr} {}_1F_1(l+1+i\eta, 2l+2, -2ikr) \tag{1.93}$$

and their asymptotic form at the origin is given by Eq. (1.61), we find for the partial-wave decomposition of (1.86) the following expression

$$\frac{1}{V_l^s} = -2\mu k^{2l+1} C_l^2(\eta) \cot \delta_l + \mathrm{Re} \left[\lim_{r,r'\to 0} \frac{G_l^c(r,r',E)}{(rr')^l} \right]. \tag{1.94}$$

Finally, by substituing this relation into (1.91) we obtain the quantization condition (1.87) in partial waves

$$\boxed{2\mu k^{2l+1} C_l^2(\eta) \cot \delta_l = \mathrm{Re} \left[\lim_{r,r'\to 0} \frac{G_l^c(r,r',E)}{(rr')^l} \right] - \lim_{r,r'\to 0} \frac{G_l^{c\omega}(r,r',E)}{(rr')^l}.} \tag{1.95}$$

As we already remarked, the Coulomb Green's function is known and is given by [33, 35]

$$G_l^c(r,r',E) = 2\mu(2ik)^{2l+1}\frac{\Gamma(l+1+i\eta)}{(2l+1)!}(r_< r_>)^l e^{ik(r_< r_>)}\times$$
$$\times\, {}_1F_1(l+1+i\eta, 2l+2, -2ikr)U(l+1+i\eta, 2l+2, -2ikr), \tag{1.96}$$

where U is the confluent hypergeometric function of the second kind and $r_<$ ($r_>$) means the lesser (greater) of the two values r and r'. The Green's function in the HO trap, $G_l^{c\omega}$, is not known analytically but it can be can found by numerically solving (1.89), that is

$$G_l^{c\omega}(r,r',E) = G_l^{\omega}(r,r',E) + \int_0^\infty dr''\, r''^2 G_l^{\omega}(r,r',E)V_c(r'')G_l^{c\omega}(r'',r',E), \tag{1.97}$$

where

$$G_l^{\omega}(r,r',E) = -\frac{1}{\omega(rr')^{3/2}}\frac{\Gamma(\frac{l}{2}+\frac{3}{4}-\frac{E}{2\omega})}{\Gamma(l+\frac{3}{2})}\times$$
$$\times\, \mathcal{M}_{\frac{E}{2\omega},\frac{l}{2}+\frac{1}{4}}(\mu\omega r_<^2)\mathcal{W}_{\frac{E}{2\omega},\frac{l}{2}+\frac{1}{4}}(\mu\omega r_>^2), \tag{1.98}$$

is the HO Green's function [34] and $\mathcal{M}$, $\mathcal{W}$ are Whittaker function of the first and second kind.

1.2.2.2 Numerical Solution

It turns out that the application of the formula (1.95) is not as simple as it may seen on first glance owning to the fact that both G_l^{ω} and $G_l^{c\omega}$ are UV divergent[1]. This can be easily seen by considering the limiting forms of $\mathcal{M}$ and $\mathcal{W}$ [22] as the argument goes to zero

$$\mathcal{M}_{a,b}(r) \xrightarrow[r\to 0]{} r^{b+\frac{1}{2}}, \tag{1.99}$$

$$\mathcal{W}_{a,b}(r) \xrightarrow[r\to 0]{} \frac{\Gamma(2b)}{\Gamma(\frac{1}{2}+b-a)}r^{\frac{1}{2}-b} + \frac{\Gamma(-2b)}{\Gamma(\frac{1}{2}-b-a)}r^{\frac{1}{2}+b}. \tag{1.100}$$

It can be shown that the UV divergences cancel each other exactly. To achieve this, it is adventageous to express the Coulomb Green's function using a similar Fredholm equation as $G_l^{c\omega}$

$$G_l^c(r,r',E) = G_l^0(r,r',E) + \int_0^\infty dr''\, r''^2 G_l^0(r,r',E)V_c(r'')G_l^c(r'',r',E), \tag{1.101}$$

[1] An ultraviolet (UV) divergence is generally a divergence caused by phenomena at infinitesimaly small distances ($k \to \infty$). Here, it means that the expression diverges for $r \to 0$.

where G_l^0 is the free-particle Green's function [20, 21]

$$G_l^0 = -2i\mu k j_l(kr_<)h_l^+(kr_>) \tag{1.102}$$

and $h_l^+ = j_l + iy_l$ is the spherical Hankel function of the first kind.

The usual method to solve Fredholm equations of the second type, such as Eq. (1.97) and (1.101), is the so-called Liouville-Neumann series [36]. Let us have an integral equation in the form

$$\phi(x) = f(x) + \lambda \int_a^b K(x,t)\phi(t)dt, \tag{1.103}$$

then the solution is given by the series

$$\phi(x) = \lim_{n\to\infty} \sum_{i=0}^{n} \lambda^i u_i(x), \tag{1.104}$$

where

$$u_n(x) = \int_a^b \int_a^b ... \int_a^b K(x,t_1)K(t_1,t_2)...K(t_{n-1},t_n)f(t_n)dt_n...dt_1. \tag{1.105}$$

The n-th iteration $u_n(x)$ is obtained by first starting with $\phi(x) = u_0(x) = f(x)$, plugging it back into the original equation and then repeating this process n times. In the case of Eq. (1.101) we have $\phi = G_l^c$, $f = G_l^0$, $\lambda = 1$, $K(r,r') = Z_1 Z_2 e^2 r' G_l^0(r,r')$ and similarly for the harmonic oscillator case, Eq. (1.97).

Let us first consider the 'zeroth iteration' of the Fredholm equations (1.97) and (1.101), that is

$$G_l^c \approx G_l^0,\ G_l^{c\omega} \approx G_l^{\omega}. \tag{1.106}$$

Considering the limiting forms of Bessel functions (1.56) we get[2]

$$\lim_{r,r'\to 0} G_l^0(r,r',E) = -i2\mu k \frac{\pi(kr)^{2l}}{2^{2l+2}\Gamma^2(l+\frac{3}{2})} - \frac{\Gamma(l+\frac{1}{2})}{\Gamma(l+\frac{3}{2})}\frac{\mu}{r} \tag{1.107}$$

and using (1.99) we obtain

$$\begin{aligned}\lim_{r,r'\to 0} G_l^{\omega}(r,r',E) = &-\frac{\Gamma(l+\frac{1}{2})}{\Gamma(l+\frac{3}{2})}\frac{\mu}{r} + \\ &- \frac{1}{\omega}\frac{\Gamma(-l-\frac{1}{2})}{\Gamma(l+\frac{3}{2})}\frac{\Gamma(\frac{3}{4}+\frac{l}{2}-\frac{E}{2\omega})}{\Gamma(\frac{1}{4}-\frac{l}{2}-\frac{E}{2\omega})}(\mu\omega)^{l+\frac{3}{2}}r^{2l}\end{aligned} \tag{1.108}$$

[2] $(2l-1)!! = 2^l\Gamma(n+\frac{1}{2}) = (-2)^n\sqrt{\pi}/\Gamma(\frac{1}{2}-n)$

and hence the difference of the Green's functions is finite and well-defined because the divergent terms proportional to $1/r$ cancel. Actually, using the quantization condition we get

$$k^{2l+1}\cot\delta_l = \frac{C_l^2(0)}{C_l^2(\eta)}(-1)^{l+1}\,(4\mu\omega)^{l+\frac{1}{2}}\,\frac{\Gamma(\frac{3}{4}+\frac{l}{2}-\frac{E}{2\omega})}{\Gamma(\frac{1}{4}-\frac{l}{2}-\frac{E}{2\omega})}, \tag{1.109}$$

which is obviously just the Bush formula (1.63) barring the factor $C_l^2(0)/C_l^2(\eta)$ which is equal to 1 when $\eta = 0$.

After the first iteration, the Fredholm equations (1.97) and (1.101) have the form

$$G_l^{c\omega}(r,r',E) = G_l^{\omega}(r,r',E) + \int_0^\infty dr''\, r''^2 G_l^{\omega}(r,r',E)V_c(r'')G_l^{\omega}(r'',r',E). \tag{1.110}$$

and

$$G_l^{c}(r,r',E) = G_l^{0}(r,r',E) + \int_0^\infty dr''\, r''^2 G_l^{0}(r,r',E)V_c(r'')G_l(r'',r',E). \tag{1.111}$$

We will denote the integrals on the right-hand side $\Delta G_l^{c\omega}$ and ΔG_l^{c}, respectively. After switching the order of integration and limits (this step is justified because the spherical Bessel and Whittaker functions of the first kind do not diverge at the origin) and using the limiting forms for j_l and $\mathcal{M}$ we have

$$\begin{aligned}&\lim_{r,r'\to 0}\Delta G_l^{c\omega} = \\ &= \int_0^\infty dr''r''^2 V_c(r'')\left[\frac{1}{\omega(rr'')^{\frac{3}{2}}}\frac{\Gamma(\frac{l}{2}+\frac{3}{4}-\frac{E}{2\omega})}{\Gamma(l+\frac{3}{2})}(\mu\omega r^2)^{\frac{l}{2}+\frac{3}{4}}\mathcal{W}_{\frac{E}{2\omega},\frac{l}{2}+\frac{1}{4}}(\mu\omega r''^2)\right]^2\end{aligned} \tag{1.112}$$

and

$$\lim_{r,r'\to 0}\Delta G_l^{c} = \int_0^\infty dr''r''^2 V_c(r'')\left[2i\mu k\left(\frac{\sqrt{\pi}(kr)^l}{2^{l+1}\Gamma(l+\frac{3}{2})}\right)h_l^{(+)}(kr'')\right]^2. \tag{1.113}$$

To isolate the divergent part we split the integration into two intervals, from 0 to ε, where ε is an arbirarily small positive constant, and from ε to infinity, where the integral is well defined. Near the origin we can use limiting forms for all functions and we get, after some trivial manipulations

$$\lim_{r,r'\to 0}(rr')^{-l}\Delta G_l^{c} = -4\mu^2k^2e^2\int_0^\epsilon dr''r''\frac{\Gamma^2(l+\frac{1}{2})}{4\Gamma^2(l+\frac{3}{2})}\frac{1}{k^2(r'')^{2l+2}} + \text{Fin.}, \tag{1.114}$$

where the Fin. denotes a finite contribution of the integral, $\int_\varepsilon^\infty$. Similarly, for the other propagator we have

$$\lim_{r,r'\to 0}(rr')^{-l}\Delta G_l^{c\omega} = e^2\int_0^\epsilon dr''r''\frac{1}{\omega^2(r'')^3}(\mu\omega)^{l+\frac{3}{2}}\frac{\Gamma^2(l+\frac{1}{2})}{\Gamma^2(l+\frac{3}{2})}(\mu\omega r''^2)^{\frac{1}{2}-l} + \text{Fin.} \tag{1.115}$$

and these contributions are obviously equal. In further iterations we would just multiply the expressions by the same functions so we can conclude that the UV divergences cancel and the quantization condition (1.95) is finite and well defined. Furthemore, because we always send r, r' to zero and thus $r, r' < \varepsilon$, it suffices to numerically integrate from ε to infinity, because the contribution near origin is $\mathcal{O}(\varepsilon)$.

The Liouville-Neumann approach is equivalent to the perturbative expansion suggested in [35], in which case the Green's function in a trap is given by

$$G_{c\omega} = \frac{G_\omega}{1 - V_c G_\omega} = \sum_{n=0}^{\infty} G_\omega (V_c G_\omega)^n, \tag{1.116}$$

where we have just rewritten equation (1.89) and expanded it into a harmonic series. A similar expansion is used in case of G_c to guarantee the subtraction of UV divergences.

The problem is that the perturbative expansion (Neumann series) is not guaranteed to converge and because of that the applicability of the method suggested to obtain phase shifts from the quantization condition in Ref. [15] and used in Ref. [16] is limited. The Green's function G_l^ω has poles in the energies equal to the spectrum of the harmonic oscillator, that is

$$\frac{E}{\omega} = \frac{3}{2} + l + 2n, \tag{1.117}$$

where $n = 0, 1, 2...$ labels the excited states, and as a consequence the quantization condition diverges for these energies. However, it turns out that the Neumann series diverges in a larger interval around these eigen-energies. The reason for this is that the perturbative expansion converges only if all eigenvalues of the Green's operator are in a unit circle in the complex plane, which is not the case when E is equal to bound-state energy or not sufficiently larger; see the Chapter 1.7 of [37] or Chapter 9 of [21] for a more detailed discussion on the convergence aspects of a perturbative series.

These issues are illustrated in Figures 1.3 and 1.4. In the former Figure, s-wave pp phase shifts for the Minnesota potentail [29] calculated by iterating the Fredholm equations are compared to the exact solution of the Schrödinger equation obtained using the Numerov method. Each energy corresponds to a given trap length b - by varying b the dependence of phase shifts on energy

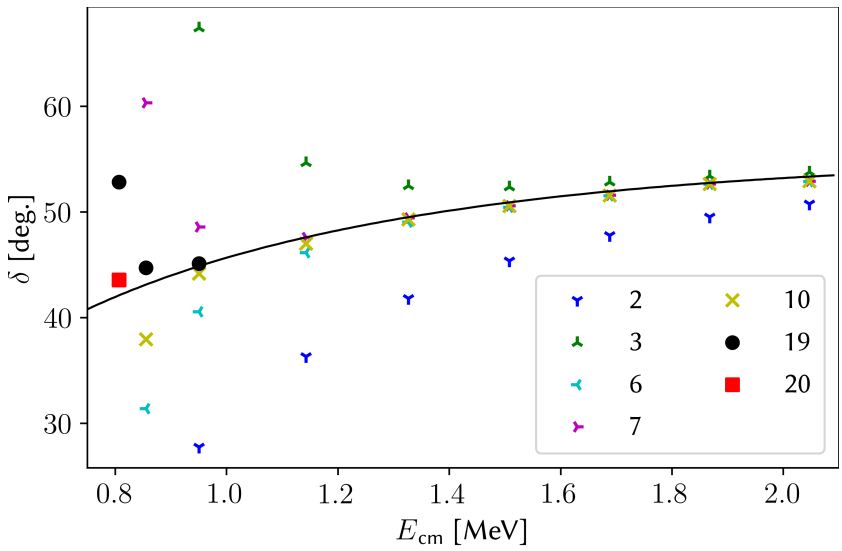

Figure 1.3 Comparison of s-wave pp phase shifts obtained by solving the Schrödinger equation with the Minnesota potential [29] using the Numerov method (solid black line) and the quantization condition in the HO trap, where the Green's functions are obtained by iterating the Fredholm equations (different symbols correspond to a certain number of iteration; see the legend). The HO frequency was varied between $\omega \in [0.7, 2]$ MeV corresponding to b between approximately 6.4 fm and 11 fm.

is obtained. We consider only the ground state of the HO trap spectrum, but higher excited states of a HO with given b can naturally be considered. While for energies around $E_{\mathrm{cm}} = 2$ MeV only 3 iterations are needed to obtain converged values of the phase shift, for energies sligthly over 0.8 MeV not even 20 iterations suffice and converged phase shitfs for energies lower than 0.8 MeV could not be obtained even after hundreds of iterations. Since the Coulomb interaction is added perturbatively in the expansion (1.116), we would expect to need more and more terms as we are nearing zero energy, but it does not explain the rapidly slowing convergence around 0.8 MeV.

The reason for this behaviour is illustrated in the Figure 1.4. Here, we did not use a concrete potential to obtain the bound state energies of the pp system in a trap. Instead, for a fixed HO length $b = 20$ fm an arbitrary range of energies is considered and phase shifts are calculated using the quantization condition. These phase shifts are thus unphysical, since a physical calculation with a given potential corresponds to only one energy; in other words, these phase shifts represent all possible shifts corresponding to the HO trap $b = 20$ fm obtainable using all possible interactions. The red bands in the Figure represent energy ranges, where the Neumann series for the Green's functions diverges and the dashed lines correspond to the first

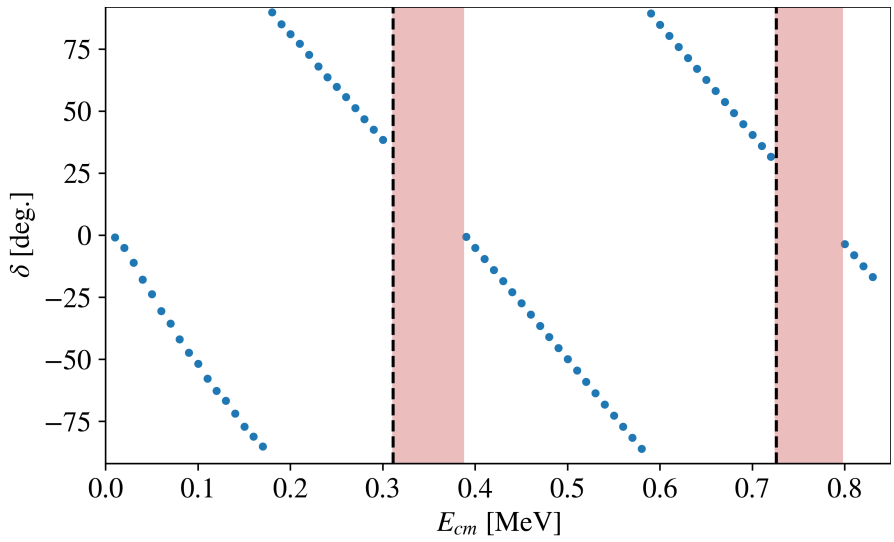

Figure 1.4 Scattering phase shifts from the quantization condition for arbitrary energies. The blue points represent s-wave pp phase shifts obtained by iterating the Fredholm equations for the Green's functions G^c and $G^{c\omega}$. The HO trap length was set to $b = 20$ fm and using the quantization condition the phase shifts were calculated for energies ranging from $E_{\text{cm}} = 0.01$ MeV to $E_{\text{cm}} = 0.85$ MeV. The red bands represent energy regions where the perturbative series diverges. Eigenenergies of the HO are depicted by the vertical dashed lines.

$(n = 0)$ and second $(n = 1)$ eigenenergy of the HO. We observe that as we cross the eigenenergies the perturbative series diverges until we are far enough from the pole of G_l^ω and then converged phase shifts can be obtained again, as we argued in the previous paragraph. Although it may not seem like a huge issue from this figure because the divergent energy regions are quite small, we have to remember that in physical calculations b (or ω) is not constant and each b has its own slightly different divergent energy interval. This means that we have to be careful when choosing b, because it needs to be large enough so that the effects of the HO potential on the scattering phase shifts are negligible but also must not correspond to an energy too close to a pole of G_l^ω. This makes the method difficult to apply for low-energy scattering since in that case b needs to be generally higher, because the system has a large wavelength $\sim 1/k$. This issue is not so troubling for higher energies because it is generally easier to find trap lengths which are not problematic, as is illustrated in Figure 1.5. Here, pp phase shifts obtained using the Numerov algorithm and the HO method are compared for higher energies, $E_{\text{cm}} > 2.5$ MeV. In this case, only 7 iterations were needed to obtained converged results.

To get around this problem we can (at least numerically) solve for the

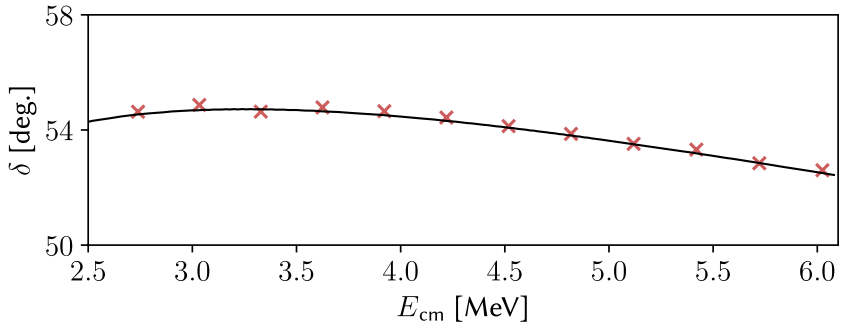

Figure 1.5 Comparison of s-wave pp phase shifts obtained by solving the Schrödinger equation with the Minnesota potential [29] using the Numerov method (solid black line) and phase shifts obtained from the quantization condition in the HO trap (red crosses), where the Green's functions are obtained by iterating the Fredholm equations just seven times. The HO frequency was varied between $\omega \in [0.7, 2]$ MeV, but this time the second eigenenergy of the HO trap spectrum was chosen.

Green's functions G_l^c and $G_l^{c\omega}$ directly. They are calculated on a numerical grid for r and r' by fixing r_{min} as the starting point and $r_{\mathrm{max}} = fb$ as the endpoint, where f is a numerical factor and b is the length of the HO trap. The value of the parameter r_{min} is key - it needs to be small enough so the Green's functions are accurate but large enough that we avoid their UV divergences. We divide the interval $(r_{\mathrm{min}}, r_{\mathrm{max}})$ in N grid points with progressively rising steps, such that

$$r_n = r_{n-1} + hq^n$$

where q is the incremental ratio and h is the step, fixed such that $r_N = r_{\mathrm{max}}$. If $q = 1$, the N points are equidistant. The limit in Eq. (1.95) is approximated as

$$\frac{\mathrm{Re}\left[G_l^c(r_{\mathrm{min}}, r_{\mathrm{min}}, E) - G_l^{c\omega}(r_{\mathrm{min}}, r_{\mathrm{min}}, E)\right]}{(r_{\mathrm{min}})^{2l}}. \tag{1.118}$$

On the grid $\{r_n\}$ the Green's functions are simply represented as the matrices

$$\mathrm{G}_{ij}^0 = G^0(r_i, r_j) \tag{1.119}$$

and the Fredholm equations become simple matrix equations

$$\begin{aligned} \mathrm{G}_l^c &= \mathrm{G}_l^0 + \mathrm{G}_l^0 \mathrm{DK} \mathrm{G}_l^c, \\ \mathrm{G}_l^{c\omega} &= \mathrm{G}_l^\omega + \mathrm{G}_l^\omega \mathrm{DK} \mathrm{G}_l^{c\omega}, \end{aligned} \tag{1.120}$$

where $\mathrm{K}_{ij} = \delta_{ij} r_i^2 V_c(r_i)$ and D is the diagonal matrix of integration weights (distances between the grid points). Given the matrix form of the Dyson

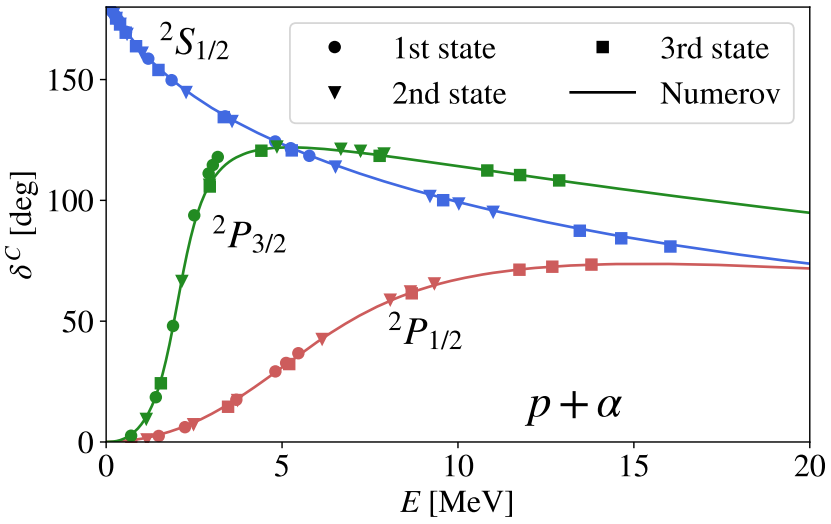

Figure 1.6 A comparison of $p\alpha$ phase shifts in the $^2S_{1/2}$, $^2P_{3/2}$ and $^2P_{1/2}$ partial waves obtained by the solution of the two-body Schrödinger equation with the potential of Eq. (1.122) using the Numerov method and the generalized Busch formula with Green's functions found by matrix inversion. This figure is taken from the author's work [17], where $E = E_{\text{cm}}$ and δ^c are the phase shifts denoted as δ in the rest of the thesis.

equations (1.120), the Green's functions are obtained through matrix inversion

$$\begin{aligned} \mathrm{G}_l^c &= \left(1 - \mathrm{G}_l^0 \mathrm{DK}\right)^{-1} \mathrm{G}_l^0, \\ \mathrm{G}_l^{c\omega} &= \left(1 - \mathrm{G}_l^\omega \mathrm{DK}\right)^{-1} \mathrm{G}_l^\omega. \end{aligned} \tag{1.121}$$

We test the above numerical procedure by applying it to a case of two-body p^4He scattering, where the α is treated as a point-like particle. Since the Coulomb force is two-times stronger than in the pp case, this example allows us to assess if our method can truly handle low-energy Coulomb repulsion. The two-body potential is taken as a simple square well in the form

$$V(r) = (1 + \beta \boldsymbol{L} \cdot \boldsymbol{\sigma}) U(r), \tag{1.122}$$

where $\boldsymbol{L}$ is the angular momentum operator, $\boldsymbol{\sigma} = \frac{2}{\hbar}\boldsymbol{S}$ the Pauli spin operator and $U(r)$ is given by

$$U(r) = U_0, \quad r < a \tag{1.123}$$

and is otherwise zero. This simple phenomenological potential is known to reproduce the experimental $p\alpha$ $s-$wave and $p-$wave phase shifts [38] using the parametrization

$$U_0 = -70.9\,\text{MeV}, \quad a = 2.5\,\text{fm}, \quad \beta = 0.15. \tag{1.124}$$

The phase shifts calculated using (1.121) and (1.95) are compared to the exact solution of the Schrödinger equation obtained using the Numerov method in Figure 1.6. We observe excellent agreement between the two methods for the s-wave as well as the two possible p-wave partial waves. Using the matrix invertion even phase-shifts for energies in the range of tenths of MeVs are calculated accurately and the computional cost is the same for all energies. However, it needs to mentioned that going to higher partial waves than $l = 1$ presents numerical challenges, since the numerators and denominators in (1.95) become very small. In the numerical implemention, one is then forced to either increase the precision of floats or increase $r_{\min}$, which may have an impact on the accuracy of the calculated phase shifts. A detailed discussion about the numerical considerations of our method can be found in Ref. [17].

Chapter 2

Correlated Gaussians Approach to Few-Body Systems

In this chapter, we briefly describe the method which we use to solve the quantum-mechanical few-body problem. Despite its conceptual simplicity, Stochastic Variational Method (SVM) with correlated Gaussian (CG) basis is one of the most powerful few-body methods and it is widely used in sub-nuclear, nuclear, chemical and condensed matter physics [18, 39]. It is especially fit for our purpose - solving the few-body Schrödinger equation with potentials derived from pionless effective field theory. As described in Chapter 3, these interactions are, in our work, given by coordinate-space Gaussians which makes the calculation of the potential matrix elements in the CG basis simple, since they can be calculated analytically. Furthemore, expansion of the wave function in CGs combined with the SVM, in which the basis-state parameters are chosen randomly using a trial-and-error procedure, converges quickly and gives numerically accurate results [19] even with the 'almost-singular' field theory potentials with very small ranges.

2.1 The Few-Body Problem

The non-relativistic N-body quantum-mechanical system is characterized by the Hamiltonian

$$H = \sum_{i=1}^{N} \frac{p_i^2}{2m_i} - T_{cm} + \sum_{i<j} V_{ij} + \sum_{i<j<k} V_{ijk} + \sum_{i<j<k<l} V_{ijkl} + ..., \qquad (2.1)$$

where m_i is the mass of the $i-th$ particle and V_{ij}, V_{ijk} and V_{ijkl} are two-body, three-body and four-body interactions, the ellipsis contains forces between more than four bodies. The center-of-mass kinectic energy $T_{\rm cm}$ needs to be

subtracted to ensure that the Hamiltonian is translationally invariant and that we describe only the intrinsic dynamics of the system. If the number of particles N is not too large, this subtraction can be done conveniently by introducing the relative (Jacobi) coordinates, as described in this section.

Our goal is to solve the Schrödinger equation $H\Psi = E\Psi$ with the Hamiltonian given by Eq. (2.1), i.e., to find the total wave function of the system Ψ and the corresponding eigenenergy E. We achieve this by expanding Ψ into a linear combination of CGs with parameters chosen by the SVM; the details about the basis-state functions are given in Section 2.2 and the variational procedure is described in Section 2.3.

2.1.1 Jacobi Coordinates

In this thesis, we will denote the single-particle coordinates $\boldsymbol{r}^T = (\boldsymbol{r}_1, \boldsymbol{r}_2, ..., \boldsymbol{r}_N)$, where each of the $\boldsymbol{r}_i$ is a vector between a fixed position in space, such as the center of mass of the system, and the praticle i. Additionally, we define the relative (Jacobi) coordinates $\boldsymbol{x}^T = (\boldsymbol{x}_1, \boldsymbol{x}_2, ..., \boldsymbol{x}_N)$, where x_N is the center-of-mass coordinate and the rest $(\boldsymbol{x}_1, \boldsymbol{x}_2, ..., \boldsymbol{x}_{N-1})$ are independent relative coordinates. These two sets are related by the transformation

$$\boldsymbol{x}_i = \sum_{j=1}^{N} U_{ij} \boldsymbol{r}_j, \tag{2.2}$$

where U is a matrix

$$U = \begin{pmatrix} 1 & -1 & 0 & \dots & 0 \\ \frac{m_1}{m_{12}} & \frac{m_2}{m_{12}} & -1 & \dots & 0 \\ \vdots & \vdots & & \ddots & \vdots \\ \frac{m_1}{m_{12\dots N-1}} & \frac{m_2}{m_{12\dots N-1}} & \dots & \dots & -1 \\ \frac{m_1}{m_{12\dots N}} & \frac{m_2}{m_{12\dots N}} & \dots & \dots & \frac{m_N}{m_{12\dots N}} \end{pmatrix}, \tag{2.3}$$

with $m_{12\dots i} = m_1 + m_2 + \cdots + m_i$. This matrix is not orthogonal and the transformation is therefore not unitary.

To calculate matrix elements of the intrinsic kinetic energy, i.e., the total kinetic energy with the center-of-mass kinetic energy subtracted, it is necessary to transform the single-particle momentum operator $\boldsymbol{p}_i = -i\hbar\frac{\partial}{\partial \boldsymbol{r}_j}$. Defining the momentum conjugate to $\boldsymbol{x}_j$ as

$$\boldsymbol{\pi}_j = -i\hbar\frac{\partial}{\partial \boldsymbol{x}_j} \tag{2.4}$$

we get the transformation relation

$$\boldsymbol{\pi}_i = \sum_{j=1}^{N} U_{ij}^{-1} \boldsymbol{p}_j. \tag{2.5}$$

The center-of-mass momentum of the system is $\boldsymbol{\pi}_N = \sum_i^N \boldsymbol{p}_j$ and the center-of-mass kinetic energy is then given by

$$T_{cm} = \frac{\pi_N^2}{2m_{12\ldots N}}. \tag{2.6}$$

This yields the following expression for the intrinsic kinetic energy

$$\sum_{i=1}^{N} \frac{\boldsymbol{p_i^2}}{2m_i} - T_{cm} = \sum_{i,j=1}^{N} \left(\frac{1}{2m_i}\delta_{ij} - \frac{1}{2m_{12\ldots N}} \right) \boldsymbol{p}_i \cdot \boldsymbol{p}_j = \frac{1}{2} \sum_{i,j=1}^{N-1} \Lambda_{ij} \boldsymbol{\pi}_i \cdot \boldsymbol{\pi}_j, \tag{2.7}$$

where we used Eq. (2.5) and defined the matrix Λ as

$$\Lambda_{ij} = \sum_{k=1}^{N} U_{ik} U_{jk}; \quad i,j \in \{1,2,\ldots,N-1\}. \tag{2.8}$$

Local potentials depend only on the relative distance $\boldsymbol{r}_i - \boldsymbol{r}_j$ between two particles i and j, which in the Jacobi coordinates can be conveniently expressed as

$$\boldsymbol{r}_i - \boldsymbol{r}_j = \sum_{k=1}^{N} (U_{ik}^{-1} - U_{jk}^{-1}) \boldsymbol{x}_k \equiv \boldsymbol{w}_{ij}^T \boldsymbol{x}, \tag{2.9}$$

where $\boldsymbol{w}_{ij}$ is a $1 \times N$ 'column' vector. This relation is very useful for evaluating potential matrix elements in CG basis, as will be seen later.

2.1.2 Antisymmetrization

The wave function composed of N fermions needs to be properly antisymmetrized. This is achieved by introducing the antisymmetrizer

$$\mathcal{A} = \frac{1}{\sqrt{N!}} \sum_{i=1}^{N!} \pi_i \mathcal{P}_i, \tag{2.10}$$

where $\mathcal{P}_i$ is an operator that permutes the particle indices and π_i is the sign (or parity) of this permutation. The sum runs over all possible permutations. If we cosider a permutation given by

$$P = \begin{pmatrix} 1 & 2 & 3 & \ldots & N \\ p_1 & p_2 & p_3 & \ldots & p_N \end{pmatrix} \tag{2.11}$$

then the operator $\mathcal{P}$ acts on the vector of single-particle coordinates as follows

$$\mathcal{P}\boldsymbol{r} = T_P \boldsymbol{r}, \tag{2.12}$$

where the matrix T_P is defined as

$$(T_P)_{ij} = \delta_{jp_i}. \tag{2.13}$$

For example, in a three-particle fermionic system, one of the possible permutations is $P = \left(\begin{smallmatrix} 1 & 2 & 3 \\ 2 & 1 & 3 \end{smallmatrix}\right)$ and the corresponding matrix T_P is

$$T_P = \begin{pmatrix} 0 & 1 & 0 \\ 1 & 0 & 0 \\ 0 & 0 & 1 \end{pmatrix}. \tag{2.14}$$

The remaining five matrixes are defined in a similar fashion.

To find how the permutation operator acts on the Jacobi coordinates we use the relations (2.2) and (2.13)

$$\mathcal{P}\boldsymbol{x}_i = \sum_{k=1}^{N} U_{ik} \mathcal{P}\boldsymbol{r}_k = \sum_{k,l=1}^{N} U_{ik}\delta_{lp_k}\boldsymbol{r}_l = \sum_{k,l=1}^{N} U_{ik}U_{lj}\delta_{lp_k}\boldsymbol{x}_j. \tag{2.15}$$

Then, the matrix elements $(\widetilde{T}_P)_{ij}$ of operator $\mathcal{P}$ in Jacobi coordinates, corresponding to the permutation of single-particle coordinates P, are

$$(\widetilde{T}_P)_{ij} = \sum_{k=1}^{N-1} U_{ik} U^{-1}_{p_k j}. \tag{2.16}$$

Here, we do not include the center-of-mass coordinate in the sum since it remains unaffected by the permutation. The transformation of T_P to Jacobi coordinates can be conveniently expressed in matrix form

$$\widetilde{T}_P = U T_P U^{-1}. \tag{2.17}$$

2.2 Correlated Gaussian Basis

In this work, the correlated Gaussians have the form

$$F_A(\boldsymbol{x}) = \exp\left(-\frac{1}{2}\boldsymbol{x}^T A \boldsymbol{x}\right). \tag{2.18}$$

They are spherically symmetric and are thus only fit to describe systems with zero total angular momenta, $L = 0$. In this thesis, we are interested in the

description of s-wave sytems, but generalizations to non-zero L can be done by multiplying $F_A(\boldsymbol{x})$ by solid spherical harmonics within the so-called Global Vector Representation, which describes the orbital motion [18].

The $(N-1)\times(N-1)$ matrix A describes the correlations between the particles. It is positive-definite, symmetric and therefore contains $N(N+1)/2$ nonlinear parameters.

One of the nice properties of CGs is their behaviour under linear transformations. For example, the permutation operator $\mathcal{P}$ acts on F_A as

$$\mathcal{P}F_A(\boldsymbol{x}) = \exp\left(-\frac{1}{2}\boldsymbol{x}^T\widetilde{T}_P^T A\widetilde{T}_P\boldsymbol{x}\right), \tag{2.19}$$

where we have used the relation $\mathcal{P}\boldsymbol{x} = \widetilde{T}_P\boldsymbol{x}$. This means that to antisymmetrize the wave function one only needs to change the parameters A and the evaluation of matrix elements is thus quite simple, as we show in the Appendix B.

2.3 Stochastic Variational Method

In Ritz variational methods one solves the Schrödinger equation approximately by expanding the wave function of the system into a sum of suitable basis functions. We consider the total wave function of the form

$$\Psi = \sum_{i=1}^{K} c_i\psi_i = \sum_{i=1}^{K} c_i\mathcal{A}\{F_{A_i}(\boldsymbol{x})\chi^i_{SM_S}\xi^i_{TM_T}\}, \tag{2.20}$$

where χ_{SM_S} (ξ_{TM_T}) is the spin (isospin) part of Ψ with the total spin S (isospin T) and spin projection M_S (isospin projection M_T). They are constructed by successive coupling of the single-particle spin or isospin functions, i.e. for χ_{SM_S} we have

$$\chi_{SM_S} = \left[[[[\chi_{\frac{1}{2}}\chi_{\frac{1}{2}}]_{S_{12}}]\chi_{\frac{1}{2}}]_{S_{123}}\dots\right]_{SM_S}, \tag{2.21}$$

where $S_{12\dots}$ is the intermmediate spin coupling. The ξ_{TM_T} is constructed similarly.

The linear parameters c_i in Eq. (2.20) are determined by the generalized Ritz variational principle, which states that the Hamiltonian H is stationary with respect to an arbitrary change of c_i in the neighbourhood of its discrete eigenvalues. This condition leads [18] to the generalized eigenvalue problem

$$\sum_{j=1}^{K}\left(\mathcal{H}_{ij} - E\mathcal{B}_{ij}\right)c_j = 0, \tag{2.22}$$

where the matrices $\mathcal{H}$ and $\mathcal{B}$ are defined as

$$\mathcal{H}_{ij} = \langle \psi_i | H | \psi_j \rangle \,, \tag{2.23}$$

$$\mathcal{B}_{ij} = \langle \psi_i | \psi_j \rangle \,. \tag{2.24}$$

After we solve the eigenvalue problem (2.22) we obtain K eigenenergies E_k, which give the upper bounds for the ground-state and excited bound-state energies of the Hamiltonian, as per the Hylleraas-Undheim theorem.

The question is how to optimize the non-linear paramaters contained in matrices $\{A_i\}$ of the correlated Gaussians (2.18) so the eigenenergies are predicted as accurately as possible while keeping the dimension of the basis small enough for the problem to be computationally tractable. Due to the non-orthogonality of the CGs, each of the parameters is equally important and there exist several different choices that approximate the wave function equally well. This fact makes systematic optimization cumbersome, but opens the door to random selection.

The crux of the SVM is the trial and error search procedure which selects the most relevant basis states. It works as follows: let us assume that we have already chosen the first $A_1, \ldots, A_{i-1}$ matrices and solved the $(i-1)$-dimensional eigenvalue problem. Then, to select the optimal matrix A_i, we:

1. Randomly generate n different matrices $A_i^1, \ldots, A_i^n$, where the matrix elements a_{ij} of A are selected from physically relevent intervals ($1/\sqrt{a_{ij}}$ corresponds to 'distance' between the particles)

2. Determine $E_i^1, \ldots, E_i^n$ by solving the generalized eigenvalue problem

3. Select the matrix A_i^m which corresponds to the lowest energy E_i^m from among the set $\{E_i\}$ to be the i-th basis state.

4. Increase i to $i+1$

This process is repeated until the ground-state energy converges. Thanks to the Hylleraas-Undheim theorem, the same process may be used to optimize the energy E_k of the k-th excited bound state. However, while it may be that the basis which gives a converged ground state also gives a good prediction for the excited state (with the same conserved quantum numbers), it is generally not the case and optimization with respect to E_k is usually required. Atleast k basis states are required at the start to obtain the k-th eigenvalue; it is a good idea to first converge the energies $E_1, ..., E_{k-1}$ and then enlarge the basis to optimize E_k.

The advantage of this procedure is that the entire Hamiltonian matrix does not need to be recomputed and diagnolized for each and every trial basis state corresponding to A_i^m, only the last row and column need to be changed. In the $i+1$-th step the eigenvalue problem has the form

$$\begin{pmatrix} E_1 & 0 & \dots & 0 & h_1 \\ 0 & E_2 & \dots & 0 & h_2 \\ \vdots & \vdots & \ddots & \vdots & \vdots \\ 0 & 0 & \dots & E_i & h_i \\ h_1^* & h_2^* & \dots & h_i^* & h_{i+1}^* \end{pmatrix} \begin{pmatrix} c_1 \\ c_2 \\ \vdots \\ c_i \\ c_{i+1} \end{pmatrix} = E \begin{pmatrix} 1 & 0 & \dots & 0 & b_1 \\ 0 & 1 & \dots & 0 & b_2 \\ \vdots & \vdots & \ddots & \vdots & \vdots \\ 0 & 0 & \dots & 1 & b_i \\ b_1^* & b_2^* & \dots & b_i^* & b_{i+1}^* \end{pmatrix} \begin{pmatrix} c_1 \\ c_2 \\ \vdots \\ c_i \\ c_{i+1} \end{pmatrix},$$

where $h_1, \dots, h_i$ are the matrix elements of the Hamiltonian between the orthogonalized eigenstates $\Psi_1, \dots, \Psi_i$ corresponding to eigenvalues $E_1, \dots, E_i$ and the new trial basis state ψ_{i+1}

$$h_k = \langle \Psi_k | H | \psi_{i+1} \rangle \,, \tag{2.25}$$
$$h_k^* = \langle \psi_{i+1} | H | \Psi_k \rangle \tag{2.26}$$

and similarly, $b_1, \dots, b_i$ are the overlaps

$$b_k = \langle \Psi_k | \psi_{i+1} \rangle \,, \tag{2.27}$$
$$b_k^* = \langle \psi_{i+1} | \Psi_k \rangle \,. \tag{2.28}$$

We can now orthogonalize ψ_{i+1} with respect to the eigenfunction Ψ by e.g. the Gram-Schmidth method

$$|\overline{\psi}_{i+1}\rangle = \frac{|\psi_{i+1}\rangle - \sum_{k=1}^{i} |\Psi_i\rangle \langle \Psi_i | \psi_{i+1} \rangle}{\langle \psi_{i+1} | \psi_{i+1} \rangle - \sum_{k=1}^{i} \langle \psi_{i+1} \Psi_i \rangle \langle \Psi_i | \psi_{i+1} \rangle} \tag{2.29}$$

and the eigenvalue problem becomes

$$\begin{pmatrix} E_1 & 0 & \dots & 0 & q_1 \\ 0 & E_2 & \dots & 0 & q_2 \\ \vdots & \vdots & \ddots & \vdots & \vdots \\ 0 & 0 & \dots & E_i & q_i \\ q_1 & q_2 & \dots & q_i & a \end{pmatrix} \begin{pmatrix} c_1 \\ c_2 \\ \vdots \\ c_i \\ c_{i+1} \end{pmatrix} = E \begin{pmatrix} c_1 \\ c_2 \\ \vdots \\ c_i \\ c_{i+1} \end{pmatrix}, \tag{2.30}$$

where

$$q_k = \langle \Psi_k | H | \overline{\psi}_{i+1} \rangle \,, \tag{2.31}$$
$$a = \langle \overline{\psi}_{i+1} | H | \overline{\psi}_{i+1} \rangle \,. \tag{2.32}$$

To gauge the relevance of the would-be basis state we need to only know the lowest eigenvalue. This is given by the solution of the equation [18]

$$E - h_{i+1} = \sum_{k=1}^{i} \frac{|h_k|^2}{E - E_k}. \tag{2.33}$$

The limitation of the SVM with CGs stems from the sheer number of parameters that needs to be optimized. The size of the matrix A grows as $N(N+1)/2$ and for larger systems the number of basis functions needed to obtain converged results grows considerably. As a consequence, one also needs to compute larger and larger number of matrix elements between the basis function. Furthermore, the antisymmetrization for fermions mandates the repetition of this calculation $N!$ times.

Chapter 3

Pionless Effective Field Theory

The construction of nuclear interactions from underlying principles has a long history [3, 40]. We can consider the one-meson exchange potential of Yukawa [41] as a first field-theoretical attempt to tackle this problem. He theorized that the force between nucleons is mediated by a particle with mass between the electron and the proton. The existence of this particle, named pion, was later confirmed experimentally and its mass was measured to be $m_\pi \approx 140$ MeV. Since then, more types of mesons were discovered. Following the work of Yukawa, one-boson-exchange potentials were constructed and they were succesful in describing low-energy nucleon-nucleon scattering data [42]. Later, models going beyond the exchange of single particles were developed [43].

However, as it became clear that the fundamental theory of strong interaction is quantum chromodynamics (QCD), the boson-exchange potentials were reduced to mere phenomenology and effort had to be made to derive the nuclear interaction from QCD. But there, one encounters a seemingly insurmountable problem. QCD is a Yang-Mills quantum field theory with local SU(3) gauge invarience. These properties guarantee that the running of the strong coupling constant α_s is (at one-loop level) given by

$$\alpha_s(Q) = \frac{2\pi}{b_0 \ln\left(\frac{Q}{\Lambda_{\mathrm{QCD}}}\right)}, \tag{3.1}$$

where $b_0 = 11 - 2/3 n_f$ with n_f being the number of quark flavours, six in our universe [44]. The experimentally determined parameter $\Lambda_{\mathrm{QCD}} \approx 200$ MeV represents a pole of the function $\alpha_s(Q)$. In other words, at large momenta we observe the famous asymptotic freedom but for Q nearing Λ_{QCD} the coupling constant grows rapidly. While these characteristics are desired in high-energy particle physics, QCD formulated in the language of quarks and gluons is very difficult to apply in the momentum domain of nuclear physics because for momenenta smaller than $Q \sim 1$ GeV it becomes non-perturbative.

A light at the end of the tunnel appeared when Steven Weinberg applied the concept of an effective field theory (EFT) to nuclear phyics [45, 46, 47]. He simply wrote down the most general Lagrangian consistent with the symmetries of QCD in terms of nucleon and pion degress of freedom and thus guaranteed that the EFT is equivalent to low-energy QCD. The chiral EFT (χEFT) was born and has been the preferred way of contructing nuclear potentials for use in microscopic ('*ab initio*') calculations ever since [3, 40, 48, 49]. This leads us back to the original idea of Yukawa's pion exchange, except now the pions are Goldstone bosons created by the spontaneuos braking of the approximate chiral symmetry; heavier mesons are integrated out and their contributions are 'hidden' in the low-energy constants (LECs) of the terms in the Lagrangian expansion series. In this work we go one step further and integrate out even the pions, leaving us only with nucleon degrees of freedom. This so-called pionless EFT ($\not\pi$EFT) was intially conceived as a toy model to study the renormalizibility of nuclear EFTs [50] but since has been succesfully applied to treat processes involving few-nucleon systems (see [2] for a recent review of not-only-pionless EFTs, a pedagological introduction to few-body applications of EFTs is also given in Chapter 4 of [51]).

In this chapter, we will briefly explain the idea behind EFTs, derive a potential from the $\not\pi$EFT including Coulomb interaction non-perturbatively and explain our procedure of fitting the potential parameters.

3.1 Effective Field Theories

EFTs exploit seperation of scales to calculate low-energy observables. The first step of constructing an EFT tailored to a certain system is the choice of relevant degrees of freedom according to the momentum scales of interest. Let us assume that our system is described by two scales, a low-momentum scale $M_{\rm lo}$ and a high-momentum scale $M_{\rm hi}$ (generally, there can be more than two). The corresponding Lagrangian density of the considered system is then expanded as

$$\mathcal{L} = \sum_i C_i(M_{\rm lo}, M_{\rm hi}, \Lambda) O_i(\{\psi\}), \tag{3.2}$$

where C_i are the LECs, O_i are operator terms involving the selected fields $\{\psi\}$, Λ is a regulator that ensures that states with momenta higher than Λ are excluded from the theory and as a consequence loop diagrams do not diverge [2] and the derived interactions are non-singular [52]. This is a 'bottom-up' approach of creating an EFT, alternatively one can proceed 'top-down' - exploiting the knowledge of the underlying theory, degrees of freedom that are asssumed to not be needed to describe the low-energy processes of interest

are integrated out and one is left with an effective Lagrangian, just as above. It is customary to denote by Q the typical momenta of the considered system which are of the order of $M_{\rm lo}$, $M_{\rm hi}$ is then the momentum at which we expect the theory to break down. The hard scale $M_{\rm hi}$ is usually set by the physics not included in the EFT, such as the masses of the particles which are integrated out. Observables then have an expansion [53] in the small parameter $(Q/M_{\rm hi})$

$$\mathscr{M} = \sum_{\nu} \mathscr{M}_{\nu}(Q,\Lambda) = \sum_{\nu} \left(\frac{Q}{M_{\rm hi}}\right)^{\nu} \mathcal{F}_{\nu}\left(\frac{Q}{\Lambda}, C_i\right), \tag{3.3}$$

where the index ν is bounded from below and defines the power-counting, that is the categorization of contributions to $\mathscr{M}$ at a given order.

In nuclear physics, to be able to treat many-body systems we wish to have an interaction that can be simply plugged into the Shrödinger equation. This makes the application of perturbative EFTs, meaning the calculation of observables as expansions in the parameter $(Q/M_{\rm hi})$, not as straightforward as introduced above. In general, a potential V is derived by matching the amplitude calculated from the Lagrangian density (i.e., from the relevant Feynman diagrams) to the one obtained from V in Born perturbation theory. Although V is not an observable, we still assume that it is given by a similar expansion as (3.3)

$$V(Q,\Lambda) = \sum_{\mu} V_{\mu}(Q,\Lambda) = \sum_{\mu} \left(\frac{Q}{M_{\rm hi}}\right)^{\mu} \widetilde{\mathcal{F}}_{\mu}\left(\frac{Q}{\Lambda}, C_i\right), \tag{3.4}$$

where μ is a counting index for the potential. In principle, this expansion truncated at some $\mu = \mu_0$ can be inserted into the Schrödinger equation exactly (it is said that V is 'iterated to all orders' or 'resummed'). The issue is that the indeces μ and ν do not necessarily correspond to each other and there would be no way to guarantee that a term of the iterated order μ of the potential would contribute only to the order $\nu = \mu$ of the observable. For example, a contribution to $\mathscr{M}_2$ can be obtained by either treating V_2 in first-order perturbation theory or by treating V_1 in second-order perturbation theory. Therefore, the 'correct' way to treat the potential from the EFT point of view is to use perturbation theory also at the level of the Schrödinger equation. Only some terms should be treated exactly and only if the power counting demands it [2], such as the LO of $\not\pi$EFT that needs to be iterated to produce nuclear bound states (we will discuss this in more detail later).

Another important point is that the physical observables $\mathscr{M}$ should not depend on the unphysical cutoff Λ, i.e., we would wish for our theory to be renormalized. From the modern point of view [52, 54], renormalization just means that our low-energy EFT should not be sensitive to the high-energy physics that probes very short distances. Since the potential is not

an observable it not only may, but must depend on the cutoff. As the cutoff is changed, so must the LECs of the potential because the amount of high-momentum physics excluded by the cutoff (and simulated by the LECs) is changed - it is said that the LECs run with the cutoff and the observables are renormalization-group (RG) invariant. The exact values of the LECs need to be determined by fits to the experimental data. The RG invariance of the observables is, however, only approximate because in practical calculations the series (3.3) is truncated and residual cutoff dependence remains. While in analytical calculations Λ-dependence can be examined easily, in numerical calculations it is investigated by varying the cutoff beyond the breakdown scale $M_{\rm hi}$ of the EFT. In this way, the error of the theory can be quantified [55]. Systematic evaluation of the theoretical unceirtanty is one of the biggest motivations behind applying EFTs to nuclear physics and striving for RG invariance even when it is challenging, like for example in χEFT [56, 57].

3.2 Pionless Theory

We shall now apply the abstract concepts introduced above by studying the simplest possible microscopic nuclear EFT, the pionless effective field theory ($\not\pi$EFT). The motivation behind $\not\pi$EFT is simple - the characteristic momenta in low-energy processes involving only a few nucleons are generally much smaller than the pion mass, $Q \ll m_\pi$. As a consequence, these systems should not be sensitive to details resolved by pion, or heavier meson exchanges - their effects are small enough to be contained in the low-energy coupling constants of the contact interactions in the Lagrangian. The breakdown scale of $\not\pi$EFT is estimated by $M_{\rm hi} \sim m_\pi$. Recently, using Bayesian statistics a median value of $M_{\rm hi} = 1.4 m_\pi$ was inferred [58].

We will proceed using the 'bottom-up' approach. Since there is only one degree of freedom left, the nucleon field N, the corresponding Lagrangian density for a two-nucleon system can be expanded as [59]

$$\mathcal{L}_{2N} = N^\dagger \left(i\partial_t + \frac{\nabla^2}{2m} \right) N + C_0^{^3\mathrm{S}_1} (N^T P_t N)^\dagger (N^T P_t N) + \tag{3.5}$$

$$+ C_0^{^1\mathrm{S}_0} (N^T P_s N)^\dagger (N^T P_s N) - \frac{C_2^{^3\mathrm{S}_1}}{8} \Big[(N^T P_t N)^\dagger (N^T \overleftrightarrow{\nabla}^2 P_t N) + h.c. \Big] +$$

$$- \frac{C_2^{^1\mathrm{S}_0}}{8} \Big[(N^T P_s N)^\dagger (N^T \overleftrightarrow{\nabla}^2 P_s N) + h.c. \Big] + \frac{1}{4} (N^T \overleftrightarrow{\nabla}_x P_{ya}^{^3\mathrm{P}} N)^\dagger (N^T \overleftrightarrow{\nabla}_x P_{ya}^{^3\mathrm{P}} N) \times$$

$$\times \Big[C_1^{^3\mathrm{P}_0} \delta_{xy}\delta_{wz} + C_2^{^3\mathrm{P}_2} (\delta_{xy}\delta_{wz} - \delta_{xz}\delta_{yw}) + C_2^{^3\mathrm{P}_2} [2\delta_{xw}\delta_{yz} + 2\delta_{zy}\delta_{yw} - \frac{4}{3}\delta_{xy}\delta_{wz}] \Big] +$$

$$+\frac{C_2^{^1\mathrm{P}_1}}{4}(N^T\overleftrightarrow{\nabla}_x P^{^1\mathrm{P}}N)^\dagger(N^T\overleftrightarrow{\nabla}_x P^{^1\mathrm{P}}N)+$$
$$+\frac{C_2^{\text{S-D}}}{4}\left[(N(P_t)_iN)^\dagger(N\overleftrightarrow{\nabla}_x\overleftrightarrow{\nabla}_y(P_t)_jN)\mathcal{T}_{xyij}+h.c.\right]+...,$$

where m is the nucleon mass and the $s-$wave spin-triplet and spin-singlet projectors are given by

$$(P_t)_i=\frac{1}{\sqrt{8}}\sigma_2\sigma_i\tau_2,\quad (P_s)_i=\frac{1}{\sqrt{8}}\sigma_2\tau_2\tau_i, \tag{3.6}$$

where σ and τ are Pauli matrices acting in spin and isospin spaces. In the p-wave, we have the spin-triplet, isospin-triplet and spin-singlet, isospin-singlet projectors

$$P_{ia}^{^3\mathrm{P}}=\frac{1}{\sqrt{8}}\sigma_2\sigma_i\tau_2\tau_a,\quad P^{^1\mathrm{P}}=\frac{1}{\sqrt{8}}\sigma_2\tau_2, \tag{3.7}$$

where the free index a specifies the two-nucleon pair ($pp/pn/nn$). The operator $\mathcal{T}$ is defined as

$$\mathcal{T}_{xyij}=\delta_{ix}\delta_{jy}-\frac{1}{3}\delta_{ij}\delta_{xy}. \tag{3.8}$$

Here, we assume the Einstein summation convention, i.e., two identical indeces in the same term are always summed over.

The first term in (3.5) is just the Lagrangian of a free Schrödinger field - because $Q\ll m_\pi$, we are working in a non-relativistic framework and therefore do not enforce the full Lorentz but only Galilean invariance of $\mathcal{L}$. The nucleon fields N are doublets in spin and isospin space and unlike dirac fields in relativisic QFT[2], $N^\dagger$ contains only a nucleon creation operator and N only a nucleon annhilation operator since antiparticles are not relevant at these energies.

Two-body interaction terms are included up to the second power of the Galilean invariant derivative $\overleftrightarrow{\nabla}=\overleftarrow{\nabla}-\vec{\nabla}$. These include the constant interaction terms in the s-wave spin triplet and singlet channels represented by the terms $C_0^{^3\mathrm{S}_1}$, $C_0^{^1\mathrm{S}_0}$ and the derivate corrections in these channels given by the terms $C_2^{^3\mathrm{S}_1}$ and $C_2^{^1\mathrm{S}_0}$. The s-wave spin-triplet channel is mixed with the d-wave spin-triplet channel $^3\mathrm{D}_1$ due to the so-called tensor interaction given by the term $C_2^{\text{S-D}}$. This interaction is well-known from phenomenological descriptions of the nuclear force and is responsible for e.g. the experimentally measured non-zero quadrupole moment of the deuteron.

[2]The non-relativistic limit of a fermionic field can be obtained by means of the Foldy-Wouthuysen transformation [60].

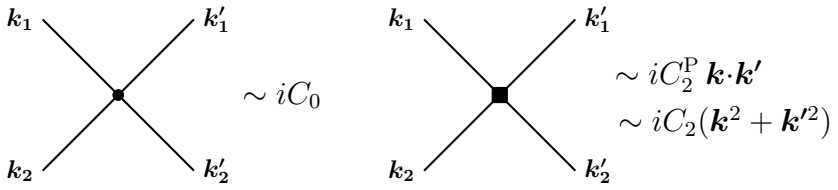

Figure 3.1 Feynman rules for the four-nucleon contact and derivative vertex. Due to Galilean invariance, the result can only depend on the differences of momenta $\boldsymbol{k} = \boldsymbol{k_1} - \boldsymbol{k_2}$, $\boldsymbol{k'} = \boldsymbol{k_1'} - \boldsymbol{k_2'}$. C_0 is equal to $C_0^{^3\mathsf{S}_1}$ or $C_0^{^1\mathsf{S}_0}$ and C_2^P is equal to any of the p-wave terms. The black square in the second diagram represents either the p-wave term or the derivative s-wave correction, in which case C_2 is equal to $C_2^{^3\mathsf{S}_1}$ or $C_2^{^1\mathsf{S}_0}$.

Lastly, the possible p-wave interactions are represented by the terms $C_2^{^1\mathrm{P}_1}$, $C_2^{^3\mathrm{P}_0}$, $C_2^{^3\mathrm{P}_1}$ and $C_2^{^3\mathrm{P}_2}$, which arise due to the spin-orbit (LS) splitting in this partial wave.

Subsequent two-body terms contained in the ellipsis of (3.5) are then generated by writing terms with higher powers of the invariant derivative, see e.g. [61]. For example, the lowest order terms contributing to partial waves with higher orbital momentum l are generated by $(N^T \overset{\leftrightarrow}{\nabla}{}^l N)^\dagger (N^T \overset{\leftrightarrow}{\nabla}{}^l N)$ and other higher order corrections such as the p-f (isospin 1) tensor interaction are constructed analagously.

The corresponding Feynman rules are given in Figure 3.1. They are not difficult to derive if we consider that a non-relavisitic field $\psi(t, \boldsymbol{x})$ representing either a proton or a neutron is given by (up to a normalization factor)

$$\psi_\alpha(t, \boldsymbol{x}) \propto \int \frac{d^3\boldsymbol{p}}{(2\pi)^3} b_\alpha(\boldsymbol{p}) e^{-i(Et - \boldsymbol{p}\cdot\boldsymbol{x})}, \tag{3.9}$$

where $b_\alpha(\boldsymbol{p})$ is the standard particle annhilation operator acting in Fock space and α is a spin projection index.

Three-body forces are also included straightforwardly, ignoring spin and isospin projections we may write

$$\mathcal{L}_{3N}^{\mathrm{int}} = D(N^\dagger N)^3 + \dots . \tag{3.10}$$

Similarly, four-body forces are generated by

$$\mathcal{L}_{4N}^{\mathrm{int}} = E(N^\dagger N)^4 + \dots . \tag{3.11}$$

Higher order corrections to these forces are contructed by inserting Galilean derivatives between the nucleon fields, see e.g. Ref. [62]. The associated trivial Feynman rules are shown in Figure 3.2.

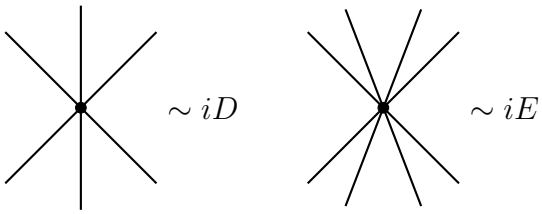

Figure 3.2 Feynman rules for the contact three- and four-body interaction.

As a last point, let us comment on the form of the propagator. The Lagrangian density for a free Schrödinger field has the form

$$\mathcal{L}_{\text{free}} = \psi^\dagger \left(i\partial_t + \frac{\nabla^2}{2m} \right) \psi, \tag{3.12}$$

where ψ is given by (3.9), which is formally very similar to the Schrödinger equation for a free particle. Indeed, it can be shown [51] that the propagator has the same form as the free-particle Green's function from QM, that is

$$D(x-y) = \int \frac{d^4k}{(2\pi)^4} \frac{e^{-ik(x-y)}}{E - \boldsymbol{k}^2/2m + i\varepsilon}. \tag{3.13}$$

Unlike in relativistic QFT, the non-relativistic propagator has only one pole. When the positive infinitesimal factor $\epsilon > 0$ is written with a plus infront, as above, the pole is $+k$. On the other hand, the choice $-i\varepsilon$ would lead to the pole $-k$. These two possibilities correspond to the advanced and retarded Green's function, respectively, and the reason for the single pole is the fact that particles and antiparticles are completely decoupled. In other words, the particles can propagate only forwards, or only backwards in time, which is why there is no point in drawing the usual arrows on the lines in non-relativistic Feynman diagrams.

3.2.1 The Return of the Effective Range Expansion

In Section 1.1.3, we have seen that the low-energy scattering behaviour of two particles can be described by a few paramaters, giving rise to the so-called effective range expansion (ERE). The ∉EFT can be regarded as a modern, field-theoretical realization of this idea.

Let us try to calculate the s-wave scattering amplitude ('the T-matrix') using the Lagrangian density (3.5). In field theory, the amplitude is usually defined with an extra factor of $4\pi/m$ compared to (1.51) [2, 63], so we have

$$T(k) = \frac{4\pi}{m} \frac{1}{k \cot\delta - ik}, \tag{3.14}$$

where k is the center-of-mass momentum of the two nucleons. We will neglect the effects of Coulomb interaction in this section. Since we are constructing a low energy theory, we assume that the ERE

$$k \cot \delta = -\frac{1}{a} + \frac{1}{2} r k^2 + \mathcal{O}(k^4) \tag{3.15}$$

describes the phase shifts well with only a few terms - the scattering length a and the effective range r. By plugging the ERE into Eq. (3.14) and Taylor expanding it around $k = 0$ we get an expansion of the amplitude in powers of momenta

$$T(k) = \frac{4\pi}{m} \left[-a + i a^2 k + a^3 k^2 - \frac{1}{2} a^2 r k^2 + \mathcal{O}(k^4) \right], \tag{3.16}$$

which is similar to the equation (3.3). We wish to match the terms of this expansion to the amplitude calculated using (3.5). The lowest k^0 term then comes from the tree-level vertex in the left side of Figure 3.1. We identify

$$C_0 = -\frac{4\pi a}{m}, \tag{3.17}$$

where C_0 is either $C_0^{^3\mathrm{S}_1}$ or $C_0^{^1\mathrm{S}_0}$, we will not distinguish between the two channels in the following.

It is obvious that this expansion can converge only if $|ak| < 1$, which implies that our theory is valid only for momenta $k < |1/a|$. This would not be a problem if the nucleon-nucleon system would be 'natural' from the point of view of the EFT, that is, it would have a small scattering length comparable to the Compton wavelength of the pion

$$\lambda_\pi = \frac{2\pi}{m_\pi} \approx 1.4\,\mathrm{fm}. \tag{3.18}$$

In that case, the EFT would be valid up to momenta of the order of pion mass, as is expected. But we know that this is not the case. According to experimental measurements [64, 65, 66], the values of proton-neutron and neutron-neutron scattering lengths are (ignoring small experimental errors)

$$a_s^{pn} = -23.71\,\mathrm{fm}, \quad a_t^{pn} = 5.41\,\mathrm{fm}, \quad a_s^{nn} = -18.95\,\mathrm{fm}, \tag{3.19}$$

where a_s and a_t refer to spin-singlet and triplet scattering lengths, respectively.

The reason for these 'unnaturaly' large scattering lenghts is known from non-relativistic theory of scattering in quantum mechanics (see e.g. Chapter 13 of [20]). The amplitude can be analytically continued for complex momenta and the poles of $T(k)$ on the imaginary axis above the origin then correspond

to bound states, poles below the origin ($\mathrm{Im}(k) < 0$) correspond to resonances or, in the s-wave, to the so-called virtual states. From Eq. (3.14), we see that $T(k)$ diverges if the equation $k \cot \delta - ik = 0$ has a solution. In the spin-triplet channel, the solution is positive and gives the binding momentum of the deuteron bound state. In the spin-spinglet channel there is a negative solution, i.e., a virtual boud state. Since both of these poles are near threshold, the ERE may be used and this leads us to the fact that the scattering length must be large, since it is proportional to the large value of $T(k)$ near the (virtual) bound state.

The breakdown scale of the theory set by e.g. $1/a_s^{pn}$ would mean that the theory is applicable only for extremely low-energy scattering, up to only about 8 MeV. This means that the perturbative treatment of NN scattering is very limited; to replicate the poles of the amplitude a non-perturbative treatment is required.

The terms in the expansion (3.16) may be regrouped [2, 67] so that we have

$$T = \frac{4\pi}{m} \left[\frac{1}{-1/a - ik} + \frac{rk^2}{2(-1/a - ik)^2} + ... \right], \tag{3.20}$$

where the first term is just a sum of the series that does not contain any effective range terms

$$\frac{1}{-1/a - ik} = -a(1 - (iak) + (iak)^2 + ...)\,. \tag{3.21}$$

In this way we have gotten rid of the large coefficients stemming from the unnatural scattering lengths of the NN system, but the series on the right-hand side of (3.21) still converges only if $|ak| < 1$, so how can such a regrouping be justified?

It turns out that the terms of expansion (3.21) correspond to a sum of the simple tree-level vertex and all its 'bubble-chain' corrections, see Figure 3.3. As is usually the case in field theories, the contributions from the loop diagrams are divergent and these divergences have to be dealt using regularization techniques. These usually involve introducing an unphysical parameter, which is later removed by renormalization, ensuring that the theory reproduces experimental data independentanly of the value of the regularization parameter. The different expansion series presented above correspond to different ways of calculating the amplitude - different renormalization schemes - but the resulting amplitude is the same; what does not remain the same are the coupling constants C_0, C_2,...

Kaplan, Savage and Wise [63, 68] have devised a regularization scheme which makes the resummation necessary (the so-called power-dimension

subtraction). Instead of (3.17), the calculation of diagrams of Figure (3.21) in their scheme yields

$$C_0(\mu) = -\frac{4\pi}{m}\left(\frac{1}{-\mu + 1/a}\right). \tag{3.22}$$

The perameter μ is an unphysical regulator parameter[1], $\mu \sim \Lambda$. Let us consider a case when μ is of the same order as the external momentum, $\mu \sim k$, and the scattering length is large, so $\mu \gg 1/a$. Then we have $C_0 \sim k^{-1}$ and the leading order contribution to the amplitude must also scale as $\mathcal{O}(k^{-1})$. Such a contribution can not stem from a single diagram because, keeping in mind the Feynman rules from the previous section and the form of the propagator (3.13), a single diagram always generates only positive powers of momenta; the whole infinite bubble chain shown in Figure 3.3 must contribute and be resummed. This means the leading order amplitude is given by the sum

$$T(k) = \frac{4\pi}{m} C_0 \left[1 + C_0 I_0 + (C_0 I_0)^2 + ...\right] = \frac{4\pi}{m} \frac{1}{C_0^{-1} - I_0}, \tag{3.23}$$

where I_0 is the integral corresponding to one bubble. It is given by a product of two propagators (3.13), one for each nucleon line.

The relation (3.22) demonstrates that it is possible to construct the theory even for large scattering lengths $a \to \infty$ but dependence of the couplings on the regularization parameter is unavoidable. Only when the scattering length is natural can we get rid of the μ completely. In other words, the existence of nuclear bound states neccessesitates the resummation of the leading order interaction.

According to experimental data [64, 65, 66], the values of the effective ranges are

$$r_s^{pn} = 2.75\,\text{fm}, \quad r_t^{pn} = 1.74\,\text{fm}, \quad r_s^{nn} = 2.83\,\text{fm}. \tag{3.24}$$

They are thus natural, $r \sim m_\pi^{-1}$, and can be treated as perturbative corrections. The amplitude is matched to the series (3.20) and we find [63, 68]

$$C_2 = -\frac{4\pi}{m}\left(\frac{1}{-\mu + 1/a}\right)^2 \frac{r}{2}. \tag{3.25}$$

Higher order corrections are constructed similarly.

[1] A reader familiar with dimensional regularization is sure to recognize it at first sight - it is the 'renormalization scale' that appears when we evaluate integrals in an arbitrary number of dimensions.

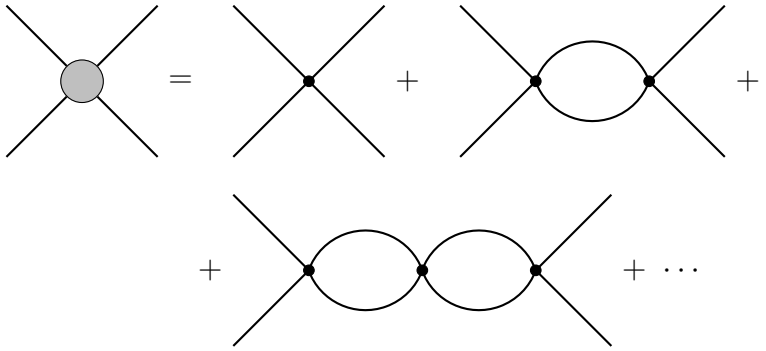

Figure 3.3 Feynman diagrams of the contributions to the LO s-wave amplitude.

So far we have made no effort to differentiate between the ${}^1S_0$ channel, which has a virtual state near the threshold, and the ${}^3S_1$ channel, which has the deuteron bound state near the threshold. As an alternative to the above treatment, the ERE (3.15) can be given as an expansion around the deuteron pole $k_d = \sqrt{mB_d} \approx 45.7$ MeV in the complex plane, where B_d is the deuteron binding energy, instead of $k = 0$. This was originally done already by Bethe [27] and the expansion then takes the form

$$k \cot \delta = -k_d + \frac{1}{2}\rho_d(k^2 + k_d^2) + \dots , \tag{3.26}$$

where $\rho_d = 1.765$ fm is the deuteron effective range [69]. Using the above equation as a starting point, the theory can be built up the same way and the couplings C are matched to it. The difference is that now the deuteron energy is fixed at LO and the pn scattering length and effective range are predictions of the theory.

The values of a_t^{pn} and $1/k_d$ differ by about 25%, which is in line with the expectation that the LO error of $\not\pi$EFT is about 30% since it is basically an expansion in the small parameter $r/a \equiv M_{\rm lo}/M_{\rm hi}$. In other words, under an appropriate power-counting we can freely choose the input parameters of the lower orders, since they are then corrected by higher order corrections, i.e., starting from a_t^{pn}, k_d is given by the expansion

$$k_d = \frac{1}{a_t^{pn}}\left(1 + \frac{r_t^{pn}}{2a_t^{pn}} + \dots\right). \tag{3.27}$$

3.2.2 Coulomb Effects

Fully seperating the contributions of strong and Coulomb interactions in scattering of charged particles is generally not possible - this lead us in

Chapter 1 to the definitions of 'additional' amplitudes and phase shifts. Therefore, if we take into account the Coulomb potential, the partial-wave amplitude due to nuclear interaction must be parametrized as

$$T_{sc}(k) = \frac{4\pi}{m} \frac{e^{2i\sigma_l}}{k \cot \delta_l - ik} \tag{3.28}$$

and the ERE is given by (1.49) - for the *pp* s-wave it has the form

$$C_0^2(\eta) k \cot \delta + 2k\eta h_0(\eta) = -\frac{1}{a_{pp}} + \frac{1}{2} r_{pp} k^2 + \mathcal{O}(k^4). \tag{3.29}$$

It is then clear that the *pp* channel deserves a special treatment, because now the couplings in the Lagrangian density need to be matched to a different ERE.

The first to study *pp* scattering in ⧸EFT were Kong and Ravndal [70, 71] and we shall follow their example. According to the phase shift analysis [72], the *pp* scattering lengths and effective ranges are

$$a_{pp} = -7.81\,\text{fm}, \quad r_{pp} = 2.79\,\text{fm}, \tag{3.30}$$

so our experience with the *pn* and *nn* channels tells us that since a_{pp} is unnatural the leading order has to once again be resummed à la Figure 3.3. But how should we include the Coulomb interaction into this framework? Since it scales as $1/k^2$ (the Fourier transform of $1/r$), it is natural that for some momentum $k = k_c$ it becomes non-perturbative and much like the strong force, it will need to be resummed.

It can be shown that each of the diagrams on the right-hand side of the Figure 3.4 diverges for $k \to 0$ due to the photon exchange [71] and we need a non-perturbative way to sum all Coulomb photon exchanges. The authors of [70, 71] were able to achieve this by using an analytic expression for pure-Coulomb Green's function from nonrelativistic scattering theory. Their calculation is sketched out below.

According to (1.79), the additional amplitude is given by

$$T_{sc}(\boldsymbol{k}) = \langle \boldsymbol{k}_c^- | V_s | \boldsymbol{k}^+ \rangle \,, \tag{3.31}$$

where V_s is the strong potential, which is read off from the Lagrangian density as

$$\langle \boldsymbol{k}' | V_s | \boldsymbol{k} \rangle = C_0 \delta(\boldsymbol{k}' - \boldsymbol{k}). \tag{3.32}$$

Then, the outgoing scattering state is given by

$$|\boldsymbol{k}^+\rangle = \sum_{n=0}^{\infty} (G_c V_s)^n \, |\boldsymbol{k}_c^+\rangle \,, \tag{3.33}$$

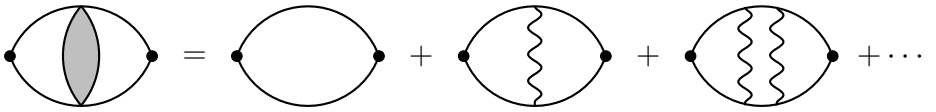

Figure 3.4 One-loop diagram dressed with a ladder of Coulomb photon exchanges

where G_c is the Coulomb Green's function as discussed in some detail in Chapter 1.2. Each insertion of G_c corresponds to adding one more photon exchange as in Figure 3.4. Then, the amplitude reads

$$T_{sc} = \langle \boldsymbol{k}_c^- | V_s \sum_{n=0}^{\infty} (G_c V_s)^n | \boldsymbol{k}_c^+ \rangle \,. \tag{3.34}$$

In priciple, $T_{sc}(k)$ could also be evaluated starting from the Lagrangian density and introducing the electromagnetic field into it, but since both the Lippman-Schwinger equation and the Lagrangian density describe non-relativistic quantum mechanics, the approaches are equivalent.

For the zeroth order ($n = 0$) one finds, after inserting two sets of complete states $|\boldsymbol{q}\rangle\langle\boldsymbol{q}|$ and $|\boldsymbol{q'}\rangle\langle\boldsymbol{q'}|$ on either side of V_s

$$T_{sc}^{(0)} = C_0 C_\eta^2 e^{2i\sigma_0}, \tag{3.35}$$

where C_η^2 is the Sommerfeld factor, see (1.50), and $2\sigma_0$ is the relative phase shift of the Coulomb functions $|\boldsymbol{k}_c^+\rangle$ and $|\boldsymbol{k}_c^-\rangle$. Similarly, for the first order one has

$$T_{sc}^{(1)} = (C_0)^2 C_\eta^2 e^{2i\sigma_0} I_0(k) \tag{3.36}$$

and higher orders are further enhanced by $C_0 I_0(k)$, where $I_0(k)$ is now the integral

$$I_0(k) = \int \frac{d^3\boldsymbol{q}}{(2\pi)^3} \int \frac{d^3\boldsymbol{q}'}{(2\pi)^3} \langle \boldsymbol{q}' | G_c(E) | \boldsymbol{q} \rangle \,. \tag{3.37}$$

Summing up the geometric series of T_{sc} contributions just like in (3.23), which corresponds to Figure 3.4, we get

$$T_{sc} = C_\eta^2 \frac{e^{2i\sigma_0}}{C_0^{-1} - I_0(k)} \tag{3.38}$$

The integral I_0 is UV divergent and can be evaluated in power-dimension subtraction scheme [71]. Plugging the result into T_{sc} and then T_{sc} into the Coulombic ERE leads us to the defintion of the renormalized coupling

$$\frac{4\pi}{m C_0(\mu)} = \frac{1}{a_{pp}} - \mu + \alpha m \left(\ln \frac{\mu\sqrt{\pi}}{\alpha m} + 1 - \frac{3}{2} C_E \right), \tag{3.39}$$

where $C_E = 0.577...$ is the Euler-Mascheroni constant and $\alpha \approx 1/137$.

So, the salient point of this subsection is that renormalization in the pp channel with electromagnetic interaction can be carried out in the same way as in the nn/pn channels but it needs to be matched to the Coulombic ERE, which unavoidably leads to different LECs of the interaction already at LO. Actually, it can be seen from (3.39) that the pp scattering length cannot be divided into a purely strong interaction and purely Coulomb part because the last term on the right-hand side of (3.39), which is caused by the addition of Coulomb interaction, depends on the renormalization scale μ (see also the discussion in [71]).

3.3 Pionless EFT Interaction

In the preceeding sections we described the applications of $\not\pi$EFT to two-nucleon systems, mostly focusing on the renormalization aspects of the theory. However, what we are ultimately interested in are systems involving more nucleons - properties of nuclear bound states and processes involving nuclear reactions. While three-nucleon systems have been treated in the dibaryon formalism, where fields representing two-nucleon states are introduced (see e.g. [2, 51]), this approach is difficult to apply beyond three particles. We therefore consider a potential approach, whose advantage is that in principle any method may be used to solve the few-body Schrödinger equation. This means that the generalization to three and more particles is straightforward and furthermore, observables may be calculated from the obtained wave functions using standard, model-independent techniques.

3.3.1 Two-Body, Three-Body and Four-Body Potential

The general way to derive a potential V from a field theory is to match the S-matrix element $S_{fi} = \langle f|\mathcal{L}|i\rangle$ obtained from the Lagrangian density, where $|i\rangle$ and $|f\rangle$ are the initial and final scattering states, to the S-matrix element obtained from non-relativistic QM, $S_{fi} = \langle f|V|i\rangle$ (see e.g. [73]). In general, V is given by a sum of all possible Feynman diagrams at the considered order.

Due to the simplicity of the pionless theory, the interaction can be written down almost immedietaly. Using the Feynman rules in Figure 3.1, the two-body potential in momentum representation decomposed into partial waves reads

$$\begin{aligned} V_{\mathrm{2B}}(\boldsymbol{k},\boldsymbol{k}') =& C_0^{^3\mathrm{S}_1} + C_0^{^1\mathrm{S}_0} + C_2^{^3\mathrm{S}_1}(\boldsymbol{k}^2+\boldsymbol{k}'^2) + C_2^{^1\mathrm{S}_0}(\boldsymbol{k}^2+\boldsymbol{k}'^2) + \\ &+ C_2^{\text{S-D}}\boldsymbol{k}^2 + C_2^{\text{D-S}}\boldsymbol{k}'^2 + (C_2^{^1\mathrm{P}_1} + C_2^{^3\mathrm{P}_0} + C_2^{^3\mathrm{P}_1} + C_2^{^3\mathrm{P}_2})\boldsymbol{k}\cdot\boldsymbol{k}'..., \end{aligned} \tag{3.40}$$

where $\boldsymbol{k}$ and $\boldsymbol{k'}$ are the incoming and outgoing center-of-mass momenta of the two nucleons. Here, each term needs to be understood as projected only to the relevant partial wave, as given by the corresponding LEC. The terms $C^{\text{D-S}}$ and $C^{\text{S-D}}$ correspond to the matrix elements $\langle {}^3\text{D}_1|V_{\text{2B}}|{}^3\text{S}_1\rangle$ and $\langle {}^3\text{S}_1|V_{\text{2B}}|{}^3\text{D}_1\rangle$, respectively.

As we have discussed in the Section 3.1, power counting mandates which terms should be included at a given order ν in the expansion (3.4) - the expansion (3.40) is just a simple case of it. To reproduce the large scattering length of the NN system we need to sum the infinite chain of bubble diagrams shown in Figure 3.3. So the LO term in the potential is naturally the one corresponding to C_0 and it reproduces the scattering length. Summation of the bubble chain means that the term is fully iterated in the Schrödinger equation, i.e., we solve it with the Hamiltonian

$$H = T + V_{\text{2B}}^{(0)}, \tag{3.41}$$

where T is the kinetic energy and $V_{\text{2B}}^{(0)}$ is the LO potential. Since a constant in momentum space is a delta function in x-representation, this potential can be written as [14]

$$V_{\text{2B}}^{(0)} = \sum_{i<j} \left(C_0^{(0)} P_{ij}^{(0,1)} + C_1^{(0)} P_{ij}^{(1,0)} \right) \delta(r_{ij}), \tag{3.42}$$

where $r_{ij} = |\boldsymbol{r}_i - \boldsymbol{r}_j|$ is the distance between the nucleons i and j, $P^{(S,T)}$ is the projector to the two-nucleon spin-isospin channel (S,T). These terms are related to the nn/pn spin singlet and triplet scattering lenghts. From the preceeding section we know that to achieve renormalization in the pp channel we need to match the interaction to the Coulombic ERE. The non-perturbative nature of the Coulomb potential requires that all exchanges of photons in Figure 3.4 be resummed. The static photon exchanges are given by the Coulomb potential, so the resummation means that we iterate the Coulomb interaction in the Schrödinger equation. We need to add another term to the LO potential, related to the pp scattering length a_{pp}, because the coupling in this channel is different, as we argued earlier. This term has the form

$$V_{pp}^{(0)} = \sum_{i<j} P_{ij}^{(0,1)} C_3^{(0)} \delta(r_{ij}) + \frac{e^2}{r_{ij}}, \tag{3.43}$$

and is projected to only the spin-singlet pp channel.

The effective range corrections are an NLO perturbative effect caused by the terms $C_2^{{}^3\text{S}_1}$ and $C_2^{{}^1\text{S}_0}$ in the Langragian density. Then, the $C_2^{{}^3\text{S}_1}$ and $C_2^{{}^1\text{S}_0}$ terms of the potential (3.40) should also reproduce the effective range and be

introduced to the Schrödinger equation in first-order perturbation theory. In coordinate representation we write them as [14]

$$V_{\rm 2B}^{(1)} = \sum_{i<j} \left(C_2^{(1)} P_{ij}^{(0,1)} + C_3^{(1)} P_{ij}^{(1,0)} \right) \times \left[\delta(r_{ij}) \vec{\nabla}^2 + \overleftarrow{\nabla}^2 \delta(r_{ij}) \right]. \tag{3.44}$$

To include the *pp* effective range correction, we must add another derivative term to the potential

$$V_{pp}^{(1)} = \sum_{i<j} P_{ij}^{(0,1)} C_3^{(1)} \times \left[\delta(r_{ij}) \vec{\nabla}^2 + \overleftarrow{\nabla}^2 \delta(r_{ij}) \right]. \tag{3.45}$$

As we will see in the next section, the perturbative treatment is essential to achieve renormalization.

In this work we will not go beyond NLO. Further corrections to the effective range expansion, such as shape parameters, are of higher orders. Generally, terms that contribute to higher partial waves must be pushed to higher orders since only the s-wave contains poles and therefore the amplitudes are enhanced by a power of $M_{\rm lo}$ (the LO s-wave amplitude scales like $\mathcal{O}(k^{-1})$, NLO like $\mathcal{O}(k^0)$ and so on, see (3.20)). Since there is no enhancement in the p-wave and the p-wave terms contain two derivatives they are N3LO [61]. It follows then that the isospin zero tensor force $C_2^{\text{S-D}}$ is N2LO, because of the enhancement in the s-wave.

The forms of the three- and four-body forces are also easy to guess based on the Lagrangian densities (3.10) and (3.11). In momentum space, their only nontrivial matrix elements are between three-body and four-body states and are equal to the constants D and E, respectively. In coordinate space, the three-body interaction is represented by two delta function acting between each pair of nucleons

$$V_{\rm 3B} \propto \sum_{i<j<k} \sum_{cyc} \delta(r_{ij}) \delta(r_{ik}), \tag{3.46}$$

where $\sum_{cyc}$ is the cyclic sum. Following Ref. [14], the four-body force is written in a hyperradial form

$$V_{\rm 4B} \propto \sum_{i<j<k<l} \delta(r_{ijkl}), \tag{3.47}$$

where $r_{ijkl}^2 = \sum_{a<b\in\{i,j,k,l\}} r_{ab}^2$ is the four particle hyper-radius.

At this point it is not clear at which order of the EFT power counting should these forces enter. The power counting of the two-body interaction was deduced based on relatively simple analytical calculations, but as we

already mentioned, generalization of these calculations to the three- and four-body sectors is rather difficult. We could try to base the power counting on naive dimensional analysis (NDA). The dimension of the non-relativisic nucleonic field N is 3/2 [51], so the three-body interaction has dimension 9 and four-body dimension 12. The NLO derivative two-body interaction is dimension 8, so more-than-two body forces should enter at N2LO. But already at two-body level we have seen that the $\not\pi$EFT power counting needs to be fine-tuned, i.e., one can not rely only on NDA which would not give us the needed resummation at LO. Furthermore, it is not immedietaly clear in which three-body spin-isospin channels should the three-body force act or if we need to consider any isospin-symmetry breaking effects as we did in the two-body sector by treating the *pp* channel seperately.

The two-body power counting is closely tied to renormalization. In the following subsection, we will discuss the connection between renormalization and the potential V and how the power counting can be derived based on potential calculations.

3.3.2 Regularization, Renormalization and Power Counting

When we apply the two-body potentials considered in the previous section in calculations of physical quantities, we run into problems. For example, if we would try to calculate the amplitude using the Lippman-Schwinger equation (1.70) we get

$$T(\boldsymbol{k}) = \langle \boldsymbol{k}_0 | V_{\mathrm{2B}} | \boldsymbol{k}_0 \rangle + \int d^3\boldsymbol{k}' \frac{1}{E - E_{\boldsymbol{k}'}} \langle \boldsymbol{k}_0 | V_{\mathrm{2B}} | \boldsymbol{k}' \rangle \langle \boldsymbol{k}' | \boldsymbol{k}^+ \rangle \,, \tag{3.48}$$

where we have inserted a set of plane wave states $|\boldsymbol{k}'\rangle$, the matrix elements of the potential are given by (3.40). Because $d^3\boldsymbol{k} \propto \boldsymbol{k}^2 dk$ and $E_{\boldsymbol{k}} \propto k^2$ we see that the amplitude diverges for $k \to \infty$ and the divergence gets more severe the more terms of the expansion (3.40) we include. Only the first term on the right side, which corresponds to the first order perturbation theory calculation, is finite. This is however expected, and it is the same situation as we have encountered in Section 3.2.1 - loop diagrams diverge and they need to be regularized. It is consistent with the fact that our effective theory does not describe high energy physics [52]; to obtain convergent amplitudes we need to get rid of high momentum states. One could use e.g. dimensional regularization known from QFT or we could simply introduce a momentum cutoff and integrate up until some finite momentum.

In order to achieve regularization of the Schrödinger equation we modify the potential V directly. The delta function $\delta(r_{ij})$ is substituted for a local

Gaussian regulator

$$\delta(r_{ij}) \to \left(\frac{\Lambda}{2\sqrt{\pi}}\right)^3 e^{-\Lambda^2 r_{ij}^2/4} \equiv \left(\frac{\Lambda}{2\sqrt{\pi}}\right)^3 \delta_\Lambda(r_{ij}), \tag{3.49}$$

where we have introduced the UV momentum cutoff Λ. In this way, we have essentialy smeared the delta function over a distance $1/\Lambda$ and we no longer probe the very short-range physics not described by the theory; in the limit $\Lambda \to \infty$ the original form of the delta function is recovered. Note, that other local and non-local choices of the regular are possible [3], but in the limit of infinite cutoff the delta functions needs to be always recovered. After Fourier transforming the regulator it takes the form e^{-k^2/Λ^2} and it is obvious that the amplitude (3.48) converges.

As we have seen in Section 3.2.1, after regularization the coupling constants C are dependent on the regularization parameter and renormalization is achieved by adjusting them so that the Lagrangian density reproduces physical data, such as the ERE. The story is the same when working with the potential instead of amplitudes and Feynman diagrams; the constants C multiplying the delta functions now must depend on Λ, $C \equiv C(\Lambda)$, and renormalization is achieved by adjusting the LECs of the potential so that it reproduces chosen experimental data.

There are two ways to treat the cutoff dependence and the renormalization of the potential. First is the so called non-perturbative renormalization, where the expansion (3.40) is truncated at some order and plugged into the Schrödinger equation, i.e., the subleading terms are also resummed. However, in this prescription the cutoff can never be varied arbitrarily beyond the breakdown scale, $\Lambda \gg M_{\rm hi}$, because it would lead to effective ranges that behave as $r < 1/\Lambda$ [74]. This would not be consistent with the physical situation of NN scattering, see (3.24), where $r \sim M_{\rm hi}^{-1} = m_\pi^{-1}$.

The reason for this behaviour is the so-called Wigner bound [75]. Derived on the basis of causality, it says that if we have a potential that is zero beyond some interaction range R, then the corresponding phase shifts obey the relation

$$\frac{d\delta}{dk} \geq -R + \frac{1}{2k}\sin(2\delta + 2kR). \tag{3.50}$$

From this inequality the following condition can be derived [74]

$$r_{\rm max}(R, a) \leq 2\left(R - \frac{R^2}{a} + \frac{R^3}{3a^2}\right), \tag{3.51}$$

which gives an upper bound $r_{\rm max}$ for the effective range r as a function of the potential range and the scattering length. Note, that the relations above

need to be modified when the long-range Coulomb interaction is present [76], however, this is not important for the present qualitative discussion. Naturally, we identify $R \sim 1/\Lambda$ and so if we try to remove the cutoff in non-perturbative renormalization by performing the limit $\Lambda \to \infty$, we inevitebly run into Wigner bound and we will never be able to reproduce the physical effective ranges of NN scattering. It is worth noting that this behaviour is not exclusive to $\not\pi$EFT, but to EFT potentials in general; including pion degrees of freedom will not save the situation [77]. Nevertheless, constructing the potential for some finite value $\Lambda < M_{\rm hi}$ is still the most used approach in nuclear physics (see e.g. [3, 40, 48] for χEFT and e.g. [78, 79] for such treatment of $\not\pi$EFT potentials).

Another problem with the non-perturbative approach is that by resumming subleading terms we do not include enough LECs necessary for renormalization. There are two types of terms at any subleading order which we need to take into account - firstly, there are the genuinely new operators that enter at that order, such as the derivative operator related to the effective range which appears at NLO or the tensor force which appears at N2LO. Secondly, there are counterterms which supress regulator dependence. For example, the N2LO $\not\pi$EFT contribution to the spin-singlet s-wave channel is given by iterating the derivative term twice, there are no new operators at this order. However, two new counterterms need to be considered, they have the same form as the constant and derivative terms but their own LECs and ensure that the renormalization conditions are met also at N2LO and no new divergences arise, i.e., the matching to ERE (or other experimental data) needs to be done anew. Only this way can we guarantee that the theory is renormalized at every order. It is said that the EFT is 'power-counting renormalizable'.

In the second renormalization scheme, perturbative renormalization with appropriate power counting, all subleading corrections are treated perturbatively. This leads to the amplitude and other observables being cutoff independent up to residual cutoff dependence which comes from truncating the expansion (3.3) at the given order. Residual cutoff dependence tells us how fast the EFT expansion converges and is improved order by order, i.e., the LO $1/\Lambda$ dependence is removed by NLO terms which give residual dependece $1/\Lambda^2$ and so on. Other sources of cutoff dependence which would lead to divergences are supressed by including the necessary counterterms. So, in general we have

$$\mathscr{M}(\Lambda \to \infty) = \mathscr{M}(\Lambda_0) + \mathcal{O}(\Lambda^{-1}), \tag{3.52}$$

where $\mathscr{M}(\Lambda_0)$ is some observable $\mathscr{M}$ evaluated at $\Lambda_0 > M_{\rm hi}$. In this way renormalization group (RG) invariance is achieved - we are able to remove the artificial regulator dependence since observables can be evaluated at

arbitrarily high cutoff values. We will also not run into issues caused by the Wigner bound, since only the LO interaction which reproduces the scattering length is iterated. Effective range is fixed perturbatively, but this is not forbidden by the Wigner bound.

It needs to be stressed that there is not necceserily the need to perform the limit $\Lambda \to \infty$, all calculations beyond the breakdown scale are equivalent [2]. However, especially in numerical calculations it is useful to vary the cutoff $\Lambda \gg M_{\rm hi}$ and check for RG invariance, since violation of the condition (3.52) hints at missing interactions and thus offers guidance in constructing the power counting [52, 80, 81]. This feature of the EFT is inevitably lost in the non-pertrubative renormalization scheme.

3.3.2.1 Three- and Four-Body Forces

It turns out that the three-body force (3.10) needs to be included at LO to describe a three nucleon system in the spherically symmetric $S = 1/2$, $T = 1/2$ channel in $\not\pi$EFT, despite the fact that according to NDA it should appear at a higher order, as argued above. The reason for this is the so-called Thomas collapse, according to which ^{3}H cannot be described only by a non-derivative short-range interaction, because as the range of the potential is sent to zero, the binding energy diverges [82]. In the spin-quartet channel this is not a problem because all three nucleons have the same spin and Pauli principle forbids them to be at the same point space - details of the short-range physics are then irrelavant. This effect was translated into the language of $\not\pi$EFT in Ref. [83]; they showed that the binding energy grows with incresing cutoff as Λ^2/m and a tower of excited bound states appears near threshold, which is an approximate realization of the Efimov effect [84]. Furthermore, it was shown that the $S = 1/2$ nd s-wave scattering amplitude does not approach a stable limit as the value of the cutoff is increased, hinting at the fact that for this three-nucleon s-wave channel a non-perturbative renormalization is required. This is similar to the case of two-nucleon scattering, where it is needed to reproduce the large scattering lenghts. We write the s-wave leading order three-body force in the form

$$V_{\rm 3B}^{(0)} = D_0^{(0)} \sum_{i<j<k} \sum_{cyc} P_{ijk}^{(1/2,1/2)} \delta_\Lambda(r_{ij}) \delta_\Lambda(r_{ik}), \tag{3.53}$$

where $P_{ijk}^{(1/2,1/2)}$ is a projector onto the three-nucleon spin-doublet, isospin-doublet channel.

It was shown relatively recently in Ref. [85] that, due to the LO Coulomb interaction, an isospin-symmetry breaking three-body force needs to included at NLO. Using strictly perturbative calculations, the authors showed that

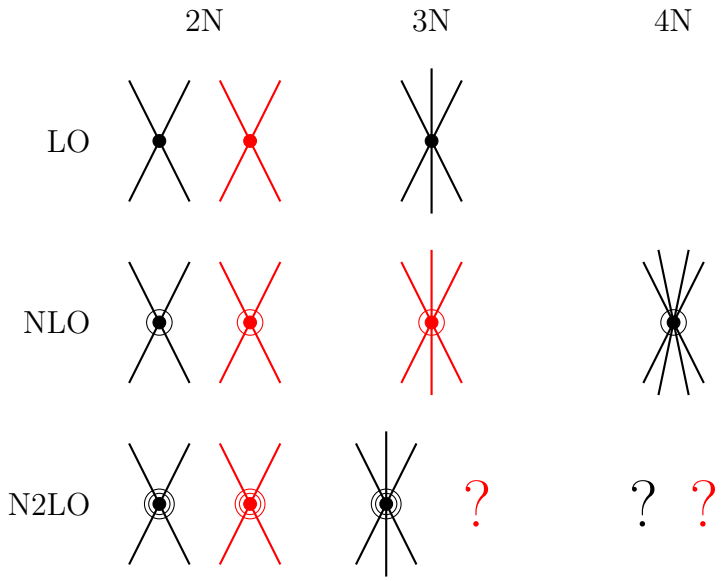

Figure 3.5 Power counting of the $\not\pi$EFT. The isospin-symmetry breaking terms which are due to the non-perturbative inclusion of the Coulomb interaction are drawn in red. The circles denote powers of (Q/M_{hi})

the s-wave pd $S = 1/2$ scattering amplitude and the ^{3}He binding energy are strongly cutoff dependant if this force is not taken into account at NLO. However, no new few-body force is needed at LO. In other words, beyond LO one needs additional input, either experimental or from more fundamental theory, to describe the pd system and its behaviour cannot be inferred just based on the nd system. The new interaction has the same form as the LO $3N$ force

$$V_{\text{3B}}^{(1)} = D_1^{(1)} \sum_{i<j<k} \sum_{cyc} P_{ijk}^{(1/2,\,ppn)} \delta_\Lambda(r_{ij}) \delta_\Lambda(r_{ik}), \tag{3.54}$$

but is projectect exclusively onto the spin-doublet, isospin-doublet ppn channel.

Although in this work we restrict ourselves to NLO, we note that a derivative three-body force enters at N2LO. This was shown in Ref. [86] for spinless bosons, which are equivalent to the three-nucleon system in $S = 1/2$. However, power-counting of the isospin-breaking Coulomb three-body force is not established beyond NLO.

Beyond three nucleons, a four-body non-derivative force given by the Lagrangian density (3.11) is needed at NLO to renormalize the spherically symmetric $(S, T) = (0, 0)$ channel, which was demonstrated for spinless bosons [87] and later for nucleons [14]. Once again, this force appears at a lower order than suggested by dimensional analysis. However, none of these calculations

included the Coulomb interaction. We write this force as

$$V_{\rm 4B}^{(1)} = E_0^{(1)} \sum_{i<j<k<l} P_{ijkl}^{(0,0)} \delta_\Lambda(r_{ijkl}), \tag{3.55}$$

where $r_{ijkl}^2 = \sum_{a<b\in\{i,j,k,l\}} r_{ab}^2$ is the four-particle hyper-radius and $P_{ijkl}^{(0,0)}$ corresponding projector to the four-body $(S,T) = (0,0)$ channel.

Due to lack of perturbative calculations beyond four nucleons (and including Coulomb), conclusions about power counting beyond NLO are difficult to make. The established power counting is summarized in Figure 3.5.

3.3.3 Fitting the Low Energy Constants

In this section, we will explain our way of fitting the LO and NLO coupling constants of the potential. However, before that, let us summarize all the considerations of the previous sections and write out the ≠EFT potential in its full form, we have

$$\begin{aligned}
V_{\not\pi}^{\rm LO} = & \sum_{i<j} \left(C_0^{(0)} P_{ij}^{(nn/pn)} + C_1^{(0)} P_{ij}^{(1,0)} \right) \delta_\Lambda(r_{ij}) + \left(\sum_{i<1} P_{ij}^{(pp)} C_2^{(0)} \delta_\Lambda(r_{ij}) + \frac{e^2}{r_{ij}} \right) + \\
& + \sum_{i<j<k} \sum_{cyc} D_0^{(0)} P_{ijk}^{(1/2,1/2)} \delta_\Lambda(r_{ij}) \delta_\Lambda(r_{ik}) + \\
V_{\not\pi}^{\rm NLO} = & \sum_{i<j} \left(C_0^{(1)} P_{ij}^{(nn/pn)} + C_1^{(1)} P_{ij}^{(1,0)} + C_2^{(1)} P_{ij}^{(pp)} \right) \delta_\Lambda(r_{ij}) + \\
& + \sum_{i<j} \left(C_3^{(1)} P_{ij}^{(nn/pn)} + C_4^{(1)} P_{ij}^{(1,0)} + C_5^{(1)} P_{ij}^{(pp)} \right) \times \left[\delta_\Lambda(r_{ij}) \vec{\nabla}^2 + \overleftarrow{\nabla}^2 \delta_\Lambda(r_{ij}) \right] + \\
& + \sum_{i<j<k} \sum_{cyc} \left(D_0^{(1)} P_{ijk}^{(1/2,pnn)} + D_1^{(1)} P_{ijk}^{(1/2,ppn)} \right) \delta_\Lambda(r_{ij}) \delta_\Lambda(r_{ik}) + \\
& + \sum_{i<j<k<l} E_0^{(1)} P_{ijkl}^{(0,0)} \delta_\Lambda(r_{ijkl}),
\end{aligned} \tag{3.56}$$

where here the projector $P_{ij}^{(nn/pn)}$ projects *exclusively* on the nn/pn spin-singlet, isospin-triplet channel (i.e., pp is excluded) and similarly $P_{ij}^{(pp)}$ projects only onto the spin-singlet, isospin-triplet pp channel. The three-body projectors $P_{ijk}^{(1/2,pnn)}$ and $P_{ijk}^{(1/2,ppn)}$ project only on the three-body pnn and ppn channels, respectively. The first two lines contain the potential $V_{\not\pi}^{\rm LO}$ that is fully iterated. The rest is the NLO potential $V_{\not\pi}^{\rm NLO}$ included as a first order perturbation. Notice also the presence of the counterterms $C_0^{(1)}, C_1^{(1)}, C_2^{(1)}$ and $D_0^{(1)}$, whose role was discussed in the previous section. The regularized delta function is given by Eq. (3.49). The LECs absorb powers of momenta so the potential is in MeV, their units can be found in Appendix C.

3.3.3.1 Leading Order

At LO there are in total four constants that need to be fitted. The two-body LECs $C_0^{(0)}$ and $C_2^{(0)}$ are fitted in free space to reproduce the experimental nn and pp scattering lengths, respectively. Let us explain the procedure on the $C_2^{(0)}$, where the process is a bit more complicated due to the Coulomb interaction. First, the regular solution $\varphi_0(r)$ of the Schrödinger equation (1.1) with $V_s(r) = C_2^{(0)}\delta_\Lambda(r)$ is obtained, where the LEC is now just an initial guess. The numerical solution is carried out using the methods of `Wolfram Mathematica` [88]. To avoid problems with singularities at the origin, the Coulomb potential is regulated with a Gaussian cutoff in momentum space. After Fourier transforming to coordinate space it has the form

$$V_c(r) = \frac{e^2}{r}\mathrm{Erf}(\kappa r), \tag{3.57}$$

where Erf is the error function and κ is an arbitrary regulator (it has nothing to do with the EFT regulators) and is chosen large enough so that the results do not depend on it, usually a few thousand fm^{-1}. Then, the corresponding amplitude due to V_s is evaluated according to equations (1.39) and (1.51)

$$f_0^{\mathrm{LO}}(k) = \frac{\mathfrak{F}_0(-k) - \mathfrak{F}_0(+k)}{2ik\mathfrak{F}_0(+k)}, \tag{3.58}$$

This amplitude is then used to obtain the scattering length, which is easy, since $k\cot\delta$ is given by

$$\mathrm{Re}\left[\frac{e^{2i\sigma_l}}{f_0^{\mathrm{LO}}(k)}\right] = k\cot\delta^{\mathrm{LO}} \tag{3.59}$$

and from there the scattering length

$$C_0^2(\eta)k\cot\delta^{\mathrm{LO}} + 2k\eta h_0 \xrightarrow[k\to 0]{} -\frac{1}{a_{pp}} \tag{3.60}$$

The LEC $C_2^{(0)}$ is varied and this process is repeated until the desired value of a_{pp} is reproduced for a range of cutoff values Λ.

The LEC $C_0^{(0)}$ is fitted in the same way to reproduce the spin-singlet scattering length a_{nn}, only difference is that due to the absence of Coulomb the Eq. (3.58) can be simplified to

$$f_0^{\mathrm{LO}}(k) = -\frac{2\mu}{k\mathfrak{F}_0(k)}\int_0^\infty dr\,\sin(kr)C_0^{(0)}\delta_\Lambda(r)\varphi_0(r) \tag{3.61}$$

and naturally, $k\cot\delta$ does not need to be regularized.

Table 3.1 The two-body LECs and the experimental data to which they are fitted.

LECs	LO exp. datum	NLO exp. datum	Ref.
$C_0^{(0)}$, $C_0^{(1)}$, $C_3^{(1)}$	$a_{nn} = -18.95$ fm	$r_{nn} = 2.75$ fm	[64, 66]
$C_1^{(0)}$, $C_1^{(1)}$, $C_4^{(1)}$	$B_d = 2.2246$ MeV	$\rho_d = 1.765$ fm	[69]
$C_2^{(0)}$, $C_2^{(1)}$, $C_5^{(1)}$	$a_{pp} = -7.8063$ fm	$r_{pp} = 2.794$ fm	[72]

In the spin-triplet channel one can either fit the LEC $C_1^{(0)}$ to the corresponding scattering length or the deuteron binding energy. To better capture the properties of the deuteron already at LO, we choose the latter. The fitting procedure is almost the same, but instead of amplitude the binding energy is calculated. The Schrödinger equation is solved the same way, but we require that the wave function is numerically zero for some large $r = r_{\max}$. The LEC is varied until this requirement is met for the experimental value of the deuteron binding energy. This process is repeated for a range of cutoff values.

The final constant that we need to fit at LO is the three-body force $D_0^{(0)}$. Here, we have two choices of experimental input - either *nd* scattering data or the ^{3}H binding energy. We choose the latter, since we want the few-body scattering results to be a prediction of the theory. Furthermore, with this choice the scattering thresholds are fixed at their experimental values. With the already adjusted two-body LECs, the three-nucleon problem is solved using SVM for an initial guess of the LEC, as explained in Chapter 2. Depending on the resulting binding energy, the LEC is adjusted until the experimental values is reproduced. The few-body calculation has to be repeated for each value of the three-body LEC.

3.3.3.2 Next-to-leading Order

There are 9 new constants at NLO. As we discussed, these terms are added in first order perturbation theory. Let us once again start with the two-body LECs of the *pp* channel, $C_2^{(1)}$ and $C_5^{(1)}$. Firstly, the inverse of the amplitude is Taylor expanded to first order around f^{LO}

$$\frac{1}{f} = \frac{1}{f^{\mathrm{LO}} + f^{\mathrm{NLO}} + \ldots} \approx \frac{1}{f^{\mathrm{LO}}} \left(1 - \frac{f^{\mathrm{NLO}}}{f^{\mathrm{LO}}}\right). \tag{3.62}$$

The real part of this expansion $\mathrm{Re}\,[e^{2i\sigma_0}/f]$ gives us the first order correction to $k \cot \delta$

$$C_0^2(\eta) k \cot(\delta^{\mathrm{LO}} + \delta^{\mathrm{NLO}}) + 2k\eta h_0 \xrightarrow[k\to 0]{} -\frac{1}{a_{pp}} + \frac{1}{2} r_{pp} k^2. \tag{3.63}$$

So to fit the two-body perturbative LECs we need to know the first order perturbative correction to the LO amplitude. This can be calculated using the so-called two-potential formula [20, 21]. The only difference to the standard textbook case is the presence of Coulomb interaction, the resulting expression is

$$f_0^{\mathrm{NLO}}(k) = -\frac{2\mu}{\mathfrak{F}_0(k)} \int_0^\infty dr \varphi_0^{\mathrm{LO}}(r) V^{\mathrm{NLO}}(r) \varphi_0^{\mathrm{LO}}(r), \tag{3.64}$$

where V^{NLO} is the relevant part of the NLO potential and $\varphi_0^{\mathrm{LO}}(r)$ is the LO regular solution obtained in the LO fit. Now, the LECs $C_2^{(1)}$ and $C_5^{(1)}$ must be adjusted so the amplitude $f^{\mathrm{LO}} + f^{\mathrm{NLO}}$ reproduces the desired pp scattering length and effective range on the right-hand side of Eq. (3.63). To compute a_{pp} and r_{pp}, the amplitude needs to be evaluated for atleast two momenta k and the ERE paramaters are then obtained from a polynomial fit of the regularized $k \cot \delta$ dependence. The NLO fit is simpler, since the Schrödinger equation does not need to be solved and not even $f_0^{\mathrm{NLO}}(k)$ needs to be evaluated for every different value of the LECs, since the integral can be split into two, the contribution from the constant and from the derivative terms, and the LECs can be factored out in front of the integral.

The NLO fitting procedure in the other two channels proceeds very similarly. The nn/pn spin singlet channels differ only in the absence of Coulomb. The difference in the spin-triplet channel is that the two constraints at NLO are the deuteron binding energy and the deuteron effective range. So, we must require that the NLO corrections to the bound-state energy $\langle \varphi_0 | V^{\mathrm{NLO}} | \varphi_0 \rangle \,/\, \langle \varphi_0 | \varphi_0 \rangle$ is zero and that the deuteron effective range is reproduced, which are the two conditions needed to fit the two LECs.

The remaining three LECs are the three-body counterterms $D_0^{(1)}$ and $D_1^{(1)}$, and the four-body force $E_0^{(1)}$. The first order correction to the binding energy is given by

$$E^{\mathrm{NLO}} = \frac{\langle \Psi^{\mathrm{LO}} | V^{\mathrm{NLO}} | \Psi^{\mathrm{LO}} \rangle}{\langle \Psi^{\mathrm{LO}} | \Psi^{\mathrm{LO}} \rangle}, \tag{3.65}$$

where Ψ^{LO} is the few-body wave function calculated with the LO potential using SVM. Since we fit the LECs to binding energies of ^{3}H, ^{3}He and ^{4}He, Ψ^{LO} corresponds to one of these nuclei, depending on which LEC is being fitted. The nice thing about the perturbative NLO fit is that the few-body calculation needs to be repeated only once (for every considered cutoff), because Ψ^{LO} is obviously unchanged by the NLO potential. Furthermore, the matrix element (3.65) also does not need to be evaluated more than once, since the corresponding LECs can be factored out in front of the expression. Then, the matrix elements of the Gaussians are evaluated according Appendix B and just a simple linear equation needs to be solved to find the value of

Table 3.2 The three- and four-body LECs and the experimental data to which they are fitted.

LECs	Experimental datum	Ref.
$D_0^{(0)}$, $D_0^{(1)}$	$B_{^3\mathrm{H}} = 8.482$ MeV	[89]
$D_1^{(1)}$	$B_{^3\mathrm{He}} = 7.718$ MeV	[89]
$E_0^{(1)}$	$B_{^4\mathrm{He}} = 28.296$ MeV	[90]

the LEC.

The concrete experimental values used in fits of the LECs with the corresponding references are found in Tables 3.1 and 3.2.

To close out this section, in Figure 3.6 we compare our fit of the two-body *pp* potential to a phase shift analysis. The phase shift predictions of our potential are obtained by extrapoling from the Coulomb-modified ERE (1.50). The leading order calcaulation is denoted by the red band. At LO the effective range is not fixed and decreases with increasing cutoff, this is consistent with the fact the in this case it can be related to the range of the potential $\sim 1/\Lambda$. At the smallest cutoff which we consider, $\Lambda = 1$ fm^{-1}, its value is $r_{pp}(1) = 2.975$ fm and at the highest value which we consider, $\Lambda = 20$ fm^{-1}, $r_{pp}(20) = 0.1$ fm. In the limit of inifinite cutoff it tends to zero, consistent with the Wigner bound. The red band was created by considering all possible effective ranges between zero and 2.975 fm - cutoff variation gives an estimate of the error of the theory.

We see that the theoretical errors of the LO calculation are reasonable up until about 1 MeV, beyond that point the phase shifts cannot be described by a single constant. At NLO the description is much improved and the ERE, i.e. our ⧸EFT potential, gives an excellent agreement with the experimental phase shifts until $E_{cm} = 15$ MeV, which is equal to $E_{\mathrm{lab}} = 30$ MeV. Naturally, the same considerations as for the *pp* channel hold also for the *s*-wave phase shifts in the $S = 0$ *pn* and *nn* channels and as such they do not warrant seperate discussions.

To check the numerical consistency and accuracy of our fit it might be worth it to calculate phase shifts a different way, which does not rely on using the ERE (and the formulas which we used to fit the potential) directly. We have presented such a method in Chapter 1.2, the binding energies in the trap are a genuine prediction of the theory and we may use them to extract phase shifts and the ERE parameters. The Figure 3.7 depicts the bound-state energies of the *pp* system trapped in harmonic oscillator potential, which were obtained by solving the Schrödinger equation with the LO ⧸EFT potential

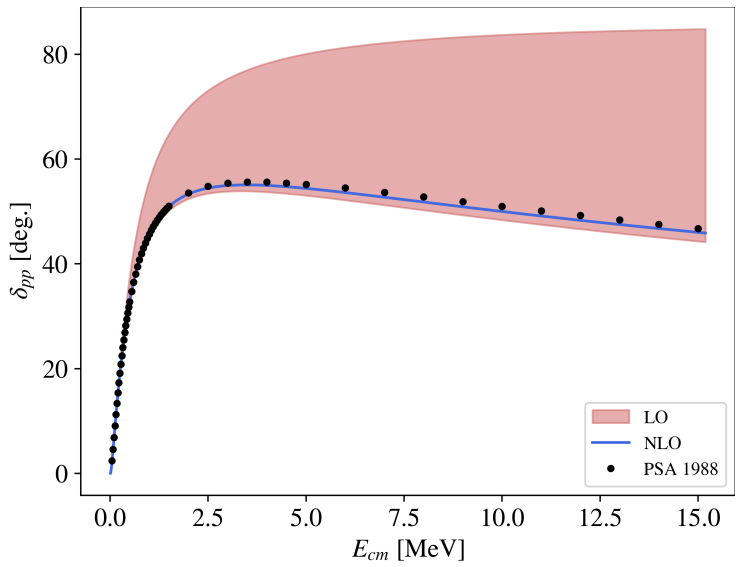

Figure 3.6 Comparison of low-energy pp $s-$wave phase shifts obtained from the phase shift analysis [72] to our LO and NLO $\not\pi$EFT potential.

and the HO potential exactly, the NLO corrections were obtained using (3.65). The leading order shows large cutoff dependence, which is of course expected, but the NLO energies vary by about only 0.01 MeV. These energies are then plugged into the quantization condition (1.95) to obtain phase shifts, which are then fitted by the ERE to obtain the running of the scattering length and effective range.

The running of the pp scattering length and effective range obtained this way are shown in Figure 3.8. In an ideal case, we would expect the dependence of the scattering length to be flat both at LO and at NLO. However, it is difficult to completely avoid numerical errors in this procedure and there are three main sources in this case - first is the error stemming from the numerical solution of the Schrödinger equation; the bound-state energy is obtained by demanding that the wavefunction is zero at a sufficient distance and there is an error stemming from the numerical method itself that solves the equation. However, we expect them to be small, not larger than 10^{-5} MeV, which we checked explicitly by also calculating the two-body energy using SVM. The largest error probably comes from applying the Coulomb-corrected Bush formula, which depends largely on the size of the trap and on the energy used as input, but these errors are difficult to quantify. Lastly, one needs to fit the ERE expansion to the obtained phase shifts, which inherently creates small errors in the ERE parameters. Alltogether, we observe discrepancies in the scattering no larger than 0.01 fm compared to the value used for the

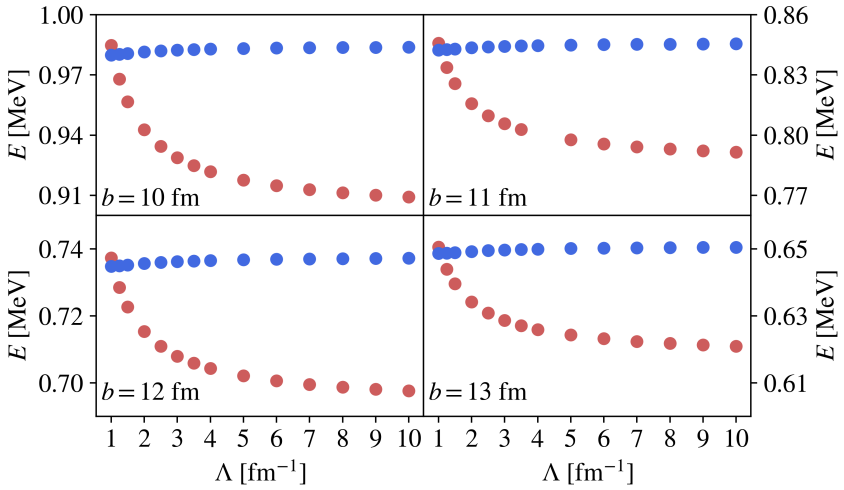

Figure 3.7 Convergence of the bound-state energy for the pp system trapped in a HO trap with four different trap lenghts b as a function of the cutoff. The LO calculations are represented by the red points, the NLO by the blue points.

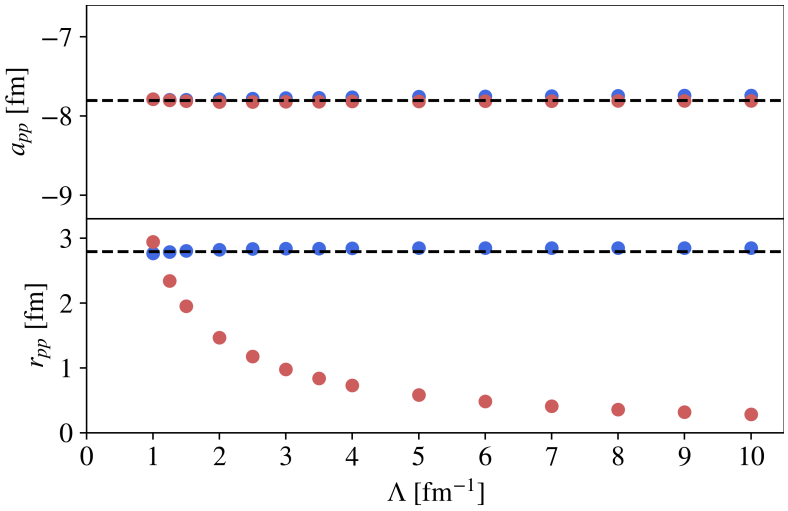

Figure 3.8 The pp scattering lenght (top) and effective range (bottom), obtained by trapping the system in an HO trap and using the quantization condition to calculate s-wave phase shifts, as functions of the cutoff. The LO calculations are represented by the red points, the NLO by the blue points, the dashed lines depict the values of ERE used to fit the $\not\pi$EFT potential.

fit (dashed lined in the figure). The same is true for the effective range at NLO, at LO the effective range is not fixed and tends to zero with increasing cutoffs, as was discussed earlier.

Overall, we conclude that our potential reproduces s-wave phase shifts very accurately up to $E_{\rm lab} = 30$ MeV, presumably even for energies a few MeV higher.

Chapter 4

Few-Nucleon Scattering Results

In this chapter, we apply the few-body scattering method developed in Chapter 1 and the potential constructed in Chapter 3 in a study of few-body nuclear systems. We investigate in detail various possible s-wave configurations of three and four nucleons up to next-to-leading order of $\not\pi$EFT. These include the bound states of the helion (^{3}He) and the alpha particle (^{4}He), proton-deuteron (pd) scattering in the elastic spin-doublet ($S = 1/2$) and spin-quartet ($S = 3/2$) channels, deuteron-deuteron (dd) scattering in the spin-quintet ($S = 2$) elastic channel and proton-helion (p^3He) scattering in the spin-singlet ($S = 0$) and triplet ($S = 1$) elastic channels. The nd and n^3H scattering was already treated in Ref. [14] and as such it is not studied here; we concentrate on the channels where the Coulomb interaction and its effects on the NN potential are relevant, as explained in the previous chapter. A more comprehensive study would need to include also various rearengement and breakup channels, however, these are currently out of scope of this work. This is especially relevant for coupled-channel n^3He and p^3H scattering, which is left for future studies.

Using the perturbative renormalization scheme, as presented in the previous chapter, we perform calculations with cutoffs up to $\Lambda = 10$ fm^{-1}, or up to $\Lambda = 20$ fm^{-1} in the case of ^{3}He and ^{4}He bound states and spin-doublet pd scattering. These values are well beyond the breakdown scale of the $\not\pi$EFT set by the pion mass, which allows us to verify the power-counting of our potential (3.56). Furthermore, by studying residual (i.e., beyond the breakdown scale) cutoff dependence, we are able to estimate the theoretical error of our results caused by truncating the EFT expansion (3.4) at LO or NLO.

The binding energies of nuclei are calculated using the SVM, as presented in Chapter 2. Perturbative corrections to the energies are obtained using the relation (3.65). In case of scattering calculations, the binding energies of the system trapped in a HO potential are calculated the same way and serve as

input into the quantization condition (1.95), where the Green's function are generally obtained by matrix inversion, i.e., using (1.121).

4.1 Three Nucleons

4.1.1 Binding Energy of ^{3}He

First, we study the binding energy of the helion in order to verify our power counting scheme. The ^{3}He is the lightest nucleus where we can observe the effects of the inclusion of the Coulomb interaction in the *pp* channel (3.43) and more importantly verify that the NLO *ppn* isospin-symmetry breaking interaction (3.54) is needed for renormalization.

The Figure 4.1 shows our results for the binding energy of ^{3}He for cutoffs in the range $\Lambda \in [1, 20]$ fm^{-1}. At leading order, all two-body forces are relevant, that is $C_0^{(0)}$, $C_1^{(0)}$ and $C_2^{(0)}$, as well as the three-body force $D_0^{(0)}$ adjusted to the ^{3}H ground-state binding energy. We observe that once the cutoff is much larger than the breakdown scale, the $B(^3\text{He})$ at LO (red points) converges as its value is increased. This is not surprising, from Eq. (3.52) we know that the residual cutoff dependence should behave like $\mathcal{O}(1/\Lambda)$. Consequently, we extrapolate $B(^3\text{He})$ to the zero-range limit $\Lambda \to \infty$ using the function

$$\mathfrak{M}(\Lambda) = \mathfrak{M}(\infty) + \frac{c}{\Lambda}, \tag{4.1}$$

where $\mathfrak{M}$ represents an observable, in this case the binding energy. The zero-range limit extrapolated value $\mathfrak{M}(\infty)$ and the constant c are determined by the fitting procedure. In general, Eq. (3.52) holds only for $\Lambda \gg M_{\text{hi}}$ and therefore only cutoffs $\Lambda \geq 4\,\text{fm}^{-1}$ are considered in the fit. The extrapolated LO binding energy then reads $B(^3\text{He}; \infty) = 7.7085(4)$ MeV , where the error is the statistical unceirtanty of the fit. This value is in excellent agreement with the experimental datum 7.718 MeV [89], however, it needs to be noted that each of the results beyond the breakdown scale is equivalent from the EFT point of view. The value of $B(^3\text{He})$ with the error estimated as the maximum spread of the energy with respect to the LO cutoff dependence is $B(^3\text{He}) = 7.80(9)$ MeV.

We also note that we have performed a similar calculation without the LO *pp* force $C_2^{(0)}$ but with the Coulomb interaction still included (purple points in Figure 4.1), meaning the *pp* and the *pn*/*nn* channel in the spin-singlet channel have the same LEC, adjusted to the *nn* scattering length a_{nn}. We have found the $C_2^{(0)}$ term to be necessary for renormalization of ^{3}He, i.e. one does not get a converging binding energy without it. This is in agreement with Ref. [91].

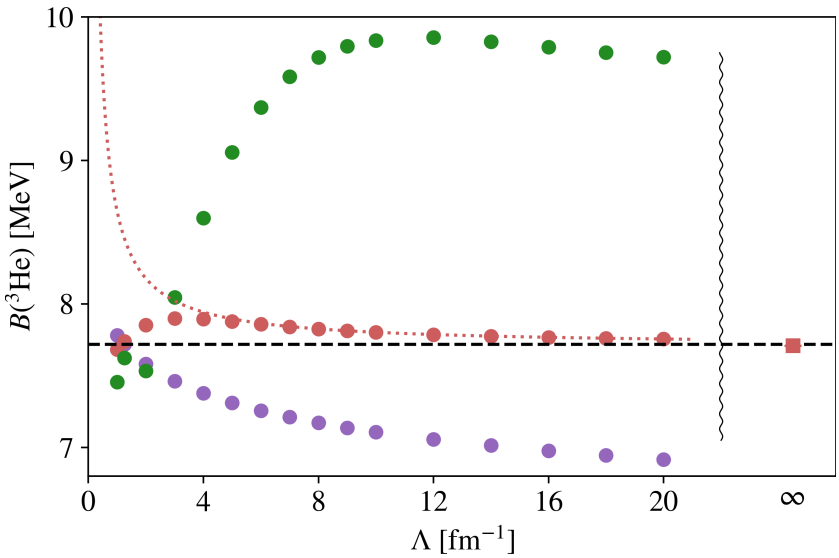

Figure 4.1 The calculated binding energy of ^{3}He, $B(^3\mathrm{He})$, as a function of the momentum cutoff Λ. The red points denote the LO calculation. The green points represent the NLO calculation, when the isospin-symmetry breaking three-body force emerging at NLO is not taken into account. The purple points are a LO calculation with a potential that treats the pp channel on equal footing with the other spin-singlet channels (pn/nn), and Coulomb is added without any modifications to the strong interaction. The wavy line seperates the LO extrapolated value at $\Lambda \to \infty$, denoted by the red square, from the finite-cutoff results. The dotted line represents the fitted extrapolating function, Eq. (4.1). The dashed line shows the experimental value.

According to the power counting, we need to include a new type of three-body force which distinguishes between ^{3}H and ^{3}He at NLO. To test this assumption, we calculated the NLO binding energy of the helion without the three-body isospin-symmetry breaking term $D_1^{(1)}$. While for cutoffs below 1.5 fm^{-1} the predictions are reasonable, as we increase Λ the energy grows rapidly reaching values of almost 10 MeV and then steadily declines. This is in contradiction with the assertion of Eq. (3.52) that, under an appropriate power counting, residual cutoff dependence should behave as $\mathcal{O}(1/\Lambda)$ and suggests our Lagrangian density is lacking terms necessary to achieve proper renormalization and RG-invariance. We have thus come to the same conclusion as the authors of Ref. [92], where the binding energy of ^{3}He was calculated analytically using the dibaryon formalism.

4.1.2 Proton Scattering off the Deuteron

Low-energy three-nucleon scattering is of lasting interest in nuclear physics and has been studied for decades using various potential models, see e.g. [93]

and references therein. For example, only very recently has the longstanding A_y puzzle been seemingly solved by considering three-body contact terms that appear at N3LO of χEFT [9], which speaks for the importance of the contact interactions for low-energy observables. Moreover, there is a large discrepancy between different phase shift analysis (PSA) predictions of the pd quartet scattering length. While the 1974 analysis [94] yields the value $a_{pd}^{3/2} = 11.88^{+0.4}_{-0.1}$ fm and the 1983 predicts $a_{pd}^{3/2} = 11.11^{+0.25}_{-0.24}$ fm [95], the most recent 1999 prediction $a_{pd}^{3/2} = 14.7(2.3)$ fm [96] differs significantly. The $a_{pd}^{3/2}$ scattering length therefore presents an important testing ground for nuclear EFTs and potential models.

The predictions of various interactions, be it purely phenomenological like AV18 or inspired by χEFT, are consistent and the values hover around $a_{pd}^{3/2} = 13.6$ fm [6, 93, 97]. Hence, they agree with the most recent 1999 analysis. The pd quartet scattering length was also studied at N2LO of $\not\pi$EFT by Konig et al. [98]. They obtained the value $a_{pd}^{3/2} = 10.9(4)$ fm, contradicting the PSA. However, they argue that the discrepancy comes from different subtraction schemes of Coulomb effects in the considered Feynman diagrams. This means that the scattering length they extract is not equivalent to the one obtained by the Coulomb-modified ERE of Eq. (1.49).

Our LO and NLO $\not\pi$EFT results for $a_{pd}^{3/2}$ are depicted in Figure 4.2 as functions of the cutoff. They were extracted by calculating the binding energies of the pd system trapped in HO potentials with lengths approximately $b \in [13.84, 45.52]$ fm, which give scattering energies E_{cm} between 0.1 to 1 MeV. Using the quantization condition, phase shifts were extracted from the calculated energies and fitted by the Coulomb ERE of Eq. (1.49). According to the adapted $\not\pi$EFT power counting, the three-body force terms D are not needed in the spin-quartet channel. The same is true for the two-body forces projected to the spin singlet channels, so none of the terms stemming from the inclusion of the Coulomb potential contribute in this case. Unsurprisingly, the well-established two-body power counting shows no deviations from the expected cutoff dependence. The LO residual cutoff dependence is quite large and the theoretical error of the LO prediction is thus significant. This is, however, in line with the fact that $\not\pi$EFT is an expansion in the small parameter r_{pn}/a_{pn}, see e.g. Eq. (3.27) or Eq. (3.20), and as such an error of about 30% is expected at LO.

Extrapolation of NLO proceeds similarly to LO, except now the residual cutoff dependence should be proportional to $1/\Lambda^2$. The extrapolating function then has the form

$$\mathfrak{M}(\Lambda) = \mathfrak{M}(\infty) + \frac{c}{\Lambda^2}, \tag{4.2}$$

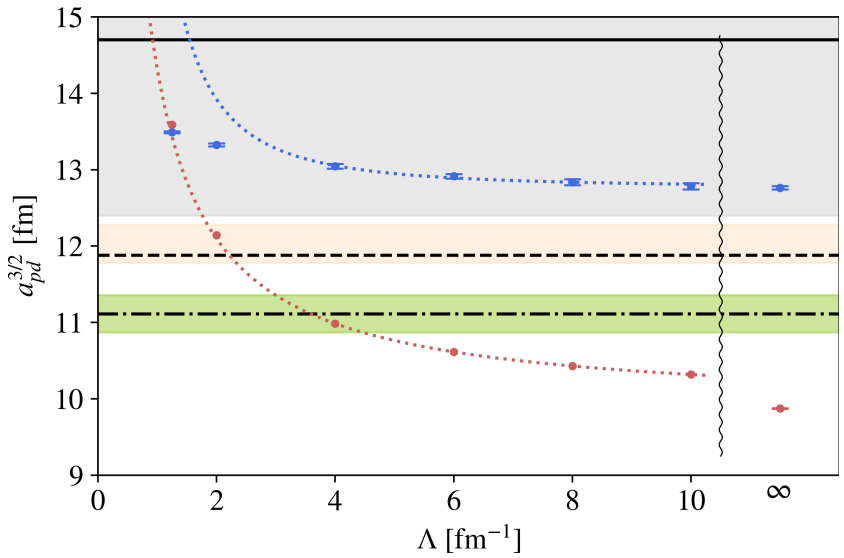

Figure 4.2 The pd scattering length in the $S = 3/2$ channel as a function of the cutoff Λ. The LO results are denoted by the red points, the NLO by the blue points. Corresponding extrapolations at $\Lambda \to \infty$ are seperated from the rest of the calculations by the wavy line. The dotted red and blue lines denote the extrapolating functions Eq. (4.1) and Eq. (4.2), respectively. The solid black line and the grey band represent the most recent experimental value and its error from the 1999 phase shift analysis [96], the dashed-dotted line and green band the 1983 phase shift analysis [95] and the dashed line and light orange band the 1974 phase shift analysis value [94].

where $\mathfrak{M}(\Lambda)$ and c have the same meaning as in Eq. (4.1). Just like at LO, we generally fit from $\Lambda = 4$ fm^{-1}. We obtain the NLO result $a_{pd}^{3/2} = 13.13(37)$ fm, where the error comes from the residual cutoff dependence (errors from fits of the ERE to the phase shifts are negligible) and is consistent with the naive NLO unceirtanty estimate $(r_{pn}/a_{pn})^2 \sim 9\%$. Our prediction thus agrees with the most recent phase shift analysis and is close to the predictions of potential models.

Nucleon-deuteron scattering in the spin-doublet channel is characteristic by having an 'anomalous' effective range expansion. In general, it may happen that the amplitude vanishes for some complex k at some point other than the origin. Consequently, the phase shift is zero at this point and the convergence radius of the $k \cot \delta$ Taylor series is limited by the absolute value $k_0 = |k|$. In spin doublet Nd scattering, k_0 happens to be so small that the usual effective range expansion defined by Eq. (1.50) is no longer a useful parametrization

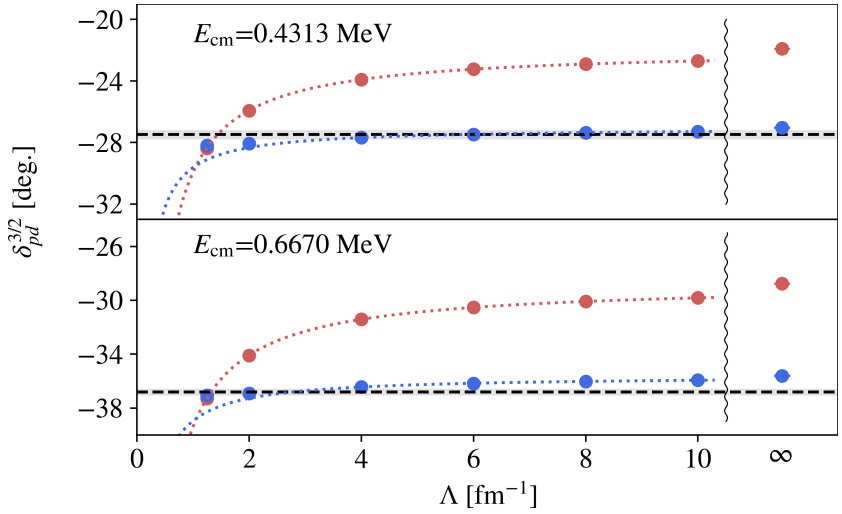

Figure 4.3 The calculated s-wave pd scattering phase shifts in the $S = 3/2$ channel as a function of the cutoff Λ. The LO results are denoted by the red points, the NLO by the blue points. Corresponding extrapolations at $\Lambda \to \infty$ are seperated from the rest of the calculations by the wavy line. The dotted red and blue lines denote the extrapolating functions. The dashed line denotes the result of the PSA [102], where its errors are given by the grey bands.

of the scattering data. The expansion

$$\varkappa_l(\eta) = \frac{-1/a + 1/2rk^2}{1 \pm k^2/k_0^2}, \tag{4.3}$$

needs to be used instead [99, 100, 101]. The sign in the denominator is plus if the pole is in the positive-mometum plane and minus otherwise.

The nd scattering length was already studied in NLO $\not\pi$EFT in Ref. [14] and the authors found the predictions to be in good agreement with the experimental value and other theoretical predictions which hower around $a_{nd}^{1/2} = 0.65$ fm. However, the pd doublet scattering length is even harder to determine since the pole is very close to the pd threshold and extremely precise calculations (or measurements) for energies less than 0.1 MeV are needed to pinpoint its precise position [96]. Currently, experimental $a_{pd}^{1/2}$ predictions are not accurate [96] and theoretical results for various potentials contradict each other [6, 93]. It is not even clear whether the scattering length is positive or negative, but its value should be very close to zero. We made attempts to fit the modified ERE (4.3) to our phase shift calculations in the energy region $E_{\rm cm} \in [0.1, 1]$ MeV, but we were not able to pinpoint the pole position precisely and obtain precise values of the ERE parameters which would not be weighed by large systematic errors. For these reasons we do

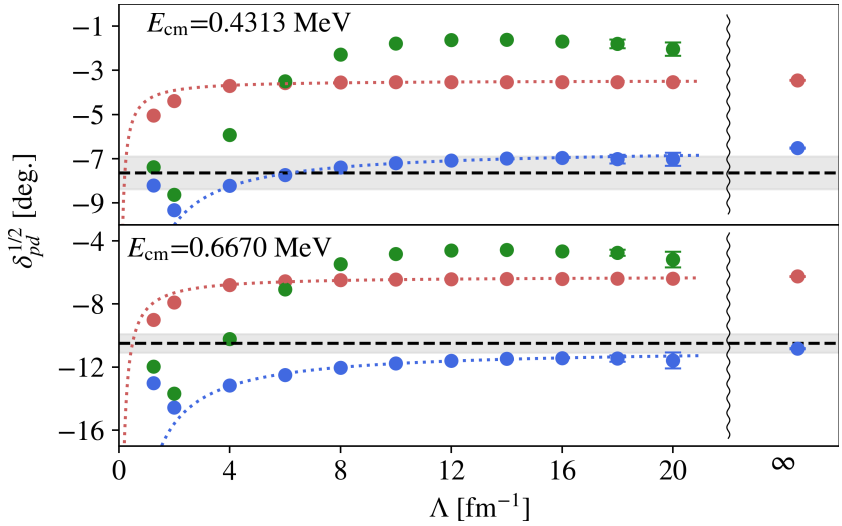

Figure 4.4 The pd s-wave scattering phase shifts in the $S = 1/2$ channel as a function of the cutoff Λ. The green points denote the NLO calculation without the new isospin-symmetry-breaking force emerging at NLO. The rest of the symbols have the same meaning as in Figure 4.3.

not compare the doublet length $a_{pd}^{1/2}$ to other calculations and experiments. Rather, we restrict our comparison with experimental data only to phase shifts.

Our results for the spin-quartet and spin-doublet s-wave phase shifts as functions of the cutoff Λ are shown in Figures 4.3 and 4.4, respectively. Here, calculations for two different center-of-mass energies E_{cm} are presented and compared to values from the PSA [102]. At NLO, the agreement with experimental data for both energies is excellent in the $S = 3/2$ channel, with a theoretical error estimated from the residual cutoff dependence being only about 1.5 degrees. Compared to the spin-quartet, the calculations for the spin-doublet are a bit more involved, since now pairs of nucleons can couple to the total two-body spin either $S = 1$ or $S = 0$, which means that all types of the two-body contact terms need to be included. Furthermore, the LO three-body force and the NLO ppn are required. Consequently, we can test if the NLO isospin-symmetry breaking three-body force correctly renormalizes the calculated phase shift. The calculations without this interaction are represented by the green points in Figure 4.4. Similarly to the binding energy of ^{3}He in Figure 4.1, the value of the phase shift rises with the cutoff up to $\Lambda = 12$ fm^{-1}, then steadily declines and does not converge. In contrast, the LO and NLO calculation which include all forces mandated by the power counting show the expected $\mathcal{O}(1/\Lambda)$ dependence on residual cutoff.

Table 4.1 Our results for the *ppn* observables, for details see the text.

Channel	Observable	LO $\not\pi$EFT	NLO $\not\pi$EFT	Experiment	Ref.
$S = 1/2$	$B(^3\mathrm{He})$	7.80(9) MeV	7.718 MeV (fit)	7.718 MeV	[89]
$S = 1/2$	$\delta_{pd}(0.4313)$	$-4.25(79)^\circ$	$-7.9(1.4)^\circ$	$-7.64(74)^\circ$	[102]
$S = 1/2$	$\delta_{pd}(0.6670)$	$-7.6(1.3)^\circ$	$-12.2(1.4)$	$-10.50(59)^\circ$	[102]
$S = 3/2$	$\delta_{pd}(0.4313)$	$-25.1(3.2)^\circ$	$-27.96(91)^\circ$	$-27.48(25)^\circ$	[102]
$S = 3/2$	$\delta_{pd}(0.6679)$	$-33.0(4.2)^\circ$	$-36.33(73)^\circ$	$-36.81(19)^\circ$	[102]
$S = 3/2$	a_{pd}	11.7(1.8) fm	13.13(37) fm	14.7(2.3) fm	[96]

Interestingly, compared to the spin-quartet calculations, the spin-doublet phase shifts at NLO are more dependent on the cutoff, with a theoretical error of about 3 degrees for both energies, which means that pd $S = 1/2$ s-wave scattering phase shifts converge rather slowly within the EFT expansion. Similar behaviour was discussed by Vanasse et al. in Ref. [92], where analytical calculations of pd scattering observables were performed. The authors concluded that the inclusion of a NLO *ppn* force leads to larger cutoff dependence in this channel.

We note that the larger error bars of the values for $\Lambda = 18$ fm^{-1} and $\Lambda = 20$ fm^{-1} in Figure 4.4 are because these calculations were not fully converged with respect to the size of the CG basis and had to be extrapolated. Our results for all considered three-nucleon channels are summarized in Table 4.1.

4.2 Four Nucleons

4.2.1 Binding Energy of ^{4}He

The Figure 4.5 shows the calculated LO and NLO binding energies of ^{4}He as functions of the cutoff. Our results might be compared to those of Ref. [14], except here we consider the nonperturbative Coulomb potential and the necessary isospin-symmetry breaking terms in the nuclear interaction. We observe that at LO it converges to the value $B(^4\mathrm{He}) = 28.11(3)$ MeV obtained using Eq. (4.1), where the error here is of statistical nature and stems from the extrapolation. This value is in good agreement with the experimental one 28.296 MeV [90], but once again we have to keep in mind the LO uncertainty based on the residual cutoff dependence, which is about 5 MeV. The green points in Figure 4.5 depict NLO values calculated without the four-body force given by Eq. (3.55). As expected based on Refs. [14, 87], a four-body

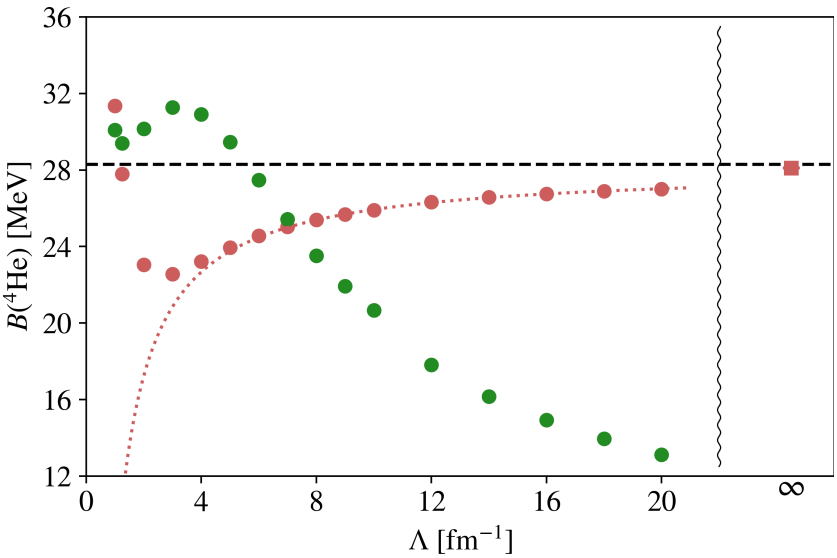

Figure 4.5 The binding energy of ^{4}He, $B(^4\mathrm{He})$, as a function of the momentum cutoff Λ. The red points represent the LO results and the green points the NLO without the perturbative four-body force. The red dotted line denotes the corresponding extrapolating functions and the extrapolated value in the infinite-cutoff limit is depicted by the red square on the right side of the squiggly line. The dashed line depicts the experimental datum.

force is needed to properly renormalize the four-nucleon system at NLO. The inclusion of the Coulomb interaction does not affect this requirement in any way.

4.2.2 Scattering of Two Deuterons

There are no experimental data concerning low-energy elastic deuteron-deuteron scattering in the $S = 2$ channel below the break-up threshold. From the theoretical side, dd s-wave scattering in the spin-quintet channel was investigated using the Faddeev-Yakubovsky equations with a phenomenological potential in Refs. [103, 104]. In the first reference, a simple Gaussian potential was employed and the reported value of the scattering length was $a_{dd}^2 = 7.8(3)$ fm. In the second reference, a Yukawa-type potential was used, the so called MT-I/III [105]. The reported scattering length was $a_{dd}^2 = 7.5$ fm.

Our results for the dd scattering length and effective range in the $S = 2$ channel at LO and NLO of $\not\pi$EFT are shown in Figure 4.6. Here, all nucleon pairs must couple to $S = 1$ and consequently only the terms $C_1^{(0)}$, $C_1^{(1)}$

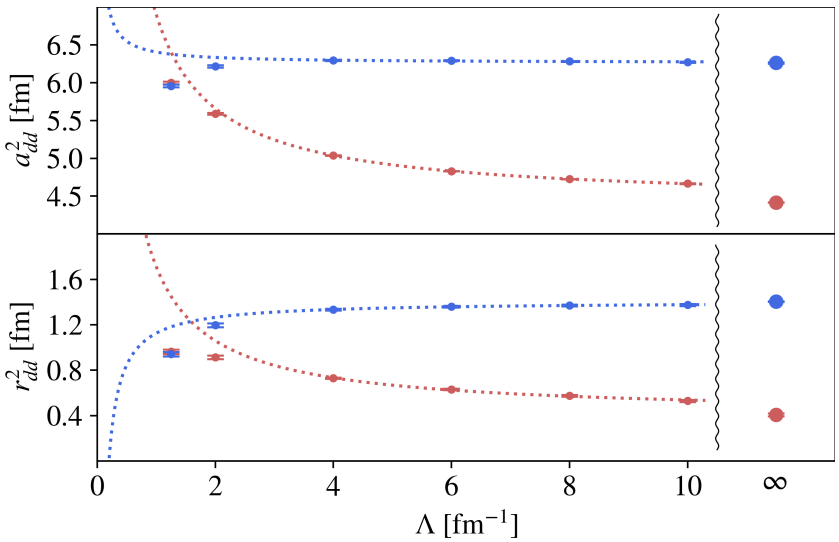

Figure 4.6 The LO and NLO scattering length and effective range of dd in the $S = 2$ channel as a function of momentum cutoff. The notation is the same as in Figure 4.2.

and $C_4^{(1)}$ contribute to this calculation. In this regard, the situation is thus somewhat similar to the pd spin quartet scattering. The final values of the ERE parameters with errors given by the residual cutoff dependence are at LO

$$a_{dd}^2 = 5.21(80)\,\text{fm}, \quad r_{dd}^2 = 0.68(28)\,\text{fm}, \tag{4.4}$$

and at NLO read

$$a_{dd}^2 = 6.13(17)\,\text{fm}, \quad r_{dd}^2 = 1.17(23)\,\text{fm}. \tag{4.5}$$

They are thus in a small disagreement in comparison with the other theoretical calculations.

4.2.3 Proton Scattering off ^{3}He

Much like the three-body pd scattering, the four-body problem of scattering protons off ^{3}He has presented an important challenge for nuclear forces. Just like pd scattering, it serves as an important benchmark for especially the three-body nuclear interaction. Throughout the last few decades, various methods in combination with phenomenological as well as χEFT potentials have been used in its treatment. Notably, calculations using the Alt-Grassberger-Sandhas (AGS) equations with screened and renormalized Coulomb potential and various realistic $2N$ interactions were performed in Refs. [106, 107], the results were found to be potential model dependent. Furthermore, hyperspherical

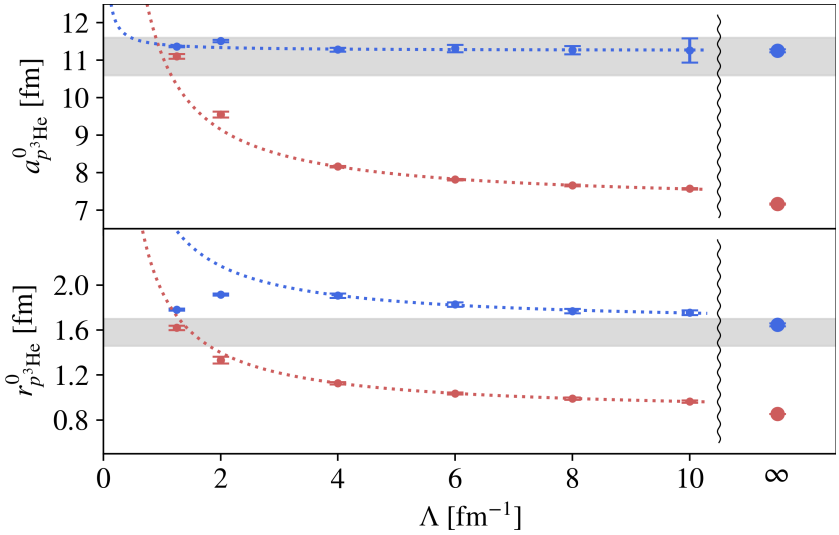

Figure 4.7 The LO and NLO scattering length and effective range of p^3He scattering in the $S = 0$ channel. The symbols have the same meaning as in Figure 4.2. The grey bands represent the results of the PSA [113].

harmonics with Kohn variational principle and $2N$ as well as $3N$ interactions were applied to this problem in Refs. [6, 10, 93, 108]. In the references [10, 108] the effect of N2LO χEFT and AV18-IL7 $3N$ forces on p^3He scattering observables was investigated. Faddeev-Yakubovsky calculations can be found in Ref. [109], where the three aforementioned methods were benchmarked with various nuclear potentials. Zero-energy p^3He scattering was studied using the correlated hyperspherical harmonics approach and Kohn variational principle with the $2N$ AV18 and $3N$ AV18 + Urbana model IX interactions in Ref. [110]. Some older calculations of scattering lengths are summarized in Ref. [111]. Last but not least, p^3He scattering was also studied at LO $\not\pi$EFT using the RGM method in Ref. [112].

Together with the apparent interest of the theoretical community in p^3He scattering, there is also a large set of experimental data available (see e.g. the references in [10]). Naturally, of particular interest to us are the scattering lengths determined from the experimental data. As of right now, the most recent phase shift analysis (PSA) was performed by Daniels et al. in Ref. [113]. They obtained the ERE parameters $a^0_{p^3\mathrm{He}} = 11.1(5)\,\mathrm{fm}$, $r^0_{p^3\mathrm{He}} = 1.58(12)\,\mathrm{fm}$ in the spin-singlet channel and $a^1_{p^3\mathrm{He}} = 9.04(14)\,\mathrm{fm}$, $r^1_{p^3\mathrm{He}} = 1.50(6)\,\mathrm{fm}$ in the spin-triplet channel. Older analyses are available in Refs. [114, 115, 116], but due to lack of experimental data at that time, there are large discrepancies in the obtained scattering lengths.

Our $\not\pi$EFT results for the ERE parameters in spin-singlet and spin-triplet

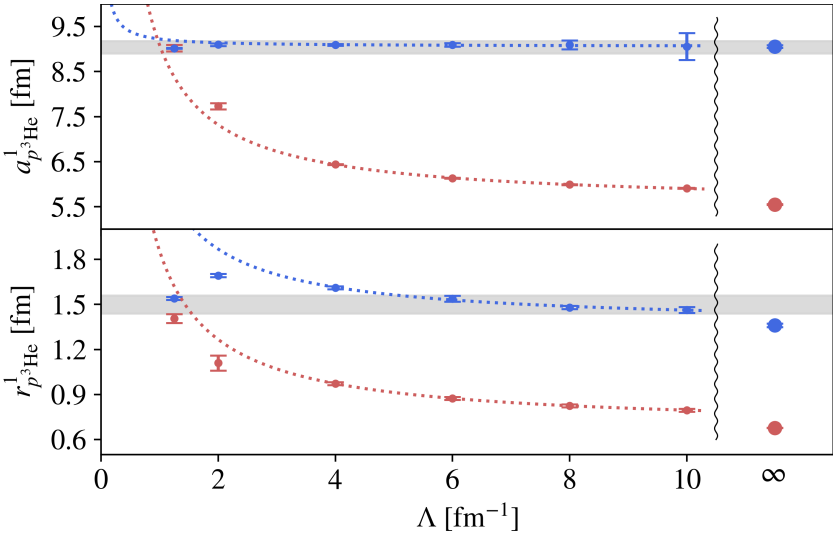

Figure 4.8 The LO and NLO scattering length and effective range of p^3He scattering in the $S = 1$ channel. The symbols have the same meaning as in Figure 4.2. The grey bands represent the results of the PSA [113].

channels are shown in Figures 4.7 and 4.8 as functions of cutoff, respectively. This four-body system is a stringent test of our interaction since, unlike in the case of *dd* scattering, all terms of the potential except the four-body force $E_0^{(1)}$ and the three-body *pnn* force $D_0^{(1)}$ play a role in the calculation. We observe very little cutoff dependence in the two scattering lengths. Especially interesting is the residual cutoff dependence of the $S = 1$ scattering length $a^1_{p^3\mathrm{He}}$ which is almost flat, suggesting that this observable is extremely well-converged already at the next-to-leading order of the ∉EFT expansion. This is further supported by the fact that values for each cutoff sit within the grey band denoting the experimental datum and its error. The same holds for the spin-singlet scattering length, although the cutoff dependence is slightly stronger, calculations for each cutoff are still located within the experimental errors. The residual cutoff dependence of the effective ranges is larger.

The final results for the ERE parameters at LO read

$$a^0_{p^3\mathrm{He}} = 9.1(2.0)\,\mathrm{fm}, \quad r^0_{p^3\mathrm{He}} = 1.24(38)\,\mathrm{fm} \tag{4.6}$$

$$a^1_{p^3\mathrm{He}} = 7.3(1.7)\,\mathrm{fm}, \quad r^1_{p^3\mathrm{He}} = 1.04(36)\,\mathrm{fm}, \tag{4.7}$$

where the errors assessed by residual cutoff dependence are about 23% for both values and agree well with the LO ∉EFT findings calculation of Ref.

[112]. The NLO predictions are

$$a^0_{p^3\mathrm{He}} = 11.40(19)\,\mathrm{fm}, \quad r^0_{p^3\mathrm{He}} = 1.79(14)\,\mathrm{fm}, \tag{4.8}$$

$$a^1_{p^3\mathrm{He}} = 9.20(17)\,\mathrm{fm}, \quad r^1_{p^3\mathrm{He}} = 1.53(17)\,\mathrm{fm}. \tag{4.9}$$

All p^3He sattering lengths and effective ranges are in excellent agreement with the PSA [113].

We insert the calculated values of $a_{p^3\mathrm{He}}$ and $r_{p^3\mathrm{He}}$ into the ERE (1.49) and show the corresponding phase shifts for the spin-singlet and triplet channels in Figures 4.9 and 4.10, respectively. The red and blue bands are constructed by considering all possible values of phase shifts given by the running scattering lenghts and effective ranges - the width of these bands represents the maximum theoretical error estimates stemming from cutoff dependence. The calculated phase shifts are compared to the PSA of Ref. [102] and other theoretical calculations. Taking into account the theoretical unceirtainty, our calculations are in excellent agreement with the experimental phase shifts - NLO $\not\pi$EFT is more accurate for very low energies in contrast to experiments, which are weighted by large errors below 2 MeV due to the strong Coulomb repulsion.

In the spin-singlet channel for energies 3 MeV and below, only the prediction of the non-local two-body $V_{\text{low-k}}$ interaction, which is characterized by almost no repulsion for low momenta [109], agrees with the PSA and our results. The discrepancies of $\not\pi$EFT compared to the predictions of the hard-core AV18 and I-N3LO interactions [109] are about 1 degree at 1.7 MeV. At higher energies, all compared phase shifts are within the NLO uncertainty band. In the spin-triplet channel, the compared calulations seem to be more consistent, but once again only our NLO $\not\pi$EFT calculations and the $V_{\text{low-k}}$ potential are able to reproduce the phase-shifts within experimental errors. However, the predictions of the AV18 and I-N3LO potentials are outside of our NLO uncertainty band only for the lowest energy phase shift. This discrepancy is about 0.7 degrees. Our LO and NLO $\not\pi$EFT results for the four-nucleon observables are summarized in the Table 4.2.

Table 4.2 Results for the four-nucleon observables, details in the text.

Channel	Observable	LO $\not\pi$EFT	NLO $\not\pi$EFT	Experiment	Ref.
$S=0$	$B(^4\mathrm{He})$	25.3(2.8) MeV	28.296 MeV (fit)	28.296 MeV	[90]
$S=0$	$a^0_{p^3\mathrm{He}}$	9.1(2.0) fm	11.40(19) fm	11.1(5) fm	[113]
$S=0$	$r^0_{p^3\mathrm{He}}$	1.24(38) fm	1.79(14) fm	1.58(12) fm	[113]
$S=1$	$a^1_{p^3\mathrm{He}}$	7.3(1.7) fm	9.20(17) fm	9.04(14) fm	[113]
$S=1$	$r^1_{p^3\mathrm{He}}$	1.04(36) fm	1.53(17) fm	1.50(6) fm	[113]
$S=2$	a^2_{dd}	5.21(80) fm	6.11(15) fm	-	-
$S=2$	r^2_{dd}	0.68(28) fm	1.17(23) fm	-	-

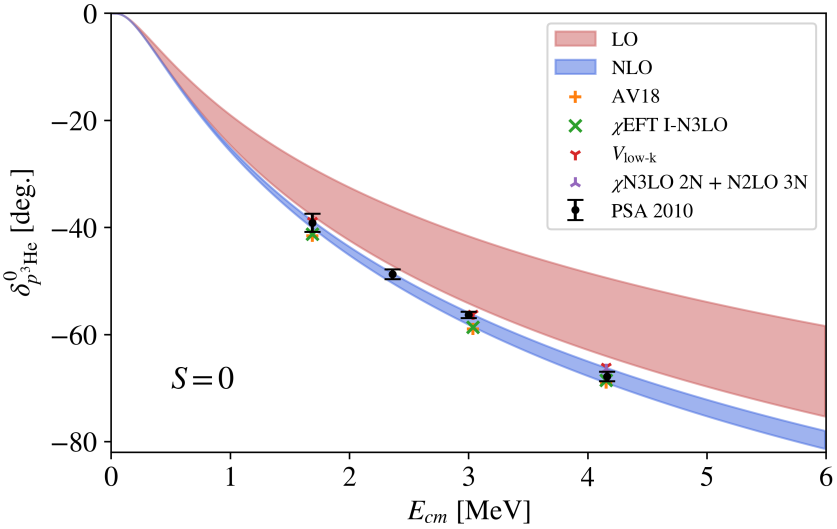

Figure 4.9 The LO (red band) and NLO (blue band) p^3He scattering phase shifts in the $S=0$ channel obtained from the ERE parameters. The black points are the results of the PSA [113]. The results for the I-N3LO, AV18, $V_{\text{low-k}}$ and χEFT N3LO with N2LO three-body force potentials are from Refs. [10, 109].

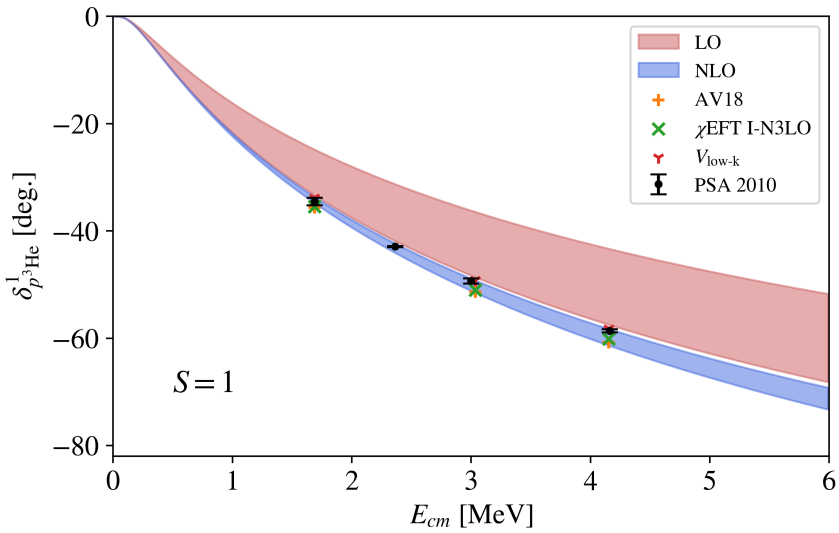

Figure 4.10 The LO (red band) and NLO (blue band) p^3He scattering phase shifts in the $S = 1$ channel obtained from the ERE parameters. The black points are the results of the PSA [113]. The results for the I-N3LO, AV18 and $V_{\text{low-k}}$ potentials are from Refs. [10, 109].

Conclusion

In this work, we explored the applications of the so-called pionless effective field theory ($\not\pi$EFT) to low-energy elastic scattering of systems of up to four nucleons.

To that effect, we devised a robust numerical solution of the quantization condition for charged particle scattering in a harmonic oscillator trap and were the first to apply it to scattering of few-body systems. The usefulness of this part of our work is not limited to only nuclear physics but can be used for extraction of scattering phase shifts of any quantum-mechanical system, where the projectile and target interact through a long-range Coulomb force and a short-range interaction.

Next, we derived a coordinate-space power-counting renormalizable potential up to the next-to-leading order of $\not\pi$EFT. The singular terms stemming from field theory are regularized by local Gaussian regulators. The main feature of our interaction compared to previous studies is that it systematically takes into account the non-perturbative Coulomb interaction and the isospin-symmetry breaking terms of the strong potential which arise because of it. The two-body interaction terms are fitted to repredoce the nn, pp effective range parameters and the deuteron binding energy and effective range; the three-body and four-body forces are adjusted to reproduce the binding energies of the triton, helion and the alpha particle. Subleading terms are included perturbatively, which allows us to vary the regulator cutoff arbitrarily beyond the breakdown scale of the theory set by the pion mass, what would otherwise be impossible due to the Wigner bound. This allows our interaction to have a well-defined power-counting scheme and we also confirm the existence of an isospin-symmetry breaking three-body force at next-to-leading order, which was recently derived in analytical calculations of pd scattering. Moreover, cutoff variation allows to estimate the theoretical error of our calculations.

Lastly, the derived interaction was used in conjunction with the harmonic oscillator trap and Stochastic Variational Method in correlated Gaussian basis to study s-wave elastic scattering of protons and deuterons, protons

and ^{3}He and two deuterons. The calculated phase shifts and effective range expansion parameters were found to be in excellent agreement with available experimental data and most other theoretical calculations. For very low-energy scattering, our potential is able to offer results which are on par or better than phenomenological potentials or interactions inspired by chiral EFT. This is apparent especially in the p^3He scattering case, where the experimental s-wave scattering phase shifts and effective range parameters are reproduced to a high accuracy by our potential and the theoretical errors stemming from the residual cutoff dependence are lower than the experimental unceirtainties.

This bodes well for future studies of nuclear reactions including also rearrangement and breakup channels within the framework of $\not\pi$EFT, which were out of scope of this work. Based on our results, $\not\pi$EFT should be able to offer very precise predictions for reactions relevant to nuclear astrophysics, which currently pose problems for experiments and theory alike.

Naturally, to achieve even higher precision further studies should go beyond NLO. Although some observables are already well-converged at this order, for others like for example the s-wave spin-doublet pd scattering phase shifts this is not the case. However, extending the calculations presented here to N2LO and further is not just a matter of fitting the relevant low-energy constants. Second-order corrections to the energy involve infinite sums over the full spectrum of the Hamiltonian and as such are impractical in many-body calculations. Other methods will have to be developed.

Lastly, in our and other works it was shown that $\not\pi$EFT is able to describe nuclei consisting of four or fewer nucleons, however, calculations for heavier systems are few and far between. Although one would except that as the characteristic momentum of the system increases contributions of pion exchanges will become too important to ignore, the precise limits of the applicability of $\not\pi$EFT are not known and should also be investigated in following studies. To that effect, scattering methods other than the harmonic oscillator (HO) trap which are able to deal with perturbative insertions of subleading potential terms will have to be developed. The usage of HO trap for heavier systems is might be challenging, due to the required precision in calculated bound-state energies.

Bibliography

[1] Heiko Hergert. "A guided tour of ab initio nuclear many-body theory". In: *Frontiers in Physics* 8 (2020), p. 379.

[2] H.-W. Hammer, Sebastian König, and U. van Kolck. "Nuclear effective field theory: Status and perspectives". In: *Rev. Mod. Phys.* 92 (2 2020), p. 025004. DOI: 10.1103/RevModPhys.92.025004.

[3] R. Machleidt and F. Sammarruca. "Recent advances in chiral EFT based nuclear forces and their applications". In: *Progress in Particle and Nuclear Physics* 137 (2024), p. 104117. ISSN: 0146-6410. DOI: https://doi.org/10.1016/j.ppnp.2024.104117.

[4] J Carbonell et al. "Bound state techniques to solve the multiparticle scattering problem". In: *Progress in Particle and Nuclear Physics* 74 (2014), pp. 55–80.

[5] D Baye. "Four-nucleon scattering with a correlated Gaussian basis method". In: *Few-body systems* 52 (2012), pp. 97–123.

[6] Laura E Marcucci et al. "The hyperspherical harmonics method: a tool for testing and improving nuclear interaction models". In: *Frontiers in Physics* 8 (2020), p. 69.

[7] Peng Guo and Bingwei Long. "Nuclear reactions in artificial traps". In: *Journal of Physics G: Nuclear and Particle Physics* 49.5 (2022), p. 055104.

[8] L Girlanda et al. "Short-range three-nucleon interaction from A= 3 data and its hierarchical structure". In: *Physical Review C* 99.5 (2019), p. 054003.

[9] L Girlanda et al. "Effect of the N3LO three-nucleon contact interaction on p-d scattering observables". In: *Physical Review C* 107.6 (2023), p. L061001.

[10] M Viviani et al. "n+ H 3, p+ He 3, p+ H 3, and n+ He 3 scattering with the hyperspherical harmonic method". In: *Physical Review C* 102.3 (2020), p. 034007.

[11] S Kegel et al. “Measurement of the α-particle monopole transition form factor challenges theory: A low-energy puzzle for nuclear forces?” In: *Physical Review Letters* 130.15 (2023), p. 152502.

[12] Petr Navrátil and Sofia Quaglioni. “Ab Initio Nuclear Reaction Theory with Applications to Astrophysics”. In: *Handbook of Nuclear Physics*. Ed. by Isao Tanihata, Hiroshi Toki, and Toshitaka Kajino. Singapore: Springer Nature Singapore, 2020, pp. 1–46. ISBN: 978-981-15-8818-1. DOI: 10.1007/978-981-15-8818-1_7-1.

[13] Brian D. Fields. “Big Bang Nucleosynthesis: Nuclear Physics in the Early Universe”. In: *Handbook of Nuclear Physics*. Ed. by Isao Tanihata, Hiroshi Toki, and Toshitaka Kajino. Singapore: Springer Nature Singapore, 2023, pp. 3379–3405. DOI: 10.1007/978-981-19-6345-2_111.

[14] Martin Schäfer and Betzalel Bazak. “Few-nucleon scattering in pionless effective field theory”. In: *Physical Review C* 107.6 (2023), p. 064001.

[15] Peng Guo. “Coulomb corrections to two-particle interactions in artificial traps”. In: *Physical Review C* 103.6 (2021), p. 064611.

[16] Hantao Zhang et al. “Charged particle scattering in harmonic traps”. In: *Physics Letters B* 850 (2024), p. 138490.

[17] Mirko Bagnarol et al. “Accurate calculation of low energy scattering phase shifts of charged particles in a harmonic oscillator trap”. In: *Physics Letters B* 861 (2025), p. 139230.

[18] Yasuyuki Suzuki and Kálmán Varga. *Stochastic variational approach to quantum-mechanical few-body problems*. Vol. 54. Springer Science & Business Media, 1998.

[19] Hiroyuki Kamada et al. “Benchmark test calculation of a four-nucleon bound state”. In: *Physical Review C* 64.4 (2001), p. 044001.

[20] J.R. Taylor. *Scattering Theory: The Quantum Theory of Nonrelativistic Collisions*. Dover Books on Engineering. Dover Publications, 2012. ISBN: 9780486142074.

[21] R.G. Newton. *Scattering Theory of Waves and Particles*. Theoretical and Mathematical Physics. Springer Berlin Heidelberg, 2013. ISBN: 9783642881282.

[22] *NIST Digital Library of Mathematical Functions*. https://dlmf.nist.gov/, Release 1.2.4 of 2025-03-15. F. W. J. Olver, A. B. Olde Daalhuis, D. W. Lozier, B. I. Schneider, R. F. Boisvert, C. W. Clark, B. R. Miller, B. V. Saunders, H. S. Cohl, and M. A. McClain, eds.

[23] Jos Thijssen. *Computational Physics*. 2nd ed. Cambridge University Press, 2007.

[24] P Descouvemont and D Baye. "The R-matrix theory". In: *Reports on Progress in Physics* 73.3 (2010), p. 036301. DOI: 10.1088/0034-4885/73/3/036301.

[25] Sergei A Rakityansky. *Jost functions in quantum mechanics*. Springer, 2022.

[26] J SCHWINGER. "A VARIATIONAL PRINCIPLE FOR SCATTERING PROBLEMS". English. In: *PHYSICAL REVIEW* 72.8 (1947), p. 742. ISSN: 0031-899X.

[27] H. A. Bethe. "Theory of the Effective Range in Nuclear Scattering". In: *Phys. Rev.* 76 (1 1949), pp. 38–50.

[28] David Gaspard and Jean-Marc Sparenberg. "Effective-range function methods for charged particle collisions". In: *Physical Review C* 97.4 (2018), p. 044003.

[29] DR Thompson, M LeMere, and YC Tang. "Systematic investigation of scattering problems with the resonating-group method". In: *Nuclear Physics A* 286.1 (1977), pp. 53–66.

[30] Thomas Busch et al. "Two cold atoms in a harmonic trap". In: *Foundations of Physics* 28.4 (1998), pp. 549–559.

[31] Akira Suzuki, Yi Liang, and Rajat K Bhaduri. "Two-atom energy spectrum in a harmonic trap near a Feshbach resonance at higher partial waves". In: *Physical Review A—Atomic, Molecular, and Optical Physics* 80.3 (2009), p. 033601.

[32] Xilin Zhang. "Extracting free-space observables from trapped interacting clusters". In: *Physical Review C* 101.5 (2020), p. 051602.

[33] Levere Hostler and R. H. Pratt. "Coulomb Green's Function in Closed Form". In: *Phys. Rev. Lett.* 10 (11 1963), pp. 469–470. DOI: 10.1103/PhysRevLett.10.469.

[34] S. M. Blinder. "Propagators from integral representations of Green's functions for the N-dimensional free-particle, harmonic oscillator and Coulomb problems". In: *Journal of Mathematical Physics* 25.4 (Apr. 1984), pp. 905–909. ISSN: 0022-2488. DOI: 10.1063/1.526245.

[35] Peng Guo and Vladimir Gasparian. "Charged particles interaction in both a finite volume and a uniform magnetic field". In: *Phys. Rev. D* 103 (9 2021), p. 094520. DOI: 10.1103/PhysRevD.103.094520.

[36] Eric W. Weisstein. *Integral Equation Neumann Series. From MathWorld—A Wolfram Web Resource*. Last visited on 10/11/2024. URL: \url{https://mathworld.wolfram.com/IntegralEquationNeumannSeries.html}.

[37] Walter Glöckle. *The quantum mechanical few-body problem*. Springer Science & Business Media, 2012.

[38] S Ali, AAZ Ahmad, and N Ferdous. "A survey of the alpha-nucleon interaction". In: *Reviews of Modern Physics* 57.4 (1985), p. 923.

[39] Jim Mitroy et al. "Theory and application of explicitly correlated Gaussians". In: *Reviews of modern physics* 85.2 (2013), pp. 693–749.

[40] R. Machleidt and D.R. Entem. "Chiral effective field theory and nuclear forces". In: *Physics Reports* 503.1 (2011), pp. 1–75. ISSN: 0370-1573. DOI: https://doi.org/10.1016/j.physrep.2011.02.001.

[41] Hideki Yukawa. "On the Interaction of Elementary Particles. I". In: *Progress of Theoretical Physics Supplement* 1 (Jan. 1955), pp. 1–10. ISSN: 0375-9687. DOI: 10.1143/PTPS.1.1. eprint: https://academic.oup.com/ptps/article-pdf/doi/10.1143/PTPS.1.1/5310694/1-1.pdf.

[42] R. Machleidt. "High-precision, charge-dependent Bonn nucleon-nucleon potential". In: *Phys. Rev. C* 63 (2 2001), p. 024001. DOI: 10.1103/PhysRevC.63.024001.

[43] R. Machleidt, K. Holinde, and Ch. Elster. "The bonn meson-exchange model for the nucleon—nucleon interaction". In: *Physics Reports* 149.1 (1987), pp. 1–89. ISSN: 0370-1573. DOI: https://doi.org/10.1016/S0370-1573(87)80002-9.

[44] Michael E. Peskin and Daniel V. Schroeder. *An Introduction to quantum field theory*. Reading, USA: Addison-Wesley, 1995. ISBN: 978-0-201-50397-5, 978-0-429-50355-9, 978-0-429-49417-8. DOI: 10.1201/9780429503559.

[45] Steven Weinberg. "Nuclear forces from chiral lagrangians". In: *Physics Letters B* 251.2 (1990), pp. 288–292. ISSN: 0370-2693. DOI: https://doi.org/10.1016/0370-2693(90)90938-3.

[46] Steven Weinberg. "Effective chiral lagrangians for nucleon-pion interactions and nuclear forces". In: *Nuclear Physics B* 363.1 (1991), pp. 3–18. ISSN: 0550-3213. DOI: https://doi.org/10.1016/0550-3213(91)90231-L.

[47] Steven Weinberg. "Three-body interactions among nucleons and pions". In: *Physics Letters B* 295.1 (1992), pp. 114–121. ISSN: 0370-2693. DOI: https://doi.org/10.1016/0370-2693(92)90099-P.

[48] D. R. Entem, R. Machleidt, and Y. Nosyk. "High-quality two-nucleon potentials up to fifth order of the chiral expansion". In: *Phys. Rev. C* 96 (2 2017), p. 024004. DOI: 10.1103/PhysRevC.96.024004.

[49] Evgeny Epelbaum, Hermann Krebs, and Patrick Reinert. "High-Precision Nuclear Forces From Chiral EFT: State-of-the-Art, Challenges, and Outlook". In: *Frontiers in Physics* 8 (2020). ISSN: 2296-424X. DOI: 10.3389/fphy.2020.00098.

[50] U. van Kolck. "Effective field theory of short-range forces". In: *Nuclear Physics A* 645.2 (1999), pp. 273–302. ISSN: 0375-9474. DOI: https://doi.org/10.1016/S0375-9474(98)00612-5.

[51] Morten Hjorth-Jensen, Maria Paola Lombardo, and Ubirajara Van Kolck. *An advanced course in computational nuclear physics*. Vol. 936. Springer, 2017.

[52] Peter Lepage. *How to Renormalize the Schrodinger Equation*. 1997. arXiv: nucl-th/9706029 [nucl-th]. URL: https://arxiv.org/abs/nucl-th/9706029.

[53] Steven Weinberg. "Phenomenological Lagrangians". In: *Physica A: Statistical Mechanics and its Applications* 96.1 (1979), pp. 327–340. ISSN: 0378-4371. DOI: https://doi.org/10.1016/0378-4371(79)90223-1.

[54] G. Peter Lepage. *What is Renormalization?* 2005. arXiv: hep-ph/0506330 [hep-ph]. URL: https://arxiv.org/abs/hep-ph/0506330.

[55] Harald W. Grießhammer. "A consistency test of EFT power countings from residual cutoff dependence". In: *European Physical Journal A* 56.4 (2020). DOI: 10.1140/epja/s10050-020-00129-5.

[56] U. van Kolck. "The Problem of Renormalization of Chiral Nuclear Forces". In: *Frontiers in Physics* 8 (2020). ISSN: 2296-424X. DOI: 10.3389/fphy.2020.00079.

[57] Arman Margaryan, Roxanne P Springer, and Jared Vanasse. "nd scattering and the A y puzzle to next-to-next-to-next-to-leading order". In: *Physical Review C* 93.5 (2016), p. 054001.

[58] Andreas Ekström and Lucas Platter. "Quantifying the breakdown scale of pionless effective field theory". In: *Physics Letters B* 860 (2025), p. 139207.

[59] SILAS R. BEANE et al. “FROM HADRONS TO NUCLEI: CROSSING THE BORDER”. In: *At The Frontier of Particle Physics*, pp. 133–269. DOI: 10.1142/9789812810458_0011.

[60] Leslie L. Foldy and Siegfried A. Wouthuysen. “On the Dirac Theory of Spin 1/2 Particles and Its Non-Relativistic Limit”. In: *Phys. Rev.* 78 (1 1950), pp. 29–36. DOI: 10.1103/PhysRev.78.29.

[61] Gautam Rupak. “Precision calculation of np→dγ cross section for big-bang nucleosynthesis”. In: *Nuclear Physics A* 678.4 (2000), pp. 405–423. ISSN: 0375-9474. DOI: https://doi.org/10.1016/S0375-9474(00)00323-7.

[62] Luca Girlanda, A Kievsky, and M Viviani. “Subleading contributions to the three-nucleon contact interaction”. In: *Physical Review C—Nuclear Physics* 84.1 (2011), p. 014001.

[63] David B. Kaplan, Martin J. Savage, and Mark B. Wise. “Two-nucleon systems from effective field theory”. In: *Nuclear Physics B* 534.1 (1998), pp. 329–355. ISSN: 0550-3213. DOI: https://doi.org/10.1016/S0550-3213(98)00440-4.

[64] DE Gonzalez Trotter et al. “Neutron-deuteron breakup experiment at $E_n = 13$ MeV: Determination of the 1 S 0 neutron-neutron scattering length a nn”. In: *Physical Review C—Nuclear Physics* 73.3 (2006), p. 034001.

[65] Robert W Hackenburg. “Neutron-proton effective range parameters and zero-energy shape dependence”. In: *Physical Review C—Nuclear Physics* 73.4 (2006), p. 044002.

[66] Q Chen et al. “Measurement of the neutron-neutron scattering length using the π-d capture reaction”. In: *Physical Review C—Nuclear Physics* 77.5 (2008), p. 054002.

[67] Ulf-G Meißner and Akaki Rusetsky. “Nonrelativistic Effective Theories”. In: *Effective Field Theories*. Cambridge University Press, 2022, 66–160.

[68] David B. Kaplan, Martin J. Savage, and Mark B. Wise. “A new expansion for nucleon-nucleon interactions”. In: *Physics Letters B* 424.3 (1998), pp. 390–396. ISSN: 0370-2693. DOI: https://doi.org/10.1016/S0370-2693(98)00210-X.

[69] J. J. de Swart, C. P. F. Terheggen, and V. G. J. Stoks. *The Low-Energy Neutron-Proton Scattering Parameters and the Deuteron*. 1995. arXiv: nucl-th/9509032 [nucl-th]. URL: https://arxiv.org/abs/nucl-th/9509032.

[70] Xinwei Kong and Finn Ravndal. "Proton–proton scattering lengths from effective field theory". In: *Physics Letters B* 450.4 (1999), pp. 320–324. ISSN: 0370-2693. DOI: https://doi.org/10.1016/S0370-2693(99)00144-6.

[71] Xinwei Kong and Finn Ravndal. "Coulomb effects in low energy proton–proton scattering". In: *Nuclear Physics A* 665.1 (2000), pp. 137–163. ISSN: 0375-9474. DOI: https://doi.org/10.1016/S0375-9474(99)00406-6.

[72] J. R. Bergervoet et al. "Phase shift analysis of 0–30 MeV pp scattering data". In: *Phys. Rev. C* 38 (1 1988), pp. 15–50. DOI: 10.1103/PhysRevC.38.15.

[73] Omar Benhar. "From Yukawa's theory to the one-pion-exchange potential". In: *Writeup of the introductory lecture given by the author on June* 12 (2017), p. 2017.

[74] Daniel R Phillips and Thomas D Cohen. "How short is too short? Constraining zero-range interactions in nucleon-nucleon scattering". In: *Physics Letters B* 390.1-4 (1997), pp. 7–12.

[75] Eugene P Wigner. "Lower limit for the energy derivative of the scattering phase shift". In: *Physical Review* 98.1 (1955), p. 145.

[76] Sebastian König, Dean Lee, and HW Hammer. "Causality constraints for charged particles". In: *Journal of Physics G: Nuclear and Particle Physics* 40.4 (2013), p. 045106.

[77] KA Scaldeferri et al. "Short-range interactions in an effective field theory approach for nucleon-nucleon scattering". In: *Physical Review C* 56.2 (1997), p. 679.

[78] Aaina Bansal et al. "Pion-less effective field theory for atomic nuclei and lattice nuclei". In: *Physical Review C* 98.5 (2018), p. 054301.

[79] Vadim Lensky, Michael C Birse, and Niels R Walet. "Description of light nuclei in pionless effective field theory using the stochastic variational method". In: *Physical Review C* 94.3 (2016), p. 034003.

[80] Bingwei Long and C-J Yang. "Short-range nuclear forces in singlet channels". In: *Physical Review C—Nuclear Physics* 86.2 (2012), p. 024001.

[81] Harald W Grießhammer. "A consistency test of EFT power countings from residual cutoff dependence". In: *The European Physical Journal A* 56.4 (2020), p. 118.

[82] Llewellyn H Thomas. "The interaction between a neutron and a proton and the structure of H 3". In: *Physical review* 47.12 (1935), p. 903.

[83] P.F. Bedaque, H.-W. Hammer, and U. van Kolck. "Effective theory of the triton". In: *Nuclear Physics A* 676.1 (2000), pp. 357–370. ISSN: 0375-9474. DOI: https://doi.org/10.1016/S0375-9474(00)00205-0.

[84] V Efimov. "Energy levels of three resonantly interacting particles". In: *Nuclear Physics A* 210.1 (1973), pp. 157–188.

[85] Jared Vanasse et al. "He 3 and pd scattering to next-to-leading order in pionless effective field theory". In: *Physical Review C* 89.6 (2014), p. 064003.

[86] Chen Ji and Daniel R Phillips. "Effective field theory analysis of three-boson systems at next-to-next-to-leading order". In: *Few-Body Systems* 54.12 (2013), pp. 2317–2355.

[87] Betzalel Bazak et al. "Four-body scale in universal few-boson systems". In: *Physical Review Letters* 122.14 (2019), p. 143001.

[88] Wolfram Research, Inc. *Mathematica, Version 14.2*. Champaign, IL, 2024. URL: https://www.wolfram.com/mathematica.

[89] JE Purcell et al. "Energy levels of light nuclei A= 3". In: *Nuclear Physics A* 848.1-2 (2010), pp. 1–74.

[90] DR Tilley, HR Weller, and Gerald M Hale. "Energy levels of light nuclei A= 4". In: *Nuclear Physics A* 541.1 (1992), pp. 1–104.

[91] J Kirscher and D Gazit. "The Coulomb interaction in Helium-3: Interplay of strong short-range and weak long-range potentials". In: *Physics Letters B* 755 (2016), pp. 253–260.

[92] Jared Vanasse et al. "He 3 and pd scattering to next-to-leading order in pionless effective field theory". In: *Physical Review C* 89.6 (2014), p. 064003.

[93] A Kievsky et al. "A high-precision variational approach to three-and four-nucleon bound and zero-energy scattering states". In: *Journal of Physics G: Nuclear and Particle Physics* 35.6 (2008), p. 063101.

[94] J Arvieux. "Phase-shift analysis of elastic proton-deuteron scattering cross sections and 3He excited states". In: *Nuclear Physics A* 221.2 (1974), pp. 253–268.

[95] E Huttel et al. "Phase-shift analysis of pd elastic scattering below break-up threshold". In: *Nuclear Physics A* 406.3 (1983), pp. 443–455.

[96] Timothy C Black et al. "Determination of proton-deuteron scattering lengths". In: *Physics Letters B* 471.2-3 (1999), pp. 103–107.

[97] C. R. Chen et al. “Nd zero-energy scattering”. In: *Phys. Rev. C* 44 (1 1991), pp. 50–59. DOI: 10.1103/PhysRevC.44.50.

[98] Sebastian König and H.-W. Hammer. “Precision calculation of the quartet-channel $p-d$ scattering length”. In: *Phys. Rev. C* 90 (3 2014), p. 034005. DOI: 10.1103/PhysRevC.90.034005.

[99] D Eyre, AC Phillips, and Frances Roig. “Proton-deuteron scattering near threshold”. In: *Nuclear Physics A* 275.1 (1977), pp. 13–28.

[100] CR Chen et al. “Low-energy nucleon-deuteron scattering”. In: *Physical Review C* 39.4 (1989), p. 1261.

[101] Timothy Charles Black. “Proton-deuteron elastic scattering at very low energy”. PhD thesis. University of North Carolina at Chapel Hill, 1995.

[102] M. H. Wood et al. “Low-energy $p-d$ scattering: High-precision data, comparisons with theory, and phase-shift analyses”. In: *Phys. Rev. C* 65 (3 2002), p. 034002. DOI: 10.1103/PhysRevC.65.034002.

[103] John F. Carew. “Deuteron-deuteron elastic and three- and four-body breakup scattering using the Faddeev-Yakubovskii equations”. In: *Phys. Rev. C* 103 (1 2021), p. 014002. DOI: 10.1103/PhysRevC.103.014002.

[104] IN Filikhin and SL Yakovlev. “Microscopic calculation of low-energy deuteron-deuteron scattering on the basis of the cluster-reduction method”. In: *Physics of Atomic Nuclei* 63 (2000), pp. 216–222.

[105] RA Malfliet and JA Tjon. “Solution of the Faddeev equations for the triton problem using local two-particle interactions”. In: *Nuclear Physics A* 127.1 (1969), pp. 161–168.

[106] A Deltuva and AC Fonseca. “Four-Body Calculation of Proton-He 3 Scattering”. In: *Physical review letters* 98.16 (2007), p. 162502.

[107] A Deltuva and AC Fonseca. “Calculation of proton-3 He elastic scattering between 7 and 35 MeV”. In: *Physical Review C—Nuclear Physics* 87.5 (2013), p. 054002.

[108] M Viviani et al. “Effect of Three-Nucleon Interactions in p-He 3 Elastic Scattering”. In: *Physical Review Letters* 111.17 (2013), p. 172302.

[109] M Viviani et al. “Benchmark calculation of n-3 H and p-3 He scattering”. In: *Physical Review C—Nuclear Physics* 84.5 (2011), p. 054010.

[110] M Viviani, Sergio Rosati, and A Kievsky. “Neutron-H 3 and Proton-H 3 e Zero Energy Scattering”. In: *Physical review letters* 81.8 (1998), p. 1580.

[111] J. Carbonell. "The continuum spectrum of the 4N system: Results and challenges". In: *Nuclear Physics A* 684.1 (2001). Few-Body Problems in Physics, pp. 218–226. ISSN: 0375-9474. DOI: https://doi.org/10.1016/S0375-9474(01)00417-1.

[112] Johannes Kirscher. "Zero-energy neutron–triton and proton–Helium-3 scattering with EFT ($\not{p}i$)". In: *Physics Letters B* 721.4-5 (2013), pp. 335–341.

[113] Timothy Vaughn Daniels et al. "Spin-correlation coefficients and phase-shift analysis for p+ He 3 elastic scattering". In: *Physical Review C—Nuclear Physics* 82.3 (2010), p. 034002.

[114] PE Tegnér and Chr Bargholtz. "The rate of the He-3 (p, e+ nu)-He-4 reaction". In: *Astrophysical Journal, Part 1 (ISSN 0004-637X), vol. 272, Sept. 1, 1983, p. 311-316. Research supported by the Naturvetenskapliga Forskningsradet.* 272 (1983), pp. 311–316.

[115] MT Alley and LD Knutson. "Effective range parametrization of phase shifts for p- 3 He elastic scattering between 0 and 12 MeV". In: *Physical Review C* 48.4 (1993), p. 1901.

[116] EA George and LD Knutson. "Scattering lengths for p- 3 He elastic scattering from an effective-range phase shift analysis". In: *Physical Review C* 67.2 (2003), p. 027001.

[117] K Varga and Yu Suzuki. "Solution of few-body problems with the stochastic variational method I. Central forces with zero orbital momentum". In: *Computer physics communications* 106.1-2 (1997), pp. 157–168.

[118] Y Suzuki et al. "Global-vector representation of the angular motion of few-particle systems II". In: *Few-Body Systems* 42.1 (2008), pp. 33–72.

List of Figures

1.1 The effective range expansion (ERE) of the proton−proton spin singlet s-wave scattering for relative momenta k up to $k^2 = 0.12$ fm^{-2} (energies E_{cm} up to 5 MeV). The solid line depicts the Coulomb-corrected ERE as a function of k^2 and the dashed line is the 'bare' ERE $k \cot \delta$. We observe that the corrected ERE behaves linearly while the 'bare' ERE diverges as $k \to 0$. The phase shifts were calculated using the two-body R-matrix method with the effective Minnesota interaction [29]. 15

1.2 Schematic depiction of the relative radial wave function of two interacting particles trapped in a HO trap. The blue line denotes the HO potential. For regions I,II and III, see the text 18

1.3 Comparison of s-wave pp phase shifts obtained by solving the Schrödinger equation with the Minnesota potential [29] using the Numerov method (solid black line) and the quantization condition in the HO trap, where the Green's functions are obtained by iterating the Fredholm equations (different symbols correspond to a certain number of iteration; see the legend). The HO frequency was varied between $\omega \in [0.7, 2]$ MeV corresponding to b between approximately 6.4 fm and 11 fm. 28

1.4 Scattering phase shifts from the quantization condition for arbitrary energies. The blue points represent s-wave pp phase shifts obtained by iterating the Fredholm equations for the Green's functions G^c and $G^{c\omega}$. The HO trap length was set to $b = 20$ fm and using the quantization condition the phase shifts were calculated for energies ranging from $E_{\text{cm}} = 0.01$ MeV to $E_{\text{cm}} = 0.85$ MeV. The red bands represent energy regions where the perturbative series diverges. Eigenenergies of the HO are depicted by the vertical dashed lines. 29

1.5 Comparison of s-wave pp phase shifts obtained by solving the Schrödinger equation with the Minnesota potential [29] using the Numerov method (solid black line) and phase shifts obtained from the quantization condition in the HO trap (red crosses), where the Green's functions are obtained by iterating the Fredholm equations just seven times. The HO frequency was varied between $\omega \in [0.7, 2]$ MeV, but this time the second eigenenergy of the HO trap spectrum was chosen. 30

1.6 A comparison of $p\alpha$ phase shifts in the ${}^2S_{1/2}$, ${}^2P_{3/2}$ and ${}^2P_{1/2}$ partial waves obtained by the solution of the two-body Schrödinger equation with the potential of Eq. (1.122) using the Numerov method and the generalized Busch formula with Green's functions found by matrix inversion. This figure is taken from the author's work [17], where $E = E_{\rm cm}$ and δ^c are the phase shifts denoted as δ in the rest of the thesis. 31

3.1 Feynman rules for the four-nucleon contact and derivative vertex. Due to Galilean invariance, the result can only depend on the differences of momenta $\boldsymbol{k} = \boldsymbol{k_1} - \boldsymbol{k_2}$, $\boldsymbol{k'} = \boldsymbol{k'_1} - \boldsymbol{k'_2}$. C_0 is equal to $C_0^{^3\mathrm{S}_1}$ or $C_0^{^1\mathrm{S}_0}$ and C_2^P is equal to any of the p-wave terms. The black square in the second diagram represents either the p-wave term or the derivative s-wave correction, in which case C_2 is equal to $C_2^{^3\mathrm{S}_1}$ or $C_2^{^1\mathrm{S}_0}$. 46

3.2 Feynman rules for the contact three- and four-body interaction. 47

3.3 Feynman diagrams of the contributions to the LO s-wave amplitude. 51

3.4 One-loop diagram dressed with a ladder of Coulomb photon exchanges 53

3.5 Power counting of the $\not\pi$EFT. The isospin-symmetry breaking terms which are due to the non-perturbative inclusion of the Coulomb interaction are drawn in red. The circles denote powers of $(Q/M_{\rm hi})$ 61

3.6 Comparison of low-energy pp $s-$wave phase shifts obtained from the phase shift analysis [72] to our LO and NLO $\not\pi$EFT potential. 67

3.7 Convergence of the bound-state energy for the pp system trapped in a HO trap with four different trap lenghts b as a function of the cutoff. The LO calculations are represented by the red points, the NLO by the blue points. 68

3.8 The *pp* scattering lenght (top) and effective range (bottom), obtained by trapping the system in an HO trap and using the quantization condition to calculate *s*-wave phase shifts, as functions of the cutoff. The LO calculations are represented by the red points, the NLO by the blue points, the dashed lines depict the values of ERE used to fit the ≠EFT potential. . . . 68

4.1 The calculated binding energy of ^{3}He, $B(^3\mathrm{He})$, as a function of the momentum cutoff Λ. The red points denote the LO calculation. The green points represent the NLO calculation, when the isospin-symmetry breaking three-body force emerging at NLO is not taken into account. The purple points are a LO calculation with a potential that treats the *pp* channel on equal footing with the other spin-singlet channels (pn/nn), and Coulomb is added without any modifications to the strong interaction. The wavy line seperates the LO extrapolated value at $\Lambda \to \infty$, denoted by the red square, from the finite-cutoff results. The dotted line represents the fitted extrapolating function, Eq. (4.1). The dashed line shows the experimental value. 72

4.2 The *pd* scattering length in the $S = 3/2$ channel as a function of the cutoff Λ. The LO results are denoted by the red points, the NLO by the blue points. Corresponding extrapolations at $\Lambda \to \infty$ are seperated from the rest of the calculations by the wavy line. The dotted red and blue lines denote the extrapolating functions Eq. (4.1) and Eq. (4.2), respectively. The solid black line and the grey band represent the most recent experimental value and its error from the 1999 phase shift analysis [96], the dashed-dotted line and green band the 1983 phase shift analysis [95] and the dashed line and light orange band the 1974 phase shift analysis value [94]. 74

4.3 The calculated *s*-wave *pd* scattering phase shifts in the $S = 3/2$ channel as a function of the cutoff Λ. The LO results are denoted by the red points, the NLO by the blue points. Corresponding extrapolations at $\Lambda \to \infty$ are seperated from the rest of the calculations by the wavy line. The dotted red and blue lines denote the extrapolating functions. The dashed line denotes the result of the PSA [102], where its errors are given by the grey bands. 75

4.4 The pd s-wave scattering phase shifts in the $S = 1/2$ channel as a function of the cutoff Λ. The green points denote the NLO calculation without the new isospin-symmetry-breaking force emerging at NLO. The rest of the symbols have the same meaning as in Figure 4.3. 76
4.5 The binding energy of ^{4}He, $B(^4\text{He})$, as a function of the momentum cutoff Λ. The red points represent the LO results and the green points the NLO without the perturbative four-body force. The red dotted line denotes the corresponding extrapolating functions and the extrapolated value in the infinite-cutoff limit is depicted by the red square on the right side of the squiggly line. The dashed line depicts the experimental datum. 78
4.6 The LO and NLO scattering length and effective range of dd in the $S = 2$ channel as a function of momentum cutoff. The notation is the same as in Figure 4.2. 79
4.7 The LO and NLO scattering length and effective range of p^3He scattering in the $S = 0$ channel. The symbols have the same meaning as in Figure 4.2. The grey bands represent the results of the PSA [113]. 80
4.8 The LO and NLO scattering length and effective range of p^3He scattering in the $S = 1$ channel. The symbols have the same meaning as in Figure 4.2. The grey bands represent the results of the PSA [113]. 81
4.9 The LO (red band) and NLO (blue band) p^3He scattering phase shifts in the $S = 0$ channel obtained from the ERE parameters. The black points are the results of the PSA [113]. The results for the I-N3LO, AV18, $V_{\text{low-k}}$ and χEFT N3LO with N2LO three-body force potentials are from Refs. [10, 109]. 83
4.10 The LO (red band) and NLO (blue band) p^3He scattering phase shifts in the $S = 1$ channel obtained from the ERE parameters. The black points are the results of the PSA [113]. The results for the I-N3LO, AV18 and $V_{\text{low-k}}$ potentials are from Refs. [10, 109]. 84

Appendix A

Numerical Methods For Two-Body Scattering

In this work, two methods for calculating two-body scatetring phase shifts were applied; Numerov, used e.g. in Figures 1.3 or 1.6 and the R-matrix, used in Figure 1.1. Although not explicitly stated in the main text, the results of these methods were often compared to verify that the phase shifts are sufficiently accurate. In this Appendix, both methods are very briefly described.

A.1 Numerov

The Numerov method is an algorithm for solving differential equations of the type

$$\frac{d^2}{dr^2}u(r) = f(r)u(r). \tag{A.1}$$

This can be applied to the Schrödinger equation where

$$f(r) = -2\mu\left[E - \frac{1}{2\mu}\frac{l(l+1)}{r^2} - V_c(r) - V(r)\right]. \tag{A.2}$$

Expanding the $u(h)$ and $u(-h)$ up to sixth order in the small value h and adding these two expansions leads to

$$u(h) + u(-h) - 2u(0) = h^2u(0)f(0) + \frac{h^4}{12}u^{\mathrm{IV}}(0) + \frac{h^6}{360}u^{\mathrm{VI}}(0) + \mathcal{O}(h^8), \tag{A.3}$$

where $u^{\mathrm{IV}}(0)$ ($u^{\mathrm{VI}}(0)$) is the fourth (sixth) derivative of $u(r)$ evaluated at 0. Using the differential equation (A.1), the fourth derivative of u is obtained

by differentiating the right-hand side two times

$$u^{\mathrm{VI}}(0) = \frac{u(h)f(h) - 2u(0)f(0) + u(-h)f(-h)}{h^2}. \tag{A.4}$$

We then have

$$\begin{aligned}\left[1 - (h^2/12)f(h)\right] u(h) + \left[1 - (h^2/12)f(-h)\right] u(-h) \\ - 2\left[1 - (h^2/12)f(0)\right] u(0) = h^2 f(0)u(0) + \mathcal{O}(h^6),\end{aligned} \tag{A.5}$$

which is the Numerov algorithm. At the beginning, we need to know $u(-h)$ and $u(0)$ and then solution is build up iteratively using the above formula. We start with the boundary condition $u(0) = 0$ and $u(h) = h^{l+1}$, which is an approximation for the wave function's behaviour at the origin under the assumption of a well-behaved potential, $\lim_{r\to 0} r^2 V(r) = 0$. The solution is build up from there using the above formula. Although the error of the Taylor expansion at each point is $\mathcal{O}(h^6)$, they add up to the global uncertainty $\mathcal{O}(h^5)$. Phase shifts can be calculated simply using Eq. (1.21).

A.2 R-Matrix

The main idea of the R-matrix theory [24] is to divide the configuration space into two regions, an external region $r > a$ and an internal region where $r < a$. The constant a is called the channel radius and its concrete value is not important, it only needs to be larger than the range of the nuclear force so that the radial wave function $u_l(r)$ in the external region is given by (1.26). We then define the R-matrix as

$$u_l(a) = R_l(E)\left[a u_l'(a) - B u_l(a)\right], \tag{A.6}$$

where B is a dimensionless parameter [24]. For $B = 0$ it is just the inverse of the logarithmic derivative of the wave function at the channel radius.

We solve the Bloch-Schrödinger equation

$$\left[H + \mathcal{L}(B) - E\right] u_l^{\mathrm{int}}(r) = u_l^{\mathrm{ext}}(r) \tag{A.7}$$

with the boundary condition

$$u_l^{\mathrm{int}}(a) = u_l^{\mathrm{ext}}(a). \tag{A.8}$$

Due to the Bloch operator

$$\mathcal{L}(B) = \frac{\hbar^2}{2\mu}\delta(r-a)\left(\frac{\partial}{\partial r} - \frac{B}{r}\right), \tag{A.9}$$

this equation is equivalent to the Schrödinger equation $Hu_l(r) = Eu_l(r)$ with the condition that the derivative of the wave function is continuos at the boundary, that is $u'^{\text{int}}_l(a) = u'^{\text{ext}}_l(a)$. The calculable R-matrix can then be expressed as the Green's function of the Bloch-Schrödinger equation, that is

$$[H + \mathcal{L}(B) - E]\, G_l(r, r') = \delta(r - r') \tag{A.10}$$

and the solution then is

$$u^{\text{int}}_l(r) = \int_0^a G_l(r, r')\mathcal{L}(B)u^{\text{ext}}_l(r')dr'. \tag{A.11}$$

Plugging in the definition of $R_l(E)$ and $\mathcal{L}(B)$ we find that

$$R_l(E) = \frac{\hbar^2}{2\mu a} G_l(a, a). \tag{A.12}$$

To make the calculation easier, we expand this expression using a finite basis

$$u^{\text{int}}_l(r) = \sum_{i=1}^{N} c_i \varphi_i(r), \tag{A.13}$$

the only requirement for these functions is that they vanish at the origin. Projecting (A.7) onto the basis $\{\varphi_i\}$ we find

$$\sum_{j=1}^{N} C_{ij} c_j \equiv \langle \varphi_i | H + \mathcal{L}(B) - E | \varphi_j \rangle_{\text{int}} = \frac{\hbar^2}{2\mu a} \left[a u'^{\text{ext}}_l(a) - B u^{\text{ext}}_l(a) \right], \tag{A.14}$$

where we have defined the C-matrix. The subscript 'int' denotes integration only in the internal region. Comparing the above expression with the definition (A.6) we obtain

$$R_l(E, B) = \frac{\hbar^2}{2\mu a} \sum_{i,j=1}^{N} \varphi_i(a)(C^{-1})_{ij}\varphi_j(a). \tag{A.15}$$

We have thus found an expression for the R-matrix that depends only on the Hamiltonian matrix elements in the internal region; notice that it is completely independent of the expansion coefficients $\{c_i\}$. The final thing left to do is to relate it to the S-matrix. Combining (1.26) and (A.6) and setting $B = 0$ we find

$$S_l(k) = \frac{I_l(ka) - R_l I'_l(ka)}{O_l(ka) - R_l O'_l(ka)} \equiv \frac{Z}{Z^*}, \tag{A.16}$$

where we used the property $I^* = O$ to define the Z-matrix. To find the phase shifts it then suffices to know the C-matrix. Following Ref. [24], we have implemented the R-matrix method for both the Lagrange mesh and a Gaussian basis.

Appendix B

Calculation of Matrix Elements in the Correlated Gaussian Basis

One of the advantages of the CGs is that the matrix elements of various operators and potentials can be evaluated analytically. Here, we will sketch out the process and give results for the overlap, kinetic energy and Gaussian potential matrix elements.

We start with the overlap matrix element between two basis states given by Eq. (2.18) with matrices of non-linear parameters A and A'. We need to calculate the integral

$$\langle F_A(\boldsymbol{x})|F_{A'}(\boldsymbol{x})\rangle = \int d\boldsymbol{x} \exp\left(-\frac{1}{2}\boldsymbol{x}^T(A+A')\boldsymbol{x}\right). \tag{B.1}$$

Let us denote $B = A+A'$. Since B is a positive-definite and symmetric matrix, it can be diagnolized by some orthogonal matrix S, so that $D \equiv S^T B S$ is diagonal. Then, the original integral is transformed into new coordinates $\boldsymbol{y} = S^T\boldsymbol{x}$

$$\int (\mathrm{det}T)^3 d\boldsymbol{y} \exp\left(-\frac{1}{2}\boldsymbol{y}^T D\boldsymbol{y}\right), \tag{B.2}$$

where $\mathrm{det}T$ is the Jacobian of the transformation, which we can assume to be equal to $+1$, since S is orthogonal. The integration can then be performed in each coordinate seperately and we simply have

$$\prod_{i=1}^{N-1} \int d\boldsymbol{y}_i \exp\left(-\frac{1}{2}D_{ii}\boldsymbol{y}_i^2\right) = \prod_{i=1}^{N-1}\left(\frac{2\pi}{D_{ii}}\right)^{\frac{3}{2}} = \left(\frac{(2\pi)^{N-1}}{\mathrm{det}D}\right)^{\frac{3}{2}}, \tag{B.3}$$

where D_{ii} is the diagonal element of D and we leave out the N-th coordinate, which corresponds to the center of mass. Since $\det(S^T B S) = \det B$ we have

$$\langle F_A(\boldsymbol{x})|F_{A'}(\boldsymbol{x})\rangle = \left(\frac{(2\pi)^{N-1}}{\det(A+A')}\right)^{\frac{3}{2}}. \tag{B.4}$$

The calculation of the kinetic energy matrix elements proceeds similarly. Using Eq. (2.7) we find

$$\langle F_A(\boldsymbol{x})|\sum_{i=1}^{N}\frac{\boldsymbol{p}_i^2}{2m_i} - T_{cm}|F_{A'}(\boldsymbol{x})\rangle = \frac{3}{2}\hbar^2 \mathrm{Tr}\left(A'(A'+A)^{-1}A\Lambda\right)\langle F_A(\boldsymbol{x})|F_{A'}(\boldsymbol{x})\rangle\,. \tag{B.5}$$

To calculate the matrix elements of the interaction $V(\boldsymbol{r}_i - \boldsymbol{r}_j)$ it is convenient to rewrite it as $V(\boldsymbol{r}_i - \boldsymbol{r}_j) = V(\boldsymbol{r})\delta(\boldsymbol{r}_i - \boldsymbol{r}_j - \boldsymbol{r})$. Using Eq. (2.9) we find for the delta function [117]

$$\langle F_A|\delta(\boldsymbol{r}_i - \boldsymbol{r}_j - \boldsymbol{r})|F_{A'}\rangle = \langle F_A|F_{A'}\rangle\left(\frac{c_{ij}}{2\pi}\right)^{\frac{3}{2}}\exp\left(-\frac{c_{ij}\boldsymbol{r}^2}{2}\right), \tag{B.6}$$

where

$$\frac{1}{c_{ij}} = w_{ij}^T(A+A')^{-1}w_{ij}. \tag{B.7}$$

Using this intermediate result, the matrix elements of $V(\boldsymbol{r})$ are

$$\langle F_A|V(\boldsymbol{r})|F_{A'}\rangle = \langle F_A|F_{A'}\rangle\left(\frac{c_{ij}}{2\pi}\right)^{\frac{3}{2}}\int d\boldsymbol{r}V(\boldsymbol{r})e^{-c_{ij}\boldsymbol{r}^2/2}. \tag{B.8}$$

If the radial dependence of the potential has Gaussian form, i.e., $V(\boldsymbol{r}) = V(r) = r^a e^{-br^2/2}$ with $r = |\boldsymbol{r}_i - \boldsymbol{r}_j|$, such as the ones discussed in Chapter 3, then the integral can be evaluated easily

$$\int d\boldsymbol{r}\, r^a e^{-\frac{1}{2}(b+c_{ij})} = 2\pi\left(\frac{2}{b+c_{ij}}\right)^{\frac{a+3}{2}}\Gamma\left(\frac{a+3}{2}\right), \tag{B.9}$$

where we used the definition of the gamma function $\Gamma(z) = \int dx\, x^{z-1}e^{-x}$. By setting $b = 0$ we obtain the following formula

$$\langle F_A|r^a|F_{A'}\rangle = \langle F_A|F_{A'}\rangle\frac{2}{\sqrt{\pi}}\left(\frac{2}{c_{ij}}\right)^{\frac{a}{2}}\Gamma\left(\frac{a+3}{2}\right), \tag{B.10}$$

which is useful to evaluate e.g. the matrix elements of the Coulomb potential $\sim 1/r$ or the harmonic oscillator $\sim r^2$.

Matrix elements of forces that act between more than two particles can also be evaluated straightforwardly. Let us have a general three-body force $V(\boldsymbol{r}_{ij}, \boldsymbol{r}_{ik}) \equiv V(\boldsymbol{r}_i - \boldsymbol{r}_j, \boldsymbol{r}_i - \boldsymbol{r}_k)$. We can use the same trick as in the two-body case, expressing the potential using delta functions

$$\langle F_A(\boldsymbol{x})|V(\boldsymbol{r}_{ij}, \boldsymbol{r}_{ik})|F_{A'}(\boldsymbol{x})\rangle = V(\boldsymbol{\rho}_1, \boldsymbol{\rho}_2, \boldsymbol{\rho}_3)\delta(\boldsymbol{\rho}_1 - \boldsymbol{r}_{ij})\delta(\boldsymbol{\rho}_2 - \boldsymbol{r}_{ik})\delta(\boldsymbol{\rho}_3 - \boldsymbol{r}_{jk}). \tag{B.11}$$

The matrix element of the delta functions is evaluated once again using Eq. (2.9), the result is [118]

$$\begin{aligned}\langle F_A(\boldsymbol{x})|\delta(\boldsymbol{\rho}_1 - \boldsymbol{r}_{ij})\delta(\boldsymbol{\rho}_2 - \boldsymbol{r}_{ik})\delta(\boldsymbol{\rho}_3 - \boldsymbol{r}_{jk})|F_{A'}(\boldsymbol{x})\rangle = \\ = \langle F_A(\boldsymbol{x})|F_{A'}(\boldsymbol{x})\rangle \left(\frac{\mathrm{det}C}{(2\pi)^3}\right)^{\frac{3}{2}} \exp\left(-\frac{1}{2}\boldsymbol{\rho}^T C \boldsymbol{\rho}\right),\end{aligned} \tag{B.12}$$

where now $\boldsymbol{\rho}^T = (\boldsymbol{\rho}_1, \boldsymbol{\rho}_2, \boldsymbol{\rho}_3)$ and C is a symmetric 3×3 matrix with the elements

$$\left(C^{-1}\right)_{\alpha\beta} = w_\alpha^T (A + A')^{-1} w_\beta, \tag{B.13}$$

where $\alpha = ij, ik, jk$. Then, the potential matrix element is given by integrating over the coordinates $\boldsymbol{\rho} = (\boldsymbol{\rho}_1, \boldsymbol{\rho}_2, \boldsymbol{\rho}_3)^T$

$$\begin{aligned}\langle F_A(\boldsymbol{x})|V(\boldsymbol{\rho})|F_{A'}(\boldsymbol{x})\rangle = \\ = \langle F_A(\boldsymbol{x})|F_{A'}(\boldsymbol{x})\rangle \left(\frac{\mathrm{det}C}{(2\pi)^3}\right)^{\frac{3}{2}} \int d\boldsymbol{\rho} V(\boldsymbol{\rho}) \exp\left(-\frac{1}{2}\boldsymbol{\rho}^T C \boldsymbol{\rho}\right).\end{aligned} \tag{B.14}$$

This result can be easily generalized to n-body forces. In that case we need a matrix element of a product of $m = n(n-1)/2$ delta functions, one for each possible particle pair. The matrix C is then $m \times m$ dimensional, still given by Eq. (B.13), except the indeces α, β run over all particle pairs and $\boldsymbol{r}$ are the coordinates of all possible pairs $\boldsymbol{\rho} = (\boldsymbol{\rho}_1, \boldsymbol{\rho}_2, \boldsymbol{\rho}_3, ...)^T$. The only formal difference in equations (B.12) and (B.13) is that the factor $(2\pi)^3$ becomes $(2\pi)^m$,

$$\begin{aligned}\langle F_A(\boldsymbol{x})|V(\boldsymbol{\rho})|F_{A'}(\boldsymbol{x})\rangle = \\ = \langle F_A(\boldsymbol{x})|F_{A'}(\boldsymbol{x})\rangle \left(\frac{\mathrm{det}C}{(2\pi)^m}\right)^{\frac{3}{2}} \int d\boldsymbol{\rho} V(\boldsymbol{\rho}) \exp\left(-\frac{1}{2}\boldsymbol{\rho}^T C \boldsymbol{\rho}\right).\end{aligned} \tag{B.15}$$

Just like in the two-body case, an analytical expression can be found if we assume that the n-body potential dependence is given by a local, central Gaussian

$$V(\boldsymbol{r}_{ij}, \boldsymbol{r}_{ik}, ...) \equiv V(r_{ij}, r_{ik}, ...) = \exp\left(b \sum_{i<j} r_{ij}^2\right), \tag{B.16}$$

where the sum in the exponent is the hyperradius, sum of distances of all possible particle pairs, i.e. $\sum_{i<j} r_{ij}^2 = \sum_\alpha \rho_\alpha^2$ in the notation introduced above. Using Eq. (B.15) we find

$$\langle F_A(\boldsymbol{x})|V(\boldsymbol{\rho})|F_{A'}(\boldsymbol{x})\rangle = \\ = \langle F_A(\boldsymbol{x})|F_{A'}(\boldsymbol{x})\rangle \left(\frac{\det C}{(2\pi)^m}\right)^{\frac{3}{2}} \int d\boldsymbol{\rho} \exp\left(-\frac{1}{2}\boldsymbol{\rho}^T(C+b)\boldsymbol{\rho}\right), \quad \text{(B.17)}$$

where the integral is equivalent to the one we needed to evaluate for the overlap matrix element, we just need to do the substitutions $N-1 \to m$ and $B \to (C+b)$. The final result then reads

$$\langle F_A(\boldsymbol{x})|V(\boldsymbol{\rho})|F_{A'}(\boldsymbol{x})\rangle = \langle F_A(\boldsymbol{x})|F_{A'}(\boldsymbol{x})\rangle \left(\frac{\det C}{\det(C+b)}\right)^{\frac{3}{2}}. \quad \text{(B.18)}$$

Appendix C

Low-Energy Constants

In this Appendix, we present the fitted values of the LECs of the potential, Eq. (3.56), devised in this work, which were left out of Chapter 3 for brewity.

Table C.1 The leading order low energy constants of the potential fitted and used in this work, see Chapter 3 for details. Except Λ, all values in MeV.

Λ [fm^{-1}]	$C_0^{(0)}$	$C_1^{(0)}$	$C_2^{(0)}$	$D_0^{(0)}$
1.00	-24.865367586	-44.4533354532	-24.50369836097	-1.0902644426
1.25	-39.701746253	-63.7137148334	-39.79620695114	7.0398708093
2.00	-105.07232243	-142.368753293	-107.2271275520	65.4012765781
3.00	-240.92326467	-295.942886782	-246.8644112838	259.9229231906
4.00	-432.42573237	-505.172616626	-442.9298795416	661.3437507804
5.00	-679.58136224	-770.057198773	-695.2114105224	1381.982349198
6.00	-982.39071657	-1090.59635473	-1003.589797019	2588.287156701
7.00	-1340.8539842	-1466.78995544	-1367.987704277	4531.604711067
8.00	-1754.9713560	-1898.63794746	-1788.351249694	7595.462006271
9.00	-2224.7429098	-2386.14029607	-2264.640498161	12369.08472518
10.00	-2750.1685273	-2929.29697072	-2796.824693679	19762.68241655
12.00	-3967.9824859	-4182.57326470	-4028.784179687	48855.17650645
14.00	-5408.4133846	-5658.46659397	-5484.082031250	118747.4251171
16.00	-7071.4613989	-7356.97738148	-7162.617187500	289144.7353992
18.00	-8957.1262457	-9278.10517693	-9064.306640625	713096.1556883
20.00	-11065.408265	-11421.8500959	-11189.08996582	1793521.309372

Table C.2 The two-body next-to-leading order low energy constants of the potential fitted and used in this work, see Chapter 3. The values of $C_0^{(1)}$, $C_1^{(1)}$ and $C_2^{(1)}$ are in MeV, the values of $C_3^{(1)}$, $C_4^{(1)}$ and $C_5^{(1)}$ in MeV^{-1}.

Λ [fm^{-1}]	$C_0^{(1)}$	$C_1^{(1)}$	$C_2^{(1)}$	$C_3^{(1)}$	$C_4^{(1)}$	$C_5^{(1)}$
1.00	1.9136457	8.86324	1.97045470	3.459959	8.435742	0.95218829
1.25	-3.704192	1.53305	-6.4866069	-4.17064	1.011191	-5.2853806
2.00	-67.16251	-65.124	-33.224738	-28.3167	-19.2003	-76.729955
3.00	-336.5471	-305.01	-69.373330	-61.5596	-43.5069	-378.16881
4.00	-936.4254	-793.45	-105.30159	-95.1752	-66.6387	-1041.7942
5.00	-1997.311	-1613.8	-141.18151	-128.960	-89.2651	-2206.5976
6.00	-3649.528	-2849.9	-176.72942	-162.827	-111.631	-4003.9381
7.00	-6023.448	-4585.1	-212.26093	-196.741	-133.846	-6573.6838
8.00	-9249.448	-6903.1	-247.70659	-230.685	-155.967	-10049.477
9.00	-13457.90	-9887.6	-283.08435	-264.649	-178.024	-14566.198
10.00	-18779.18	-13622.	-318.40715	-298.627	-200.035	-20258.537
12.00	-33281.72	-23676.	-388.92910	-366.610	-243.969	-35708.589
14.00	-53800.07	-37733.	-459.32611	-434.618	-287.826	-57475.272
16.00	-81377.24	-56464.	-529.59978	-502.641	-331.635	-86627.956
18.00	-117057.0	-80536.	-599.82044	-570.678	-375.411	-124246.17
20.00	-161898.1	-110619	-670.00445	-638.786	-419.165	-171405.30

Table C.3 The three- and four-body next-to-leading order low energy constants of the potential fitted and used in this work, see Chapter 3. Except Λ, all values in MeV.

Λ [fm^{-1}]	$D_0^{(1)}$	$D_1^{(1)}$	$E_0^{(1)}$
1.00	4.5427770226	-0.8081848767	103.5228990939
1.25	-2.9117895760	-0.4230133270	236.4354323502
2.00	-9.7494030483	-2.1160506396	14208.0838631457
3.00	299.4564661766	10.4129706033	342948.1303553
4.00	1824.3327656964	67.7159368079	2684937.32826296
5.00	6318.2932709560	226.8565963343	9779975.17747876
6.00	16955.2205301366	578.5617813824	-766982.701414396
7.00	39275.6260143234	1291.2241202424	-280007556.475623
8.00	82770.8785784885	2639.8869734163	-2488212294.53687
9.00	163532.759679412	5090.8572256851	-15633885395.0337
10.00	308696.833513123	9428.3661977998	-83030842973.9286
12.00	1005980.22755858	30052.6791798949	-1317627875179.97
14.00	3057178.61008101	90160.4294515948	-2000787054312.21
16.00	8986872.72462052	263719.467984001	-1824664504764.31
18.00	26126250.3631177	767382.032061582	-1510665023508.18
20.00	76168337.4497947	2244977.65980085	200326702870.834